European Commission

JRC TECHNICAL REPORTS

Circuit and Containment Aspects of PHÉBUS Experiment FPT-2

Final Interpretation Report

Marco Sangiorgi
Aleksander Grah
Luca Ammirabile

2015

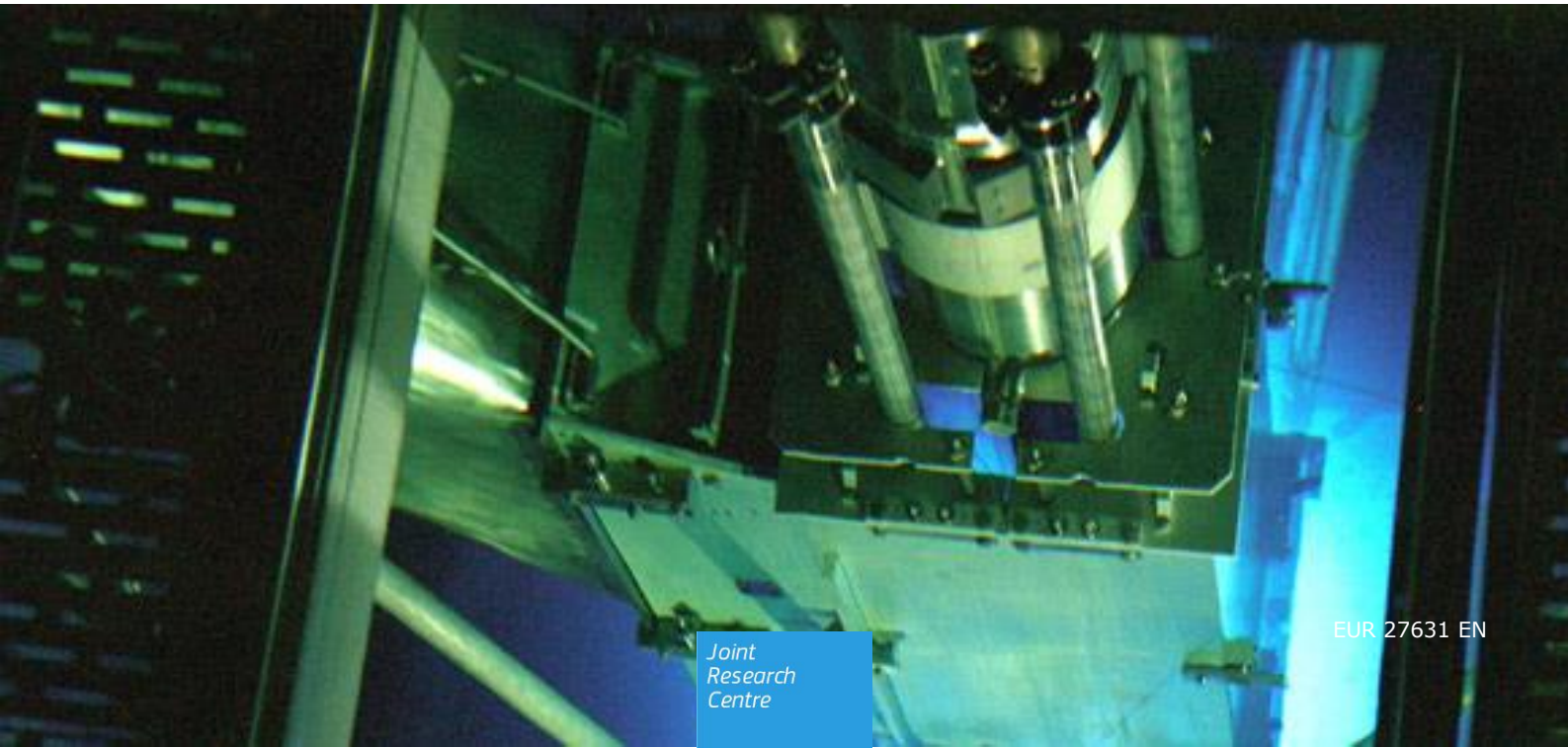

Joint Research Centre

EUR 27631 EN

Circuit and Containment Aspects of PHÉBUS Experiment FPT-2

JRC Science Hub
https://ec.europa.eu/jrc

JRC99477

EUR 27631 EN

ISBN 978-92-79-54085-1 (online)
ISBN 978-92-79-54086-8 (print)

ISSN 1831-9424 (online)
ISSN 1018-5593 (print)

doi:10.2790/94418 (online)
doi:10.2790/716808 (print)

How to cite: Authors; title; EUR; doi

Table of contents

Acknowledgements

Thanks are due to our former colleagues Alan Jones (JRC), Roland Zeyen (JRC), and the SARNET members for detecting errors and omissions and for supplying additional information.

Abstract

The international reactor safety project Phebus FP is devoted to the study of core meltdown in the case of a severe accident scenario. Its main objective is to study the fuel degradation, the release and transport of fission products and structure material in the reactor coolant system (RCS) and containment building, with special attention to iodine radiochemistry. The test sequence of those experiments included an irradiation phase, a fuel bundle degradation phase and a long-term phase dedicated to the analysis of aerosol and iodine radiochemistry in the containment vessel. The FPT-2 test was performed using a bundle configuration in a steam poor environment and with injection of boric acid. On-line measurements and post-test analyses indicate that releases of noble gases (Xe, Kr) from the fuel bundle are very high (up to 80% of initial bundle inventory); other elements can be classified as high-volatile with releases higher than 50% of bundle initial inventory (FPs: Cs, I, Te, Mo), as semi-volatile with releases comprised between 10 and 50% (FPs: Rb and control rod material: Cd) and low-volatile with releases lower than 10% (FPs: Ru, Ba and control rod material: Ag, In). Important material deposition was observed in the circuit, so that material inventory reaching the containment is significantly lower than the fractions released from the degraded bundle. The release and transport kinetics of material could be determined and seems strongly correlated with bundle degradation events (first fuel Zircaloy cladding oxidation phase, late oxidation phase and fuel liquefaction and displacement). In the circuit, specific instrumentation devoted to iodine speciation revealed that iodine exists mainly in a vapour form in the hot leg (700°C), most probably as vapour of metal iodide. Between the circuit hot leg and the cold leg (150°C), condensation of those species both on the circuit surface and on transported aerosols is quite extensive. Therefore, iodine transiting through the circuit cold leg before arriving in the containment vessel was found mainly to be in an aerosol form. It is to be noted that a minor gaseous iodine fraction was evidenced in the cold leg of the circuit. The Circuit and Containment Aerosol Interpretation Circle CACIC is devoted to give a final interpretation of the main outcomes of the experiment related just to circuit and containment, reviewing all the calculation carried out and providing a code validation/quality assurance. The interpretation is based on test data, computational simulations by state-of-the-art severe accident analysing codes and on the discussions at the meetings of the Phebus CACIC organized by IRSN, Cadarache and EC JRC, Petten.

1. INTRODUCTION

1.1 Historical background

In the 1980s a series of experiments were performed in the French Phebus reactor at Cadarache on fuel response during transients leading to severe fuel damage. In the Phebus-CSD programme a bundle of reduced length fuel rods plus a central control rod was placed in the central hole of the Phebus reactor and subjected to specified neutronic power and steam flow histories, and the degradation process was captured through on-line instrumentation and post-test examination of the degraded bundle. In addition to thermocouples and pressure sensors the on-line instruments included a crude but effective neutron imaging system which provided direct information on material movements.

A solution arose focused on a reactor safety problem relating to severe accidents. If a local or more widespread core melt event took place because of an inability to dispose of decay heat, as in the Three Mile Island accident in the US (1979), it was well known that fuel melting would occur, as in the Phebus-CSD experiments, but also that potentially hazardous fission products and other materials would be released from the fuel rods and their cladding and be transported through the reactor primary circuit and into the containment building. To what extent would the radiological hazardous material be trapped in the circuit? Specifically in the tubes of the steam generator, assuming the circuit break occurred downstream of the steam generator itself, and was there scope for operator actions to enhance the trapping and maintain the fission products in the trapped state once deposited? Such local trapping would reduce the discharge to the containment, so limiting the consequences of late containment failure and the challenge to containment engineered safety features such as sprays.

The outlines of the Phebus FP experiments (FP stands for fission product) were defined (EC CEA/IPSN, 1988). A bundle configuration similar to the previous CFD tests would be used but with irradiated fuel rods. A source of short irradiated rods was identified in the Belgian BN reactor. Prior to each experiment of the envisioned series the bundle would be irradiated in situ in the Phebus reactor to build up an inventory of fast-decaying fission products, notably iodine-131. A pressurised water circuit would keep the bundle cool during this process. When sufficient irradiation had occurred (8 days or so) the reactor would be shut down and the bundle would be drained. Without disturbing the reactor or bundle a different circuit would be switched in, supplied with injected steam at the foot of the bundle and leading via a vertical line with conical inlet and a wide-bore horizontal line to the experimental circuit within a sealed caisson. An operator-controlled reactor power history would bring the bundle to extensive degradation and fuel melting, thus providing information on core material movement and interaction etc. The input to the experimental circuit would be the injected steam, partly converted to hydrogen by oxidation of cladding within the bundle, fission products, fuel and oxidised cladding particles etc. and the final element of the circuit would be a model containment vessel with controlled surface temperatures, where the steam would largely condense and the other materials would accumulate. Apart from sampling operations no outflow from the complete circuit to the environment was envisaged during the experiment.

After completion of the experiment the reactor would be shut down, the circuit would be isolated, and samples would be retrieved, data would be analysed etc. The degraded bundle would be removed for post-test examination. On completion of engineering operations the circuit would be dismantled and a new experimental circuit would be installed, and the installation would then be ready for the following experiment.

This concept was an advance on previous US tests involving irradiated bundles, such as the SFD experiments, but there were practical difficulties in taking the idea of Phebus FP forward, notably financial. The European Commission's Joint Research Centre joined a number of national organisations (Canadian, US, Japanese) in examining the French plans and helping to fund the experiments in return for access to the data. It was

necessary to refurbish the Phebus reactor extensively to allow continued operation and to permit running the reactor over several days during the pre-irradiation phase of each experiment. The JRC assumed a leading role among the international partners and allocated members of its own staff to complement the French technical and analytical teams. The JRC also played a role in deciding upon the test matrix for the Phebus series. Early ideas of using the fission product stream from the Phebus bundle to investigate pool scrubbing, circuit water injection, and even biological effects were discarded, and the focus shifted rather to:

1. Bundle degradation and FP release under different conditions e.g. excess steam, steam starved, presence of air, and possibly with different control rod designs;
2. Circuit retention in the hot (vertical and horizontal lines) and cool (steam generator tube) portions of the circuit for different sources from the bundle. The same basic circuit layout would be used for all experiments;
3. Deposition in the containment vessel and chemistry evolution with different sources.

For the first technological test fresh fuel was used (but with a pre-irradiation phase), and was designated FPT-0. Test FPT-1 would be similar but with irradiated fuel, and the following tests were numbered FPT-2, FPT-3, FPT-4 and FPT5. The tests did not span the whole range of conditions which might be expected in core melt accidents, but it was felt that six tests would provide a good basis for code assessment while remaining within the financial envelope and the residual lifetime of the reactor.

1.2 Phebus FP programme

Five tests have been performed since the beginning of the Phebus fission product program (see Appendix 1). To study degradation and melting, two kinds of initial fuel geometry were examined: fuel bundle configuration in four tests (FPT-0, FPT-1, FPT-2, and FPT-3) and debris bed geometry in one test (FPT-4). In FPT-0, fresh fuel was used, whereas in the other tests irradiated fuel was used. For these tests, steam atmosphere is required; it was obtained by steam injection at the bundle bottom. The flow rate corresponded to the reactor case when, after core uncovering, the water in the lower part of the core evaporated. In these tests, various flow rates were imposed in order to study fission product release both in highly oxidizing conditions (FPT-0, FPT-1) and steam-poor conditions (FPT-2, FPT-3) including a steam starvation period with almost full conversion of steam to hydrogen.

1.3 Analysis and Interpretation efforts

At an early stage during preparation of test FPT-0 it became obvious to the JRC that there was considerable interest among code developers, analysts and safety bodies across Europe in participation in Phebus test preparation and post-test interpretation. It was therefore decided to set up as supporting groups to the Technical Group and Scientific Analysis Working Group, which were created under the contract by which the EC took part in the Phebus programme, three Interpretation Circles (IC) which would be purely technical in nature, tasked with providing pre-calculations of Phebus tests, interpretation of experimental observations from each test and detailed post-test analysis using those best-estimate and systems codes with which the participants were most familiar. Participation was entirely voluntary, and the ICs were open to all Phebus partners. The groups were:

- Bundle Interpretation Circle (BIC). Bundle heat-up, material movement and interaction, fission product emission and transport to the bundle outlet (Point A in Phebus parlance)

- Circuit and Containment Interpretation Circle (CACIC). Thermal-hydraulic conditions in the circuit; material transport and deposition within the circuit, including chemical interactions among species and with pipe walls; specific aerosol phenomena such as revaporisation and resuspension, source to the containment vessel (Point H); thermal-hydraulics in the containment vessel, including evaporation from the water pool and condensation on a specific cooled structure (condenser) provided to remove excess injected steam; aerosol distribution and removal within the vessel
- Containment Chemistry Interpretation Circle (CCIC). Chemical aspects of fission product behaviour in the model containment, particularly the fate of gaseous iodine arriving from the circuit, fission product interactions with painted and unpainted surfaces, and long-term (several days) chemistry within the vessel, especially its sump and the overlying atmosphere.

The FPT-2 Phebus experiment (together with the previous FPT-0 and FPT-1 tests) produced a wealth of data on all aspects of the circuit and containment behaviour, from the sources arising from the degrading bundle through temperatures, pressures and flow velocities to transport and deposition behaviour in both the circuit and the model containment and particular phenomena like resuspension and revaporisation. Through work stimulated by CACIC and embodied in national programmes and through the labours of the Commission's own staff at the Joint Research Centre all circuit and containment aspects have been investigated using both detailed and system-level codes as well as ad hoc analytical models, and the results have been compared with experimental data, as summarised in the sections which follow.

Over the years a substantial amount of analytical insight has been built up through the work of the ICs, some of it published in the open literature, some in the minutes of the ICs, and some in internal reports of the EC projects or of national organisations. Concerned that some hard-won information documented only in the "grey literature" was not being sufficiently well integrated to EU governments and industry and might eventually be lost, the JRC has begun documenting interpretation reports of the main analytical features of the Phebus programme and the conclusions which may be drawn from them.

The present document is the interpretation report for CACIC activities regarding Phebus experiment FPT-2. The interpretation is based on test data, computational simulations by state-of-the-art severe accident analysing codes and on the discussions at the meetings of the Phebus CACIC organized by IRSN, Cadarache and EC JRC, Petten.

It is difficult to give an exhaustive list of code users and other specialists who contributed to the analysis of FPT-2 test results and their interpretation. A special mention is due for the work of K. Trambauer (GRS) using ATHLET-CD, J. Birchley (Paul Scherrer Institute (PSI) using MELCOR, L.E. Herranz (CIEMAT) using ASTEC, and CONTAIN, A. Bujan (JRC), J. Dienstbier (UJV) and I. Drosik (IRSN) using ASTEC/SOPHAEROS, G. Gyenes (JRC) using ASTEC/CPA (see Appendix 3).

1.4 Structure of the report

In Section 2 a brief description of test FPT-2 is provided, giving for the circuit and containment the objectives, design and scenario. The bundle degradation history is then reviewed from the viewpoint of defining the time-dependent multicomponent source to the circuit. Various phases of release are defined, useful in the discussion of results which follows.

In Section 3, the circuit section is examined, reviewing both the experimental findings and the calculated results. Thermal hydraulic conditions are reviewed, including data from the thermal gradient tubes. Deposition is considered in turn looking at both

experimental data and calculation results, together with some specific features of interest.

Elements depositing as aerosols are considered separately from those depositing partially or wholly as vapours. Dedicated subsections examine the behaviour of iodine in the circuit, from its release from the bundle till its discharge at the circuit outlet (Point H).

Attention then turns in Section 4 to the model containment vessel, looking first at the thermal hydraulics, for which there were several distinct experimental phases and where specific design features such as the suspended cylinders of the condenser played an important role, and then examining the evolving aerosol characteristics and the deposition behaviour, as measured and as calculated.

Section 5 provides a summary consolidating the findings of the studies reported regarding the circuit and the containment vessel respectively both from the viewpoint of understanding and model validation and from that of plant safety, and finally highlights some open issues.

2. PHEBUS EXPERIMENT FPT-2

The final experimental data report of FPT-2 (Gregoire et al., 2008) is available. The Phebus progress reports are also available where experimental findings and interpretation activities have been presented.

2.1 FPT-2 objectives

The main objective of the FPT-2 test was to achieve a long enough period with highly reducing conditions (by way of almost complete transformation of the injected steam into hydrogen, as a result of the Zircaloy oxidation), in the upper part of the bundle and through the experimental circuit, in order to investigate material release from the bundle, transport and deposition within the circuit under such conditions, and discharge into the containment. In this respect, the FPT-2 test aimed at providing data correlating bundle degradation phenomena with FPs release kinetics. These data would be used to quantify retention processes at various locations in the circuit where sharp changes in the carrier gas temperature are expected (at the test bundle outlet and in the steam generator tube), and to study the FP physicochemical behaviour, emphasising the impact of the steam-poor conditions.

Another main objective was to study the FP behaviour in the containment under conditions representative of a LWR severe accident. The analysis of iodine radiochemistry in the sump water and the atmosphere was specifically emphasised, with some extensive dedicated instrumentation, on the one hand, and with painted surfaces placed in both the sump water and the containment atmosphere in order to provide a scaled source for organic iodides, on the other hand. The sump water was set to be alkaline (pH 9) and set to hot evaporating conditions during the chemistry phase in order to promote the volatile iodine transfer from the sump to the atmosphere. During this period, the thermal hydraulic conditions in the containment (also called *REPF502 vessel*) were imposed by setting the temperature evolution of condensers, vessel wall and sump water (from 90 °C prior to the washing phase to 120 °C during the chemistry phase) to obtain the desired evaporation/condensation rate (about 1g/s) and a humidity ratio approx. 70% during the chemistry phase.

An additional objective was to characterise aerosols and deposition processes such as gravitational settling on the containment bottom, diffusiophoresis onto painted condensers exposed to the containment atmosphere and deposition onto the containment walls.

Complementary objectives were to characterise:

- the effect of boric acid injection on the FP behaviour (for the first time in a Phebus FP test, boric acid was added to the steam used as the test bundle coolant, with a 1000 ppm by mass of boron);
- the difference of deposition phenomena in the section next to the bundle outlet between stainless steel and Inconel (by means of post-test analyses on vertical line sections);
- aerosol sizing in the circuit cold leg.

From the analysis of the previous test results (FPT-0, FPT-1) it was known that after degradation of fuel rod cladding by high-temperature steam oxidation the temperature in the hottest bundle part had to be maintained at about 2473 K (2200 °C) to maximize the released mass of volatile, semi and low volatile fission products from the fuel. This implies that about one third of the fuel in the bundle should have been heated until relocation temperature or even higher, up to complete melting and formation of an extended molten pool in the lower third of the bundle.

Due to the lower steam flow injected at bundle inlet to investigate the transport and chemical behaviour of released radio-nuclides in novel conditions compared to the FPT-0 and FPT-1 tests, the cladding oxidation rate was limited. Thus during the main oxidation period most of the steam reduced to hydrogen and the volatile fission products were released in a hydrogen-rich atmosphere. The low steam flow rate enhanced the FP deposition in the circuit line. Boric acid was added to the injected steam to explore its eventual impact on the chemical speciation of released volatile products.

2.2 Test scenario and release to the circuit

The scenario for the FPT-2 test was similar to that of the previous FPT-0 and FPT-1 tests.

The experiment was divided into different sequential phases:

- a degradation phase starting from the fuel bundle deterioration up to the containment isolation from the circuit during which the FP were released from the fuel, transported along the circuit and injected into the containment;
- a condensation phase where the condensers continued to operate and the aerosols could settle and condense;
- a settling phase in which the "wet" condenser surfaces were heated so that steam no longer condensed upon them;
- a washing phase during which aerosols that settled on the vessel bottom were washed into the sump;
- a long-term chemistry phase.

Only the degradation/injection, condensing and aerosol settling phases are considered in this report.

The main differences with regard to the experiments FPT-0, FPT-1 were the burn-up of the fuel rods and the steam flow at the bundle inlet. Nearly fresh fuel was used for the FPT-0 bundle and lower burn-up pre-irradiated fuel (22 GWd/t) was investigated in the FPT-1 experiment, while the FPT2 test used 33 GWd/t uranium dioxide fuel enriched to 4.5% and re-irradiated in situ for 7 days to a burn-up of 130 MWd/t. As a consequence the fuel rods in FPT-1 and FPT-2 contained a significantly higher fission-product inventory compared to FPT-0. At the bundle inlet, the steam flow rates were imposed to study the fission product (FP) release both in highly oxidizing conditions (steam flow 1.0 to 2.5 g/s for FPT-0 and FPT-1) and steam-poor conditions (0.5 g/s for FPT-2). The higher rate roughly corresponds to the scaled steam flow from a completely covered core, while the lower rate corresponds to a largely uncovered core (Gregoire et al., 2008).

Common to all the three Phebus experiments, there was a thermal calibration period of the experimental setup, a FP release period when the main degradation of the bundle took place (Figure 2), an aerosol deposition period and a chemistry period. After the FP-release period the containment was isolated from the circuit.

In the FPT-2 Phebus experiment the fuel bundle was composed of 20 short (1 m long) fuel pins with a central Ag-In-Cd control. The bundle is a scaled model (1:5000) of a French 900 MW PWR reactor core. The purpose of re-irradiating the fuel in FPT-2 for 7.2 effective days prior to the degradation phase was to create a representative inventory of short-lived fission products. After that, a 37-hour transition period allowed putting the Phebus facility in test conditions at zero reactor power and gave time to the decay of neutron poisoning ^{135}Xe. Then the degradation phase of the test was conducted by gradually increasing the reactor power. The steam flow and the steam temperature at the inlet of the bundle were constant, 0.49 g/s and 438 K, respectively. During the whole transient, at the external surface of pressure tube the temperature of pressurized water flow was 438 K as well.

The degradation phase corresponded to a 5-hour transient during which the steam flow through the bundle was set to 0.5 g/s, while the driver core power was progressively increased by successive plateaus. The temperature reached during the transient, as a result of both the nuclear power increase and the Zircaloy oxidation, led to the successive thermo-mechanical failure of the fuel clad and the absorber rod, followed by the melting and relocation of fuel and structure materials. This degradation phase resulted in an extensive release of hydrogen, fission products, fuel elements and structure materials into the circuit and the containment vessel. The five main degradation phases could be observed in Figure 1 and are summarized in Table 1:

1. The calibration phase (0—7386 s): two power plateaus helped to verify the calculated thermal behaviour of the bundle; the cladding. balloons and bursts in the mid-height, in the hot zone of the bundle;
2. The pre-oxidation phase (7386—8520 s): pre-oxidation of the cladding, rupture of the control rods was expected during the P3 power plateau (8082—8520 s);
3. The main oxidation phase (8520—9960): power increased and consequently fuel rod temperature increased; there was the runaway of the Zircaloy oxidation at ca. 1550 °C with temperature escalation and hydrogen production. The oxidation front of the cladding moved from the middle of the bundle to lower and after that to higher elevations. Most of the time the hydrogen concentration at the bundle outlet was greater than seventy per cent. This gave the possibility to observe the release of fission products (FP) in reducing conditions;
4. The power plateau P4 (9960—13860 s): Since the oxidation was not finished completely in the upper part of the bundle there was a significant contribution to the total power until 10760 s; the plateau was used to stabilise the temperature at 1950 °C at mid height (500 mm); after 10760 the power was carefully increased in two steps and the temperature stabilised without significant contribution of oxidation power;
5. The heat up phase and shutdown (13860—19740 s): the bundle power increased linearly; the temperature increased to 2000—2200 °C; fuel and cladding liquefied and materials relocated forming a molten pool in the lower third of the bundle; there was a FP release in oxidizing conditions.

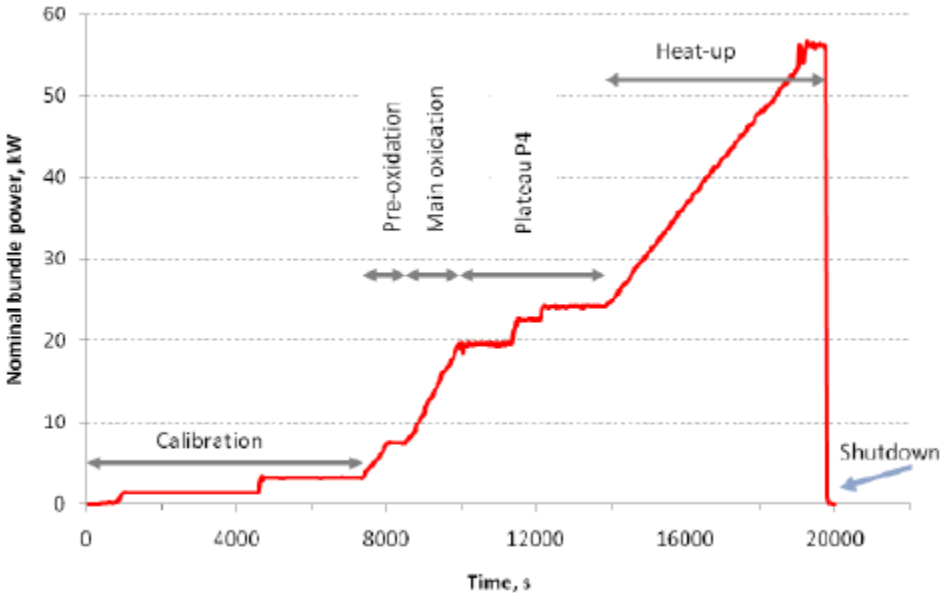

Figure 1. The nominal bundle power and the characteristic degradation periods.

During the experiment the released materials, including fission products (FP) and control and structural materials (SM) were transported through the circuit into a containment vessel, and vapour, aerosol and chemical behaviour were monitored by a variety of instrumental means.

During the test, the system pressure was maintained between 2.0 and 2.4 bars.

The release from the bundle and transport of material through the circuit during the FPT-2 transient were strongly correlated with bundle degradation events. Three main release phases could be identified:

- A first large release event was observed during a first oxidation phase, followed by a period of fairly steady release for volatile fission products and control rod materials until approximately the late oxidation phase.
- A second large material release occurred at the time when oxidation happened in the lower part of the fuel bundle, accompanied by the beginning of the fuel liquefaction and the first fuel relocation, releasing less volatile material.
- At reactor shutdown, aerosol concentration in the containment atmosphere peaked then it started to decrease suggesting that materials was transported to the containment only in small quantities that could not compensate for losses associated with deposition processes.

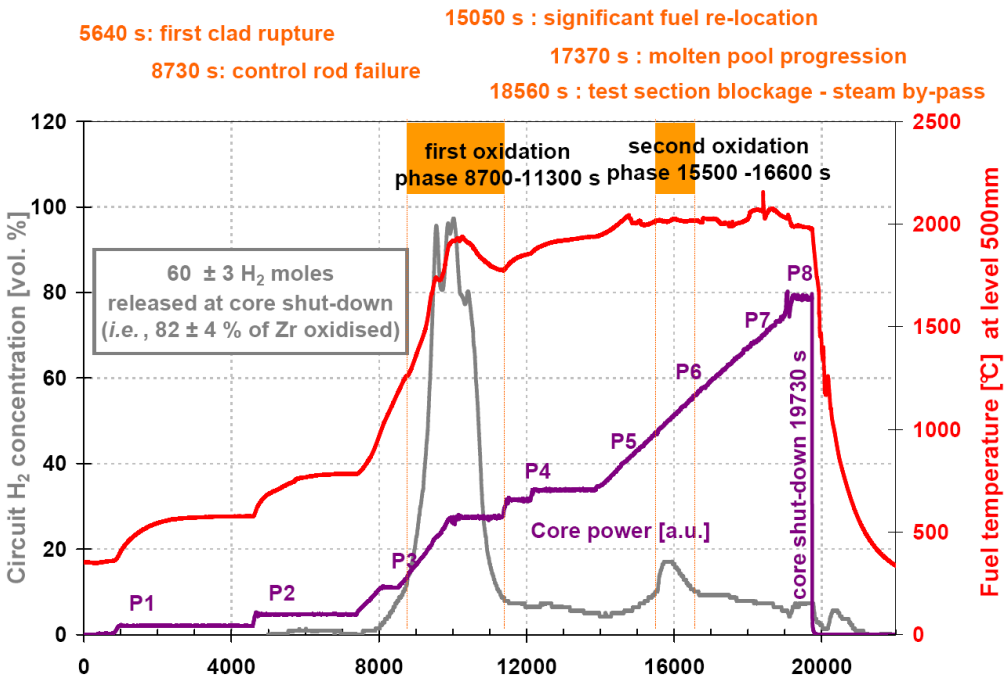

Figure 2. FPT-2 general chronology.

Table 1. The main characteristic periods of the bundle degradation phase in the FPT-2 test.

Period	Current time, s start	end	Duration, s	Reactor power, MW
Thermal calibration phase	0	7386	7386	0.21 P1 0.21 to 0.48 ramp 0.48 P2
Pre-oxidation phase and power plateau P3	7386	8520	1143	0.48 to 1.10 ramp 1.10 P3
Main oxidation phase	8520	9960	1440	1.10 to 2.74 ramp
Power plateau P4	9960	13860	3900	2.74 to 3.40 P4
Heat-up phase	13860	19215	5355	3.40 to 7.84 ramp
Power plateau P8	19215	19740	525	7.84 P8
Reactor shutdown	19740			7.84

Due to the lower steam injection rate, about 0.5 g/s in FPT-2 instead of 2 g/s in FPT-0 and FPT-1, the progression of the Zircaloy cladding oxidation front was slower in FPT-2 than in FPT-0 and FPT-1 and the bundle remained steam-starved for an extended period. The first oxidation phase lasted about 43 minutes (from 8700 up to 11300 s with a steam poor period (H_2> 75 vol%) of 18 minutes and a maximum hydrogen concentration of 97 vol%. As in FPT-0 and FPT-1, a less-significant oxidation phase was observed at a later stage of the degradation, correlated with relocation of hot material in the lower part of the degraded test bundle (from 15500 s up to 16600 s). This late oxidation phase lasted about 18 minutes (H_2 > 10 vol%), with a 3-to-4-minute long plateau corresponding to a maximum hydrogen concentration of 17%. A total production of about 60 moles of hydrogen was measured. Assuming that hydrogen was essentially produced by the oxidation of Zr about 80 % of the Zr was oxidised during the bundle degradation.

A faster release of volatile fission products was expected with regard to the FPT-0 bundle behaviour due to their greater concentration at the grain boundary and the more extensively cracked and more porous fuel pellets. But the fractional release histories did not differ greatly from those in FPT-0. A fairly constant release rate was observed for noble gases (xenon, krypton) and volatile fission products (caesium, iodine, and tellurium) during the high temperature phase. The total releases were in line with the commonly used CORSOR-M correlation (MELCOR) based on the NUREG/0772 data base (1981) which was obtained from test data from small fuel samples. However, the actual releases were slightly slower than those calculated, probably linked to the actual metallurgical condition of the fuel rod that may include additional barriers not present in tests on small samples but which slow down the release. The calculations of semi-volatile fission products release showed some discrepancies with measured values. Molybdenum and antimony release were greater than expected, while release was smaller for barium and strontium. The Phebus results show a link between releases of the semi-volatiles and their chemical forms. Those chemical forms themselves are affected by the degradation and oxidation processes.

The elements released may be classified according to their release kinetics:

- Noble gas release started during the first oxidation runaway. The released noble gases exhibited a faster initial accumulation in the containment vessel than volatile fission products;
- Volatile and semi volatile FPs release to the containment occurred at a fairly steady rate between the end of the first oxidation peak and the end of the second oxidation peak (Cs, I, Rb and Te, Mo with some delay) in qualitative agreement

with the fact that bundle degradation was progressive in FPT-2. This was also the case for In;

- Low volatile FPs (Ba, La, Y, Sr,), control rod (Ag), structure and instrumentation material (Zr, Re, W) and fuel were mostly released during the late phase of the transient (late oxidation phase and final heat up).

Data regarding the release of control rod elements are not very reliable and focus only on silver and indium. In addition, and unfortunately, silver and cadmium were not measured by on line gamma spectrometry at Point C and only ^{116}In could be measured.

The transient was ended by the reactor power shutdown and was followed by the cooling of the bundle by steam and then by the containment vessel isolation. The experimental phase then went on with a 4-day long term phase consisting of: an aerosol phase (2 days) dedicated to the analysis of aerosol deposition mechanisms in the containment (gravitational settling and wall deposition), a washing phase (20 min) which aimed at collecting aerosols into the sump, and a chemistry phase (2 days) devoted to the analysis of iodine chemistry under conditions representative of a severe LWR accident.

3. THE CIRCUIT

3.1 Design of the circuit

The circuit of the experimental set-up (Figure 3, Figure 4, Figure 5) is considered in two sections, with a division point corresponding to the main intermediate measuring station at Point C, just prior to the steam generator tube inlet. The first section comprises the conical converging zone above the fuel and control rods of the degrading bundle, the cylindrical vertical line which brings the stream of degradation products clear of the driver core, a right-angled bend into a long horizontal line of the same diameter, and several small-angle bends in three dimensions where the horizontal line enters and transits the experimental caisson, and the measuring station at Point C. These locations and components are also referred to in the literature as follows: the upper plenum (UP), vertical line (VL), horizontal line (HL), and Point C. The entrance to the upper plenum is sometimes referred to as Point B.

In the second section a diameter reduction takes place followed by a right-angled bend, the tall inverted U-tube of the model steam generator, another right-angled bend, this time without change of diameter, the measuring station at Point G, and the stretch of piping maintained at constant temperature called the cold line. This section terminates at Point H, at the connection to the containment vessel of the model.

The iodine vapour specification in the circuit was measured using specific sampling devices, thermal gradient tubes (TGTs) and transition lines (TLs), connecting 700-150 °C aerosol filters. The geometry of these sampling devices is explained in section 0.

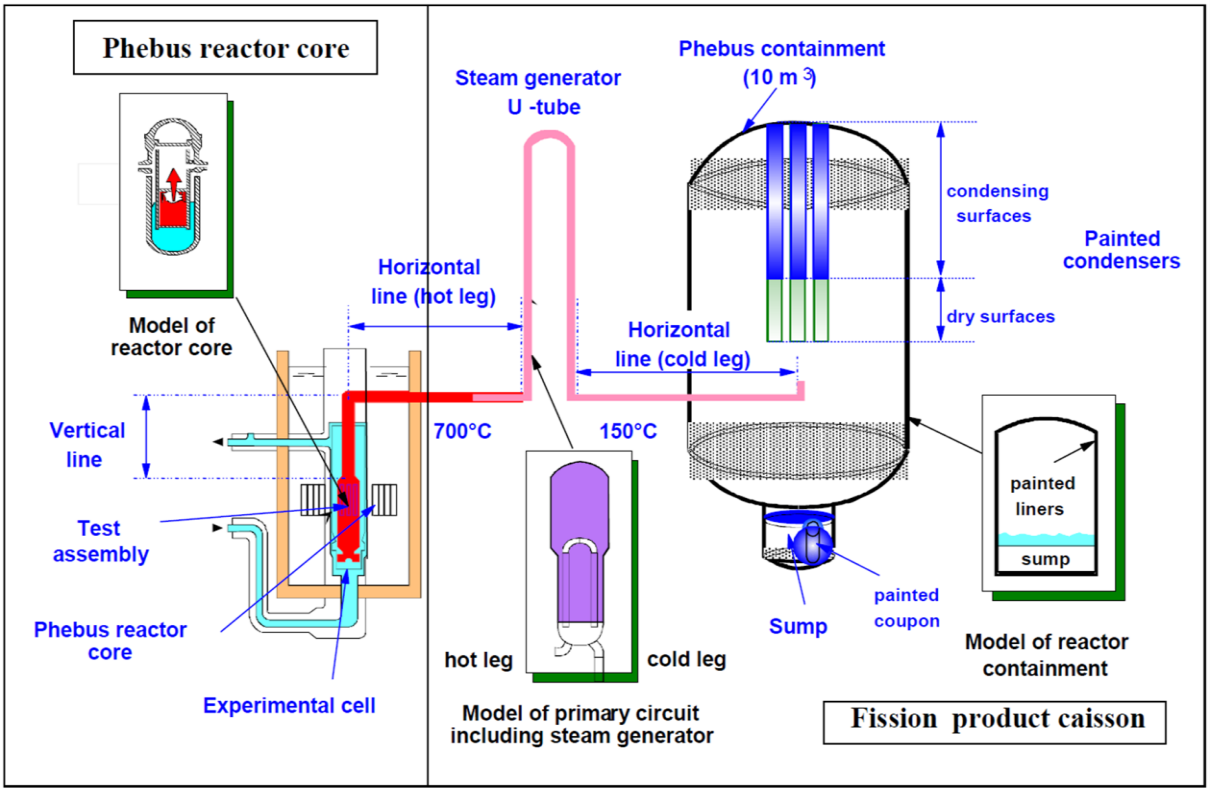

Figure 3. Schematic overview of the FPT-2 modelling.

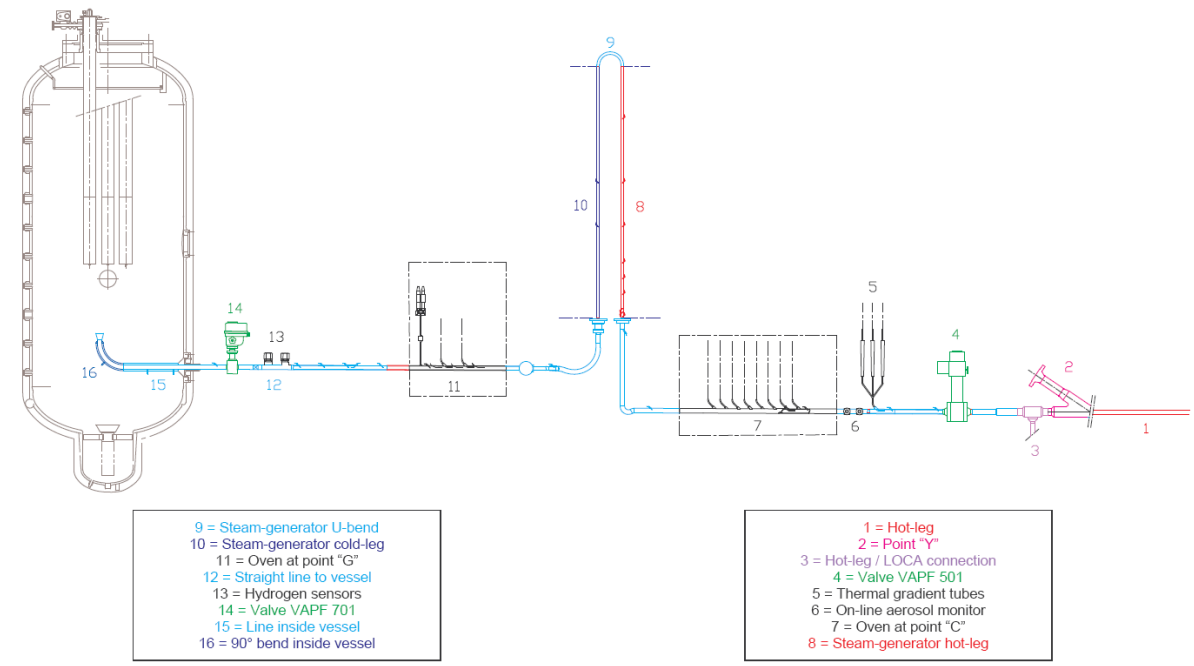

Figure 4. Circuit and instrumentation details for the experiment FPT-2 with the hot and cold line, Point C and Point G, Steam Generator and containment vessel.

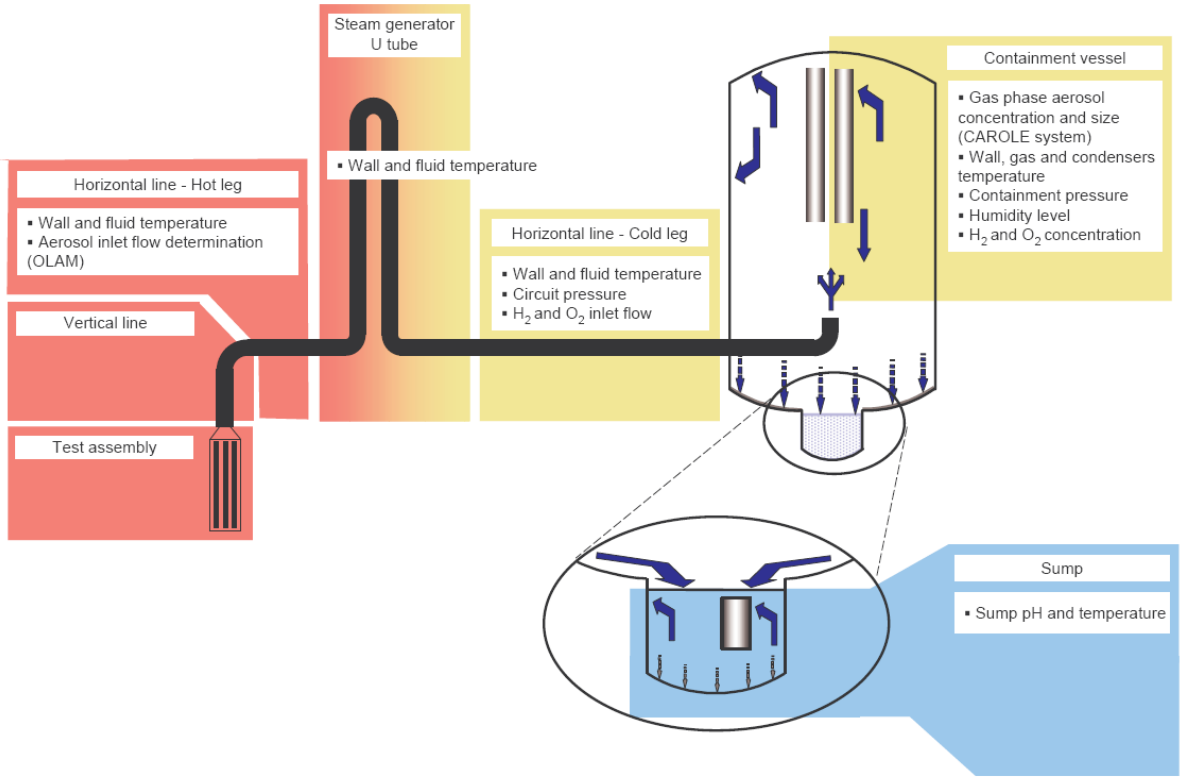

Figure 5. Main conditions overview for the experiment FPT-2.

3.2 Circuit objectives

The hot section of the circuit had two objectives: firstly, to transport the stream of released fission products (FP) and structural and control rod materials (SM) together with carrier gases from the driver core of the Phebus reactor to the experimental caisson, and secondly, to provide time-resolved and composition-dependent data on deposition and speciation at higher temperature (> 700 °C). To the extent possible the upper plenum, vertical line and horizontal line were intended to be "neutral" i.e. offering as little retention as possible, carrying an undistorted selection of elements and species to the terminal monitoring station, Point C. Their inner surface, important for interactions with fission products, was fabricated in Inconel. The main focus of attention was on the cooler portion of the circuit, and specifically the steam generator tube SG, which was designed with a diameter providing velocities and concentrations representative of a PWR cold leg break accident. Gamma scanning was provided to track the deposition of gamma emitters in real time, and the SG tube was to be sectioned for further analysis. The length of the SG tube was for practical reasons considerably shorter than the inverted U-tubes of a typical PWR steam generator, but it was assessed that most of the deposition would take place within the tube length provided, so this departure from perfect representation needs be no inconvenience. Right after the SG there is a monitoring station denoted as Point G, connected to the containment vessel by the cold leg, a length of larger diameter piping with wall temperature maintained at 150 °C, which was again intended to be "neutral" as far as FP deposition was concerned.

3.3 Thermal-hydraulics

Decisive for the evolution of the transport, deposition and eventually resuspension of fission products in the circuit were the thermal hydraulic conditions attained during the transient.

The walls of the steam generator tube were maintained at a temperature of 150°C. When material conveyed in a fluid at 700°C entered into the tube, deposition processes were observed, as discussed in § 0.

Concerning the laminar/turbulent nature of the gas flows, (Bujan et al., 2009) studied conditions in FPT-0 and FPT-1. In FPT-0, the flow remained laminar up to the beginning of the vertical line where changes to the transition regime occurred. After the steam generator inlet the flow reached the turbulent regime, but with a significant drop (by a factor of two) in the Reynolds number (11000 down to 6000) during the oxidation runaway because of consumption of steam and release of hydrogen into the fluid. In FPT-1, the total fluid mass flow rate was smaller by a factor of about 1.4, so the Reynolds number was smaller by such a factor and the flow generally remained laminar up to the steam generator inlet, gradually changing to turbulent (but to a lesser extent than in FPT-0) up the steam generator hot leg. (Clément et al., 2003) assert also that in the FPT-0 circuit cold leg the gas flow was turbulent. No similar detailed studies have been done for FPT-2/FPT-3 with their lower flow rates, but the final report of FPT-2 (Grégoire et al., 2008) states that flow is laminar in the steam generator and in the thermal gradient tubes; a similar statement is made in the FPT-3 final report (Payot et al., 2011) for the steam generator only because there were no thermal gradient tubes in that experiment.

It has been previously argued that the above-the-bundle flows in tests FPT-0 and FPT-1 can be treated as forced laminar convection leading to substantial improvements in calculation of deposits on the pipe wall. It was noticed that the progressive reduction of flow rates, FPT-0 > FPT-1 > FPT-2, indicated above-bundle flow in FPT-2 to be mixed convection, i.e., the strength of natural convection induced by the cold pipe wall was no longer negligible compared to the injected flow. (Garnier, 2009) performed a CFD study to confirm this conclusion and investigate the detailed flow structure in the vertical line for tests FPT-1 and FPT-2. Results of this study show that in the FPT-1 test the flow is

still not developed at a distance of 1m above the bundle with local Nusselt numbers ranging from 5.5 to 7.5 in the narrowing part of the pipe (y < 0.6 m). On the contrary, owing to the weaker flow in the FPT-2 test, buoyancy effects are large enough to initiate a downward counter-current along the wall, confined to the narrowing part of the pipe (Figure 6). Such a counter-current lowers gas temperature gradients at the wall, and thus reduces the Nusselt numbers. A simple diffusive model of radiation showed that radiation decreases gas temperature in the central region of the pipe in the hot scenario, but has almost no influence on the Nusselt numbers. It can be concluded that the CFD and "engineering" approaches are consistent and that re-circulating flow must be taken into account in FPT-2.

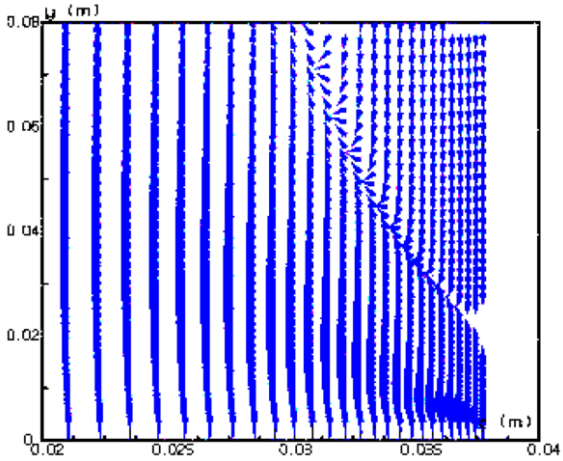

Figure 6. CFD computation of convection effects for the FPT-2 experiment. The buoyancy effects are large enough to initiate a downward counter-current along the wall.

3.4 Circuit mass balance

Releases from the fuel in FPT-2 were similar to FPT-0/FPT-1, although some of the fission products released from the fuel in FPT-2 were deposited at the top of the bundle. This appears due to the smaller flow rate and lower surface temperatures in the upper part of the bundle in FPT-2, and hence larger deposition velocity in relation to carrier gas velocity. For the same temperature difference slower flow will result in higher percentage deposition. But the slower flow in FPT-2 also changes the temperature field in the gas stream so the outcome is not so obvious. Besides in FPT-2 the flow pattern is not the same as in FPT-1 because of recirculation. The low-volatile fission products were released in only small amounts from the bundle but there was, again, evidence of some deposition at the top of the bundle. Based on the quantitative experimental results obtained in the degraded fuel bundle, and the experimental circuit, a circuit mass balance could be built for most nuclides of interest.

The lower releases observed for several elements and the significant deposits found in the circuit line may be related to the lower steam injection rate (0.5 g/s for FPT-2 and FPT-3 compared to a maximum of 2.2 g/s in FPT-1) and to a more progressive degradation of the FPT-2 fuel bundle. In FPT-2 (and in FPT-3), the low steam injection rate also resulted in a significant deposition of volatile fission products (Cs, I, Te and Mo) above the upper grid at the level of the still intact upper fuel rods, whereas in FPT-0 and FPT-1 with a higher steam injection rate deposition rather occurred in the upper plenum and the vertical line. Figure 7 shows the final state of the fuel bundle and isotope distribution for FPT-3.

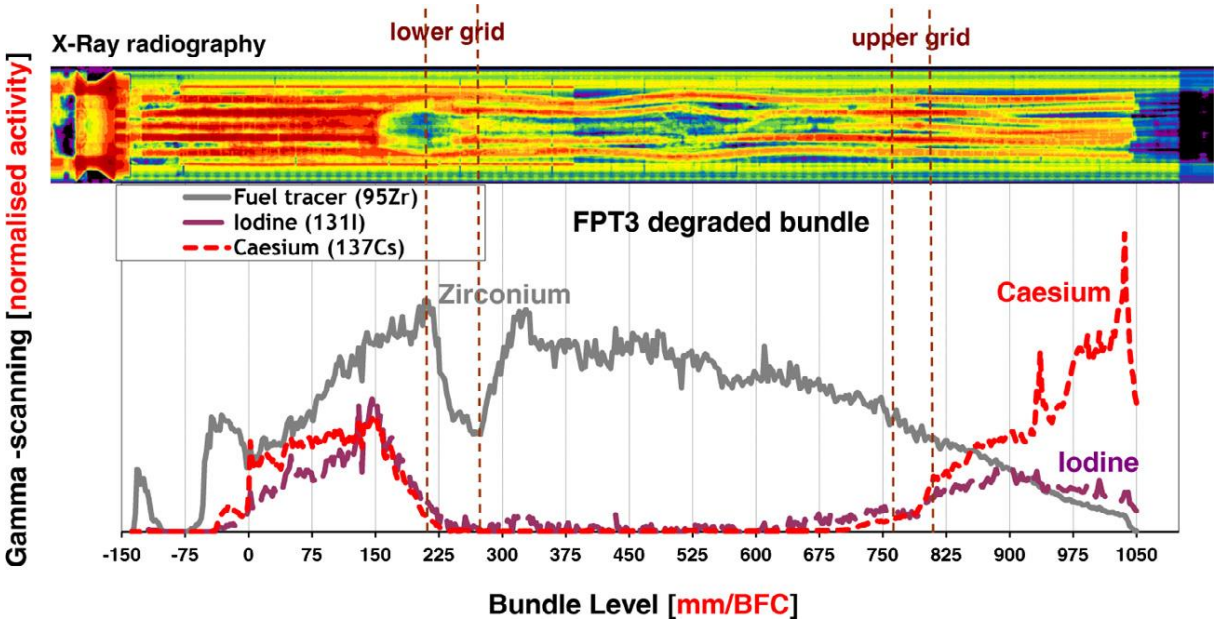

Figure 7: FPT-3 – final state of the fuel bundle and isotope distribution (95Zr, 140Ba/La, 103Ru, 131I, 137Cs) – (Payot et al., 2011

Noble gases Xe and Kr are strongly released from the fuel as observed in the previous tests; they did not interact with circuit surfaces, they reached the containment atmosphere with no circuit retention so that containment inventories corresponded to their released inventories from the bundle, respectively about 79% i.i. and 60% i.i. The volatile FPs (I, Cs, Te, Mo, Rb) are characterized by a fraction in excess of 45-75% of initial bundle inventory released from the fuel bundle. The inventories reaching the containment vessel are however lower (30-60% of initial bundle inventory) since these elements deposited partially on the circuit surfaces. These elements consequently have a low contribution to residual power in a reactor case. However, FPT-2 results indicate that released volatile FPs can deposit in the upper fuel zone; these deposits make the considered FPs available for delayed re-vaporisation as the fuel heats up.

Highly volatile FPs had containment inventories higher than 40% of the initial inventory, including Iodine (Figure 8, 57% i.i.) and Cs (41% i.i.) whose behaviours were very similar to FPT-1. Some elements were intermediately discharged into the containment ranging from 10% to 40% of the initial bundle inventory, such as Rb (32% i.i.), Mo (31% i.i), Te (28% i.i) and Cd (23% i.i). Rb, Te and Cd appear to be significantly less released than in FPT-1 where they were among the highly volatile fission products. Other elements had low release fractions in the containment such as Sn (6.8 % i.i.), In (5.7% i.i.), W (3.7% i.i.), Ag (Figure 10, 1.5% i.i.) and Tc (0.92% i.i.). Among these elements, Sn, Ag and Tc were significantly less released than in FPT-1 where they had containment inventories respectively of 33% i.i., 6.7% i.i. and 21% i.i.. Some elements had negligible discharged fractions into the containment (lower than 0.5% i.i.) such as low volatile fission products Sr (0.43% i.i.), Ba (Figure 9, 0.37% i.i.), Ru (0.083% i.i.), La (0.056% i.i.), fuel material U (0.0028% i.i.), Zr (0.0076% i.i.) coming from the structures and Re (0.33% i.i.) coming from the instrumentation. Among these elements, fuel material and Re were remarkably less discharged than in FPT-1 (by a factor of 43 and 20 respectively); Pu is not even detected in FPT-2. Ba, Ru and Zr were also less discharged than in FPT-1 where they had containment inventories respectively of 0.7% i.i., 0.5% i.i. and 0.015% i.i..

Deposits in the circuit are significant for all species (except for noble gases) both in the hot leg and in the cold leg of the circuit. For instance, a noticeable tellurium deposition process was observed in the hot leg of the circuit with almost 9% of its bundle inventory

remaining deposited there after the degradation phase. On the other hand, it was observed from cold-leg decontamination solutions that about 5% of initial bundle inventory of caesium deposited along the circuit cold leg. Important deposits were also measured for barium and silver. Low-volatile elements remain almost entirely in the fuel zone, where they contribute to the residual power. These include fuel material (U), fission products (Ba, Sr, Ru, Tc, La, Ce) and control rod material (Ag). Semi-volatile elements (Rb and Cd) comprise 8-25% of initial bundle inventory released from the fuel bundle, but due to deposition in the circuit line, the fraction reaching the containment vessel is lower: 5-15% of initial inventory. These include control-rod material (In, Cd), structure material (Sn) and material associated with bundle instrumentation (W, Re).

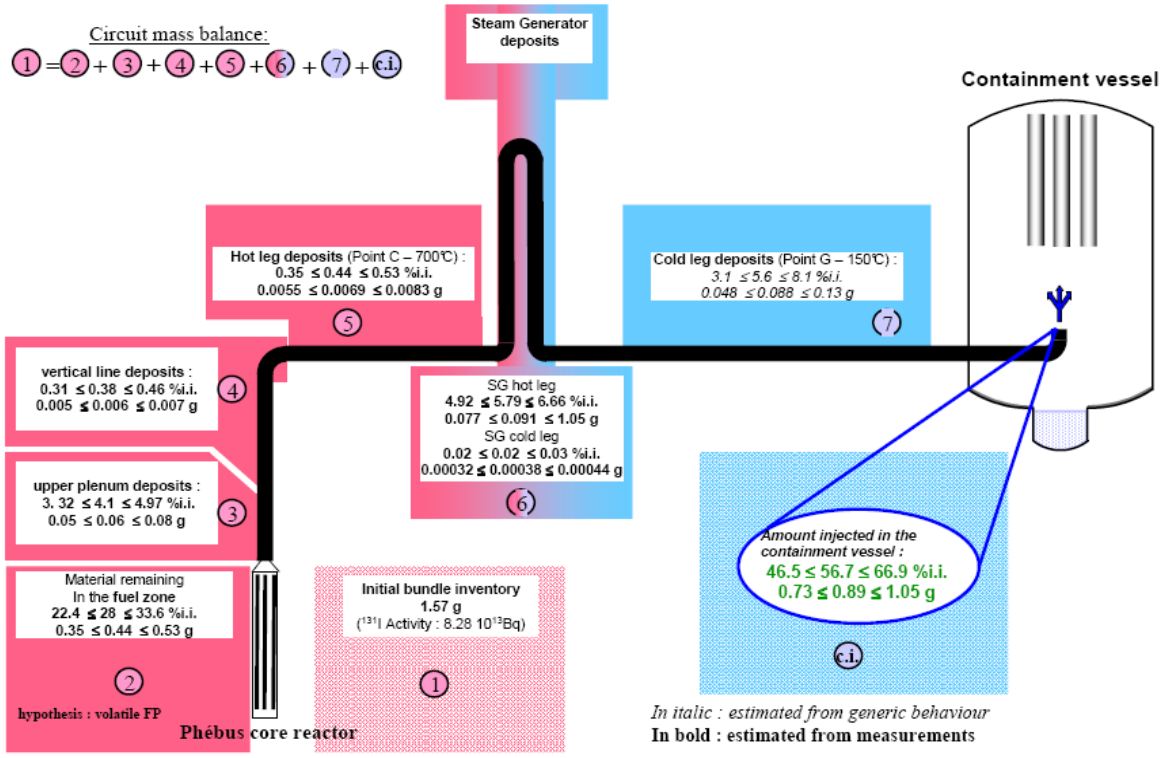

Figure 8. FPT-2 experimental circuit: mass balance of I^{131}.

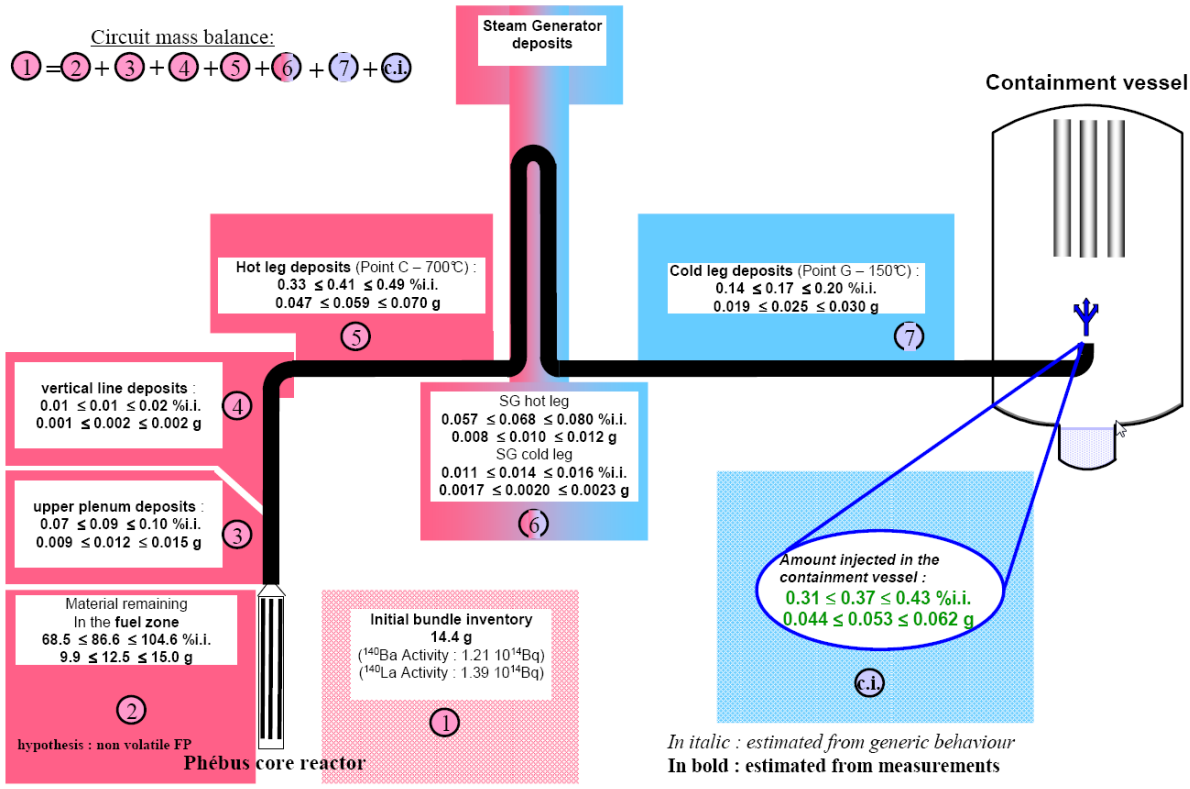

Figure 9. FPT-2 experimental circuit: mass balance of Ba (^{140}Ba / ^{140}La).

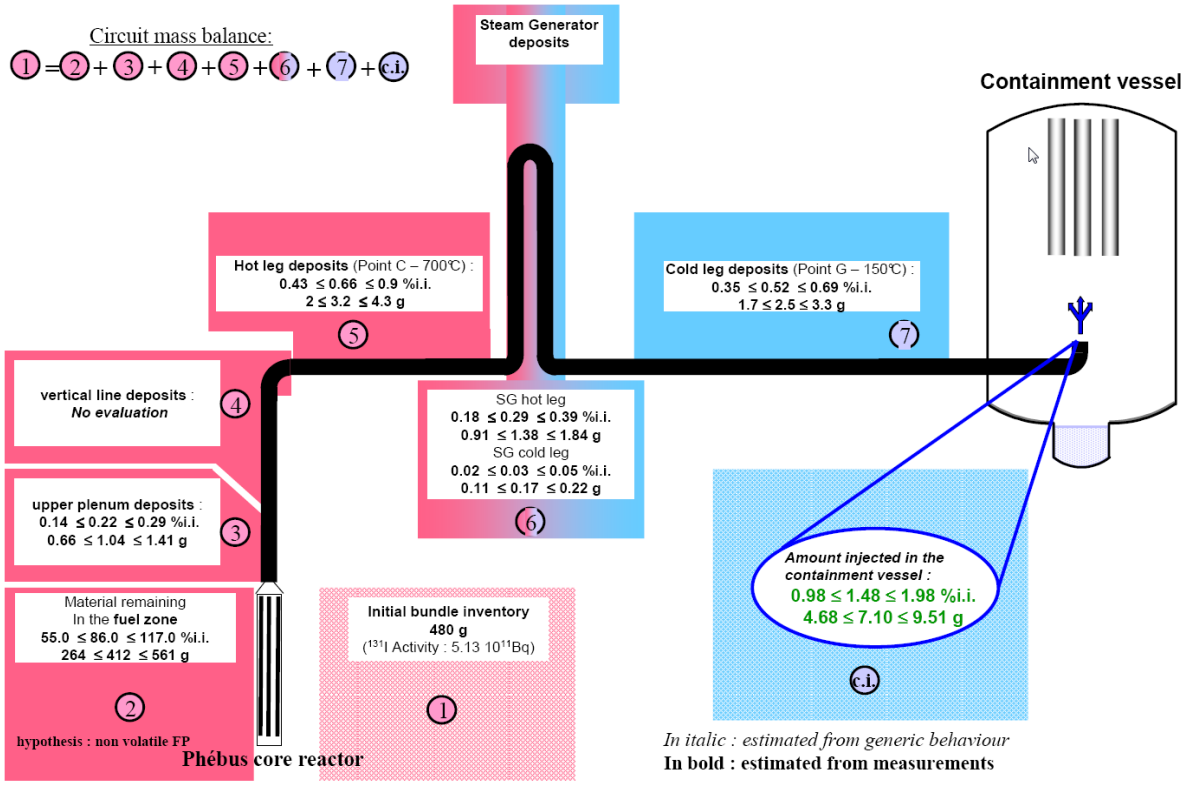

Figure 10. FPT-2 experimental circuit: mass balance of Ag^{110m}.

On the upper plenum, the vertical line, the hot leg and the cold leg, the deposition processes were:

1. Condensation, possibly followed by chemical interactions with the surfaces or with the deposited elements;
2. Aerosol impaction;
3. Thermophoresis;
4. Aerosol settling processes.

In the FPT-2 experiment, the low steam injection rate (0.5 g/s) resulted in more deposition of volatile fission products (Cs, I, Te and Mo) than in the FPT-1 in the upper section of the degraded test bundle (above the upper grid at the level of the remaining upper fuel rods). In the cold leg, experimental deposition data are available only for caesium, barium and silver. Nevertheless, compared to the mass injected into the containment, a generic behaviour could be identified for volatile (Cs) and low volatile material deposits (Ag, Ba) allowing estimating the cold leg deposits for the unmeasured elements. In the hot leg, material deposition could be determined experimentally for a larger set of elements (Cs, I, Te, Ba, Ag); for the unmeasured elements, the deposits in the hot leg were estimated using generic behaviour for volatile and low volatile material as in the cold leg.

The walls of the steam generator tube were maintained at a temperature of 150°C. When material conveyed in a fluid at 700°C entered into the tube, two deposition processes were observed:

1. Species in a vapour form (as some fraction of I and Cs) condensed on the tube walls (mainly at the entrance) or on the aerosols;
2. Species in an aerosol form (for instance Te and Ba) deposited on the tube walls under the effect of the temperature gradient between the fluid and the walls (thermophoresis).

In the inlet section of the steam generator (SG), all detected elements show a simple exponential decay deposition profile. Deposits in the raising part of the steam generator represented about 84% and 94% of the total mass deposited in the steam generator respectively for low volatile and volatile elements. The computation results with ATHLET-CD indicate a general agreement in the simulation of the fission product transport and chemical speciation, as shown for AgI in Figure 11. In comparison to test results the retention of species in the circuit is generally overestimated. With respect to large measurement uncertainty the source term into the containment is predicted fairly well (K. Trambauer et al., 2008).

The volatile-FP inventory at the level of rod-remnants in the upper part of the degraded bundle is typically doubled in FPT-2 compared to the original inventory, while it is nearly entirely depleted in FPT-1. This behaviour appears consistent with both the more extensive degradation of upper rods and the higher fluid flow in FPT-1 as compared to FPT-2.

Deposits in the upper plenum and the vertical line were less significant in FPT-2 than in FPT-0 and FPT-1, apart from the notable exception of Te, which undergoes some large deposition in both the upper plenum and the hot-leg horizontal line, and for iodine whose global deposit in the upper plenum and the vertical line was similar to that of FPT-1. Deposits were significant for all species (except noble gases) both in the hot leg and in the cold leg of the circuit.

The important deposits measured both in the cold leg of the circuit differs with those obtained for both previous tests. On the contrary, measured steam-generator deposits are significantly lower in FPT-2 than in FPT-0 and FPT-1 (less than 5% versus ~10-20% for volatile FPs). It was nevertheless observed that the fluid temperature at the steam generator inlet dropped down to 400-450°C through most of the release phase of the

FPT-2 test, instead of the expected 700°C. Although this behaviour remains unexplained, it could account for some additional inventory being deposited upstream the steam generator inlet where the temperature gradient was located (cold traps). According to (Tim Haste et al., 2013) an additional explanation is that the circuit was partly blocked by boric acid deposits.

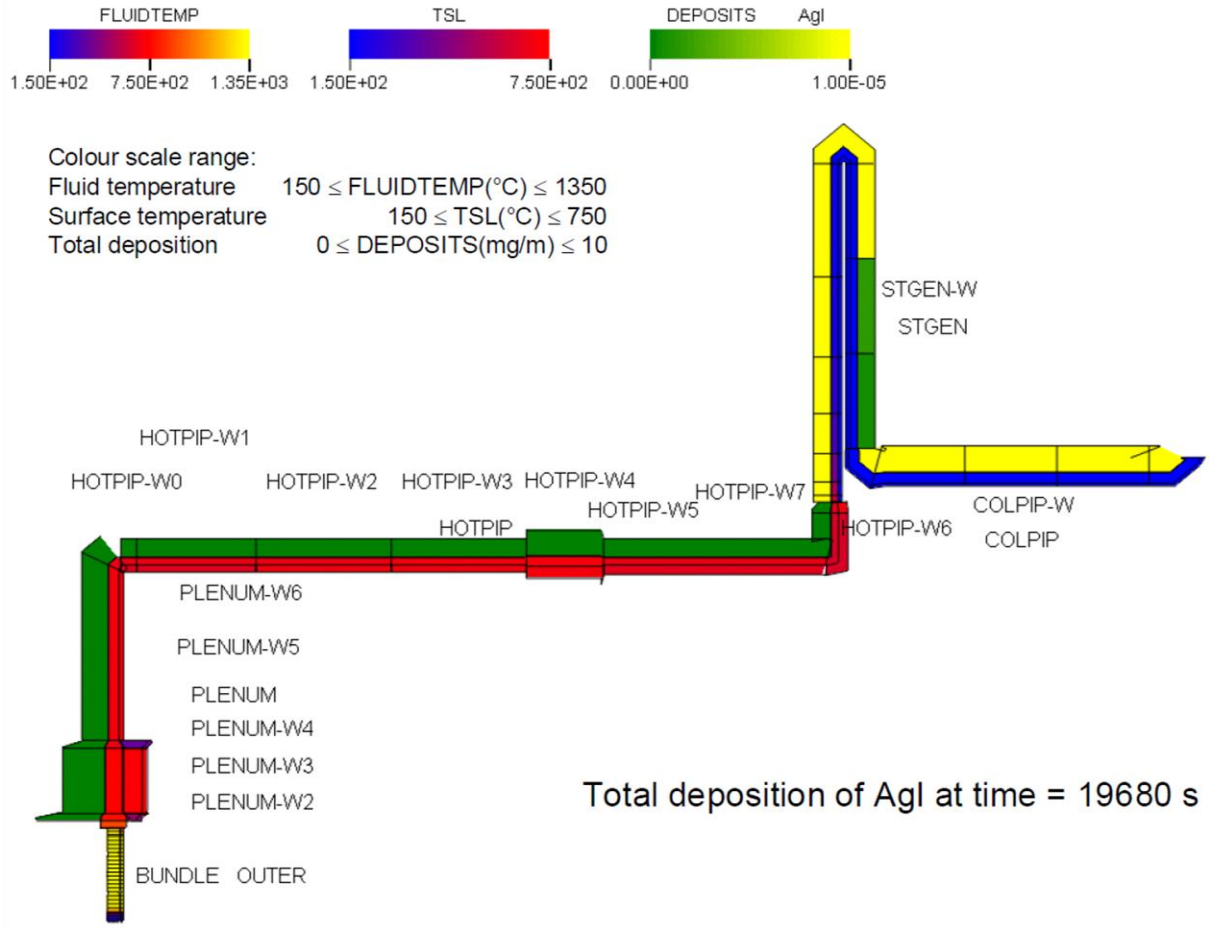

Figure 11. Calculation with ATHLET-CD: deposition before the SG plays a minor role. This is similar for other species.

In Figure 12–Figure 16 the deposition profiles of some elements in the steam generator are shown. The light blue lines represent the online analysis: the activity measurements in the "CECILE hot cell". For some parts of the SG (segments 2, 3, and 7) exist values which are based on PTA data; they are depicted by black lines with a dot. The values calculated from gamma spectrometric recordings are given as element specific deposition and as deposition of composites with iodine and caesium. The total deposition is represented by red lines.

In Figure 12 the iodine profile along the steam generator length at the end of the experiment is shown. At the inlet section of the SG the online analysis provides a value of 0.3 g/m. The corresponding calculation result is 0.67 g/m which is about twice as much. The calculated profile decreases slower along the length than the measured one. In the first part of the SG the deposits consist mainly of CsI and BaIOH. At a length of ca. 1 m AgI gains importance. In this area condensation at pipe wall plays a dominant role. The calculation shows that behind this point mostly aerosol deposition takes place, particularly after ca. 4.4 m due to "bend impaction" in the U bend of the SG; the bend impaction was not observed in the experiment.

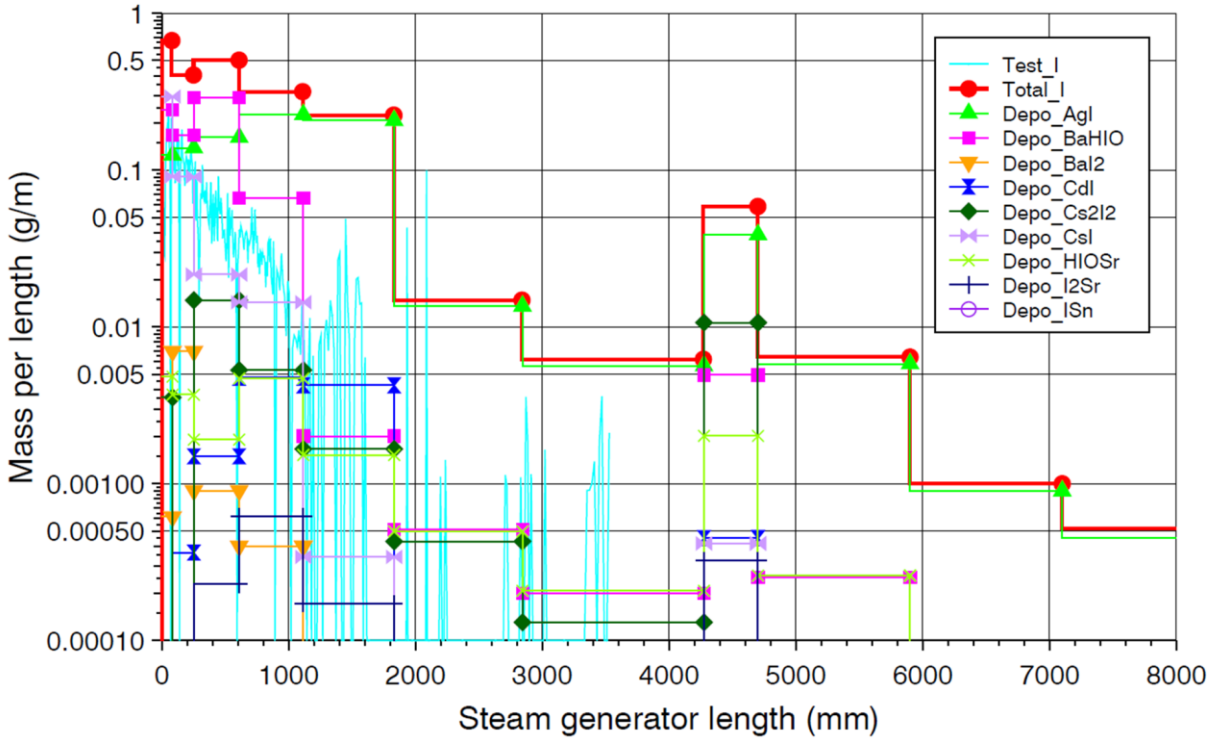

Figure 12. Deposition of Iodine in steam generator at end of experiment (t = 20000 s). The light blue line represents the online analysis; the red line represents total values calculated from gamma spectrometric recordings.

Figure 13 depicts the caesium profile over the SG length at the end of the experiment is shown. At the inlet section of the SG the online analysis provides a value of 2 g/m. The calculation result is 10.6 g/m which is about five times as much. The gradient of the calculated profile is in agreement with the measured one. Remarkably there is a certain agreement of the PTA data and the calculated profile at 2 m of SG length. At the inlet section the retention is mostly based on $CsBO_2$ and $CsReO_4$ condensates. After 1 m of length the deposition of CsOH aerosols predominates. The calculation shows enhanced aerosol deposition due to "bend impaction" in the U bend after ca. 4.4 m; this was not observed in the experiment.

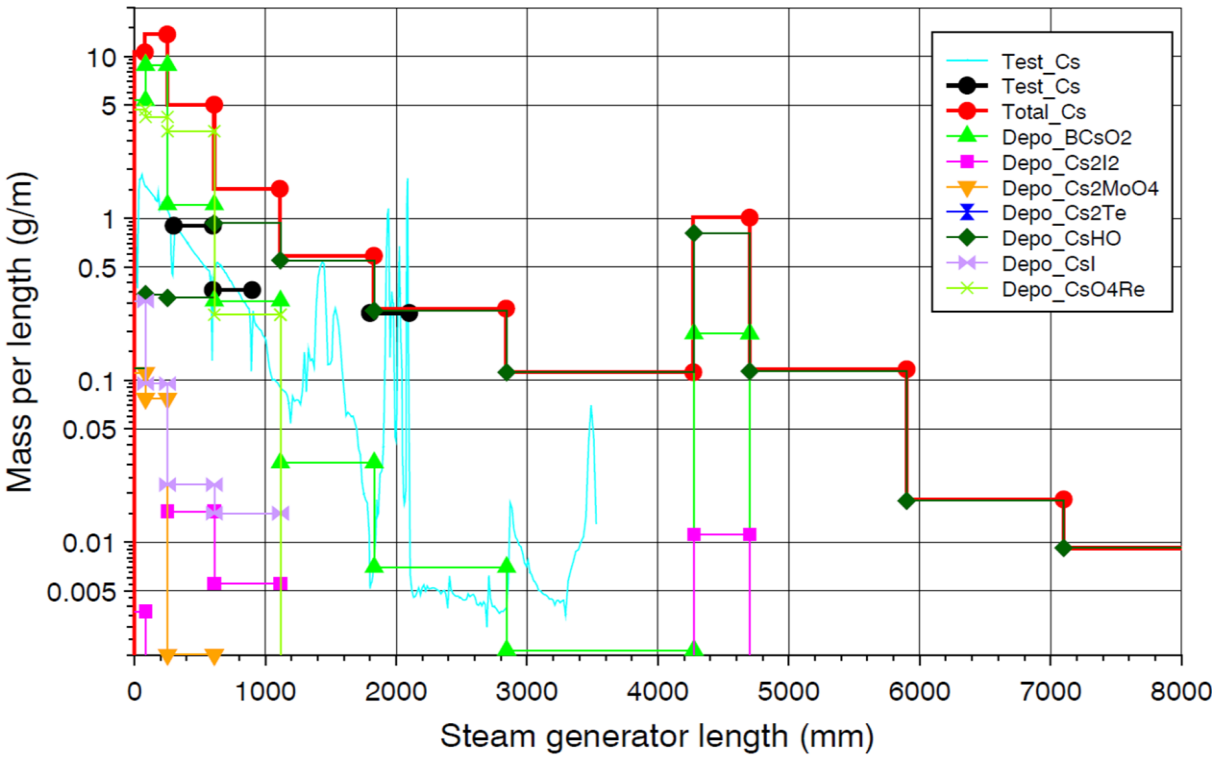

Figure 13. Deposition of caesium in steam generator at end of experiment (t = 20000 s). The light blue line represents the online analysis; the black line is based on PTA data; the red line represents total values calculated from gamma spectrometric recordings.

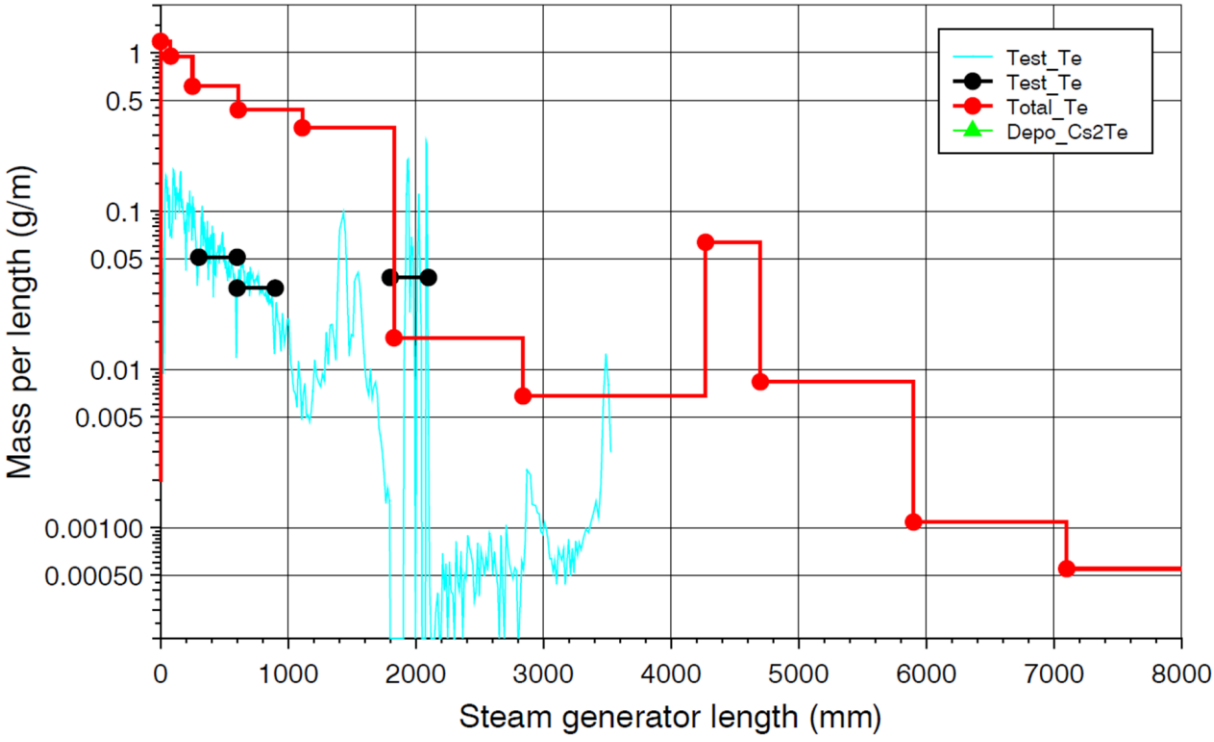

Figure 14. Deposition of Tellurium in steam generator at end of experiment (t=20000 s). The light blue line represents the online analysis; the black line is based on PTA data; the red line represents total values calculated from gamma spectrometric recordings.

Figure 14 shows the deposition of tellurium in the steam generator. The online analysis yields a value of 0.2 g/m at the inlet section. The corresponding calculated value is 1.2 g/m. The calculated profile decreases with a smaller gradient than the measured one. However, at 2 m the PTA data and calculation are in agreement. The calculation shows enhanced aerosol deposition due to "bend impaction" in the U bend after ca. 4.4 m; this was not observed in the experiment. Besides Cs_2Te with 0.1 mg/m condensate in the first volume, there are no significant compounds of tellurium with iodine or caesium.

In Figure 15 the deposition of molybdenum is shown. Hereby, no online analysis data exists, only values based on PTA. The most important compound with caesium is Cs_2MoO_4 which is represented by 35 mg of aerosol deposition in the first tree volumes. The calculation shows enhanced aerosol deposition due to "bend impaction" in the U bend after ca. 4.4 m; this was not observed in the experiment.

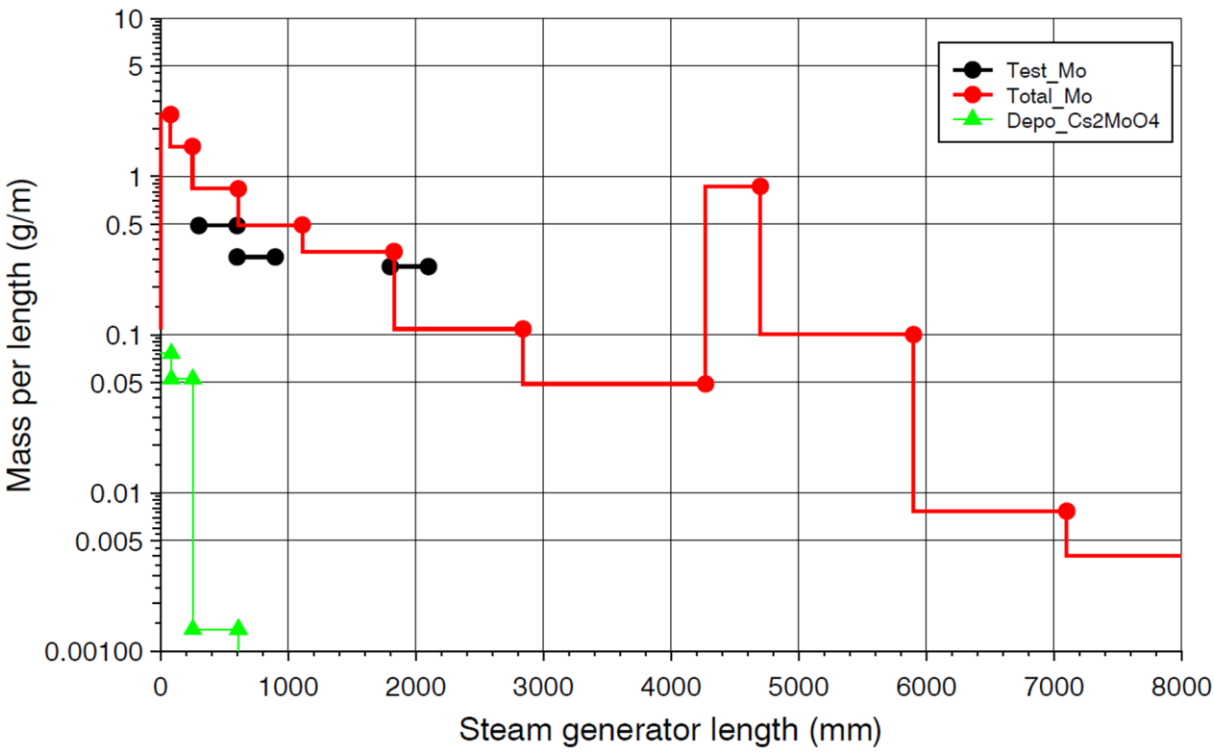

Figure 15. Deposition of Molybdenum in SG at end of experiment (t = 20000 s). The black line is based on PTA data; the red line represents total values calculated from gamma spectrometric recordings.

Figure 16 depicts the silver profile in the SG. The online analysis delivers an initial value of 2 g/m. The calculation yields 20 g/m which is 10 times larger. The gradients of the observed and calculated profiles are similar. The creation of the silver profile is mostly based on aerosol deposition. The contribution of silver iodide (AgI) is about one or two magnitudes smaller than the total silver deposition. At 2 m the calculation results match the PTA data. The calculation shows enhanced aerosol deposition due to "bend impaction" in the U bend after ca. 4.4 m; this was not observed in the experiment.

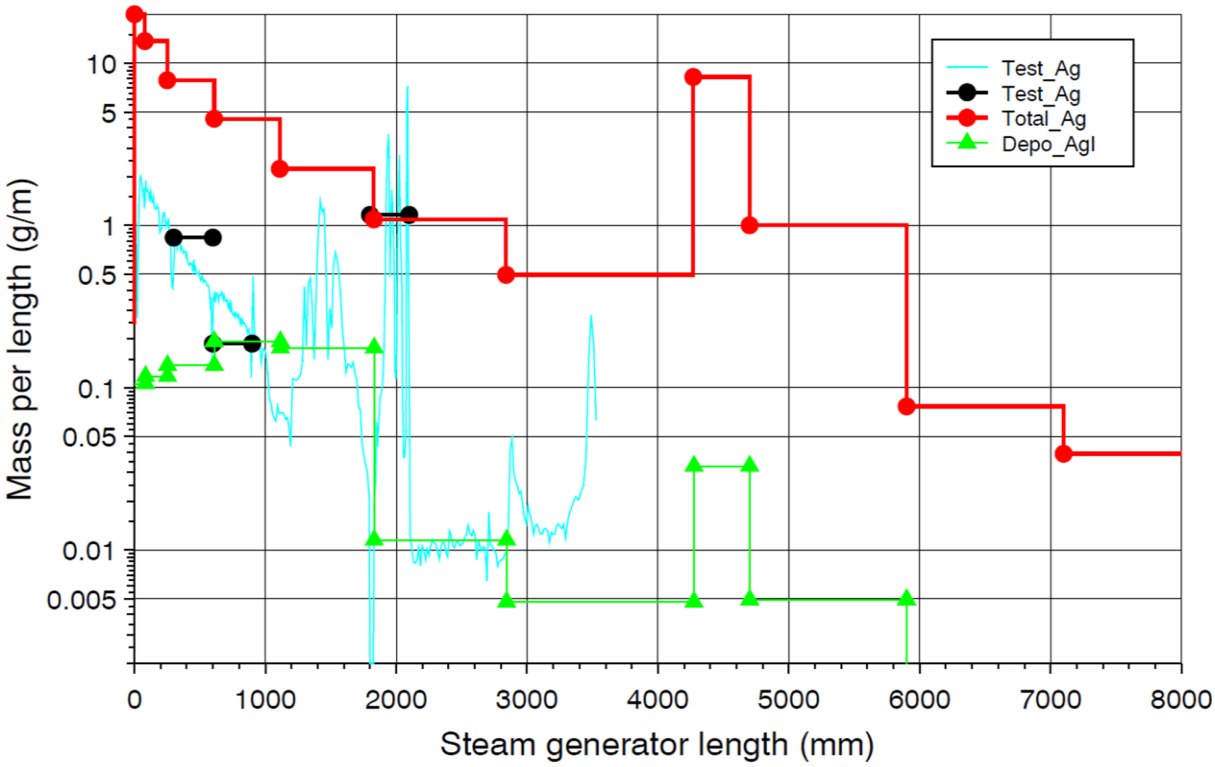

Figure 16. Deposition of Silver in steam generator at end of experiment (t = 20000 s). The light blue line represents the online analysis; the black line is based on PTA data; the red line represents total values calculated from gamma spectrometric recordings.

3.5 Point C and thermal gradient tube (TGT)

The sequential samplings of the experimental circuit (hot leg and cold leg aerosol filters and iodine specific instrumentation) were operated during the key phases of the transient (first clad rupture, main and late oxidation phases) so as to obtain a kinetic of material transport in the circuit.

Evidence concerning the speciation at Point C is available in FPT-2 from the thermal gradient tubes (Figure 17), to which a portion of the flow was sampled for each tube (TGT-700, TGT-701, TGT-702) at several instants during the transient. The analysed hot-leg samplings consist of the following components:

- 3 sequential thermal gradient tubes (TGPF) (shown in Fig.17B), with regulated/measured temperature linear profile between 700 °C and 150 °C, each equipped with an outlet aerosol filter (FIPF) maintained at 150;
- the inner tube of the main hot line maintained at 700 °C;
- 1 sequential sampling line maintained at 700 °C;
- 8 sequential aerosol filters(FIPF) maintained at 700 °C;

- 4 sequential aerosol/zeolite filters (FZPF) maintained at 150 °C, primarily dedicated to gaseous iodine analysis (zeolite stage);
- 4 sequential transition lines (shown in Fig.17A) ensuring the unregulated/unmeasured thermal transition between the FIPF (700 °C) and the FZPF (150 °C) filters.

All these components were counted by spectrometry in the CECILE hot cell after the test. Some were sent to external laboratories for chemical analysis (PTA). Counting operations were performed on sampling lines for the first time in the FPT-2 test, with the primary objective of achieving mass-balance closure along those sampling lines which were dedicated to iodine analysis. According to (Gregoire et al., 2008) the wall temperature decreased along the tube from 700 °C to 150 °C, and the deposition pattern was observed by gamma scanning and Post Test Analysis PTA.

TGPF700, was triggered at the SIC control rod rupture instant (22% of hydrogen content). The measured isotopes were ^{131}I and ^{137}Cs. Iodine and caesium are mainly transported under vapour form at that moment. The iodine profile reveals two condensation peaks (Figure 18) near the tube entrance with an improbable candidate (I_2Sr) for the first one (630°C), and no candidate for the second one (550°C). The caesium profile is flat all along the tube, except at the very entrance of the TGT where the only candidates are Cs_2Te, Cs_2MoO_4 or CsO (Gregoire et al., 2008).

TGPF701 was triggered during the starvation phase (100% of hydrogen content). The measured isotopes are ^{131}I, ^{134}Cs, ^{136}Cs and ^{137}Cs. Iodine and caesium are present under vapour and aerosol forms. Considering the very irregular profiles, no detailed analysis could be performed on this TGT (Gregoire et al., 2008).

TGPF702 (Fig.17) was triggered during the heat up phase (10% of hydrogen content). The measured isotopes are ^{131}I, ^{134}Cs, ^{136}Cs, ^{137}Cs, ^{129}Te, ^{140}La and ^{140}Ba. Tellurium and Lanthanum behave as aerosols, with an increasing activity profile towards the exit of the tube, which is in accordance with an increasing thermophoretic force along the tube. Iodine and caesium are present under vapour and aerosol forms. Three iodine species have been identified as potential candidates for the first condensation peak (580°C): CsI, Cs_2I_2 and IRb. Concerning caesium, five possible candidates for the first peak (590°C) are CsI, Cs_2I_2, CsCl, Cs_2O_4Re and Cs_2O. Presence of CsI or Cs_2I_2 seems to be very probable during this sampling (Gregoire et al., 2008).

The experimental results highlighted quite different deposition behaviour at the different sampling times which may be indicative of a variation of the chemical species transported through the hot leg during the fuel degradation process.

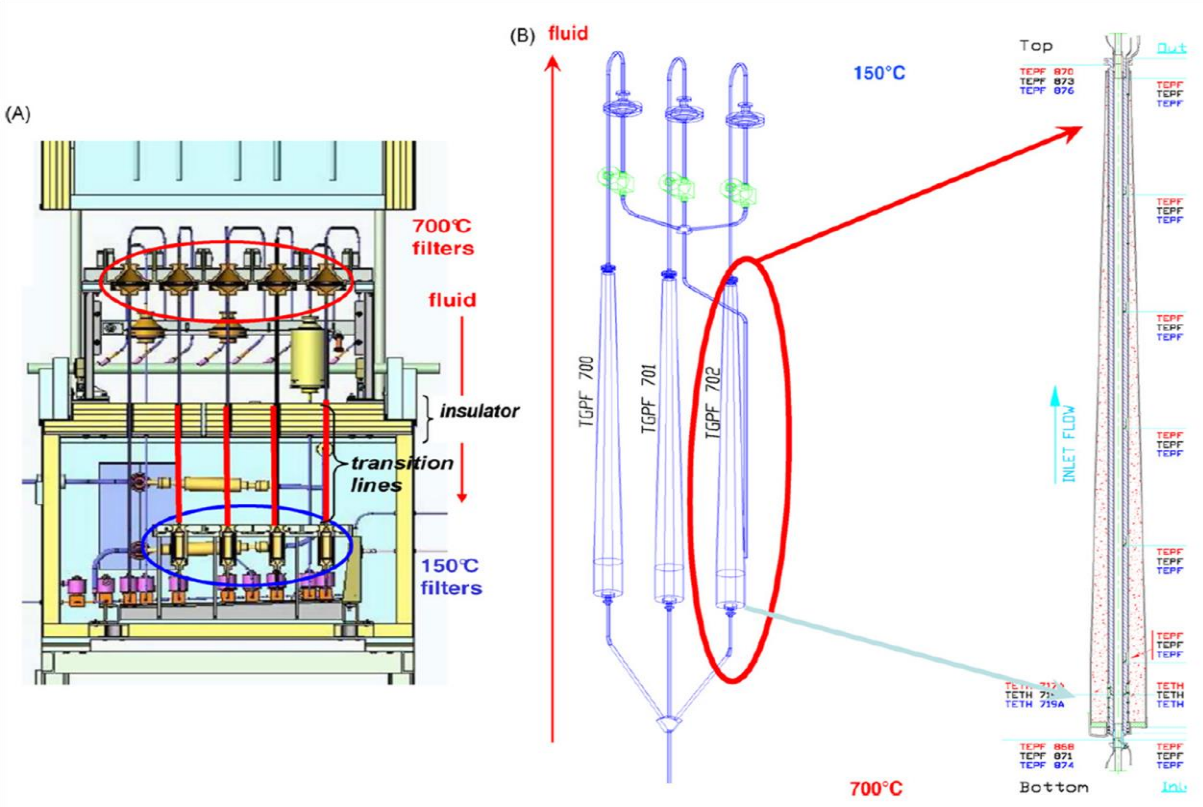

Figure 17. Experimental means to measure vapour specification at Point C: (A) transition lines (TLs) and (B) thermal gradient tubes (TGTs).

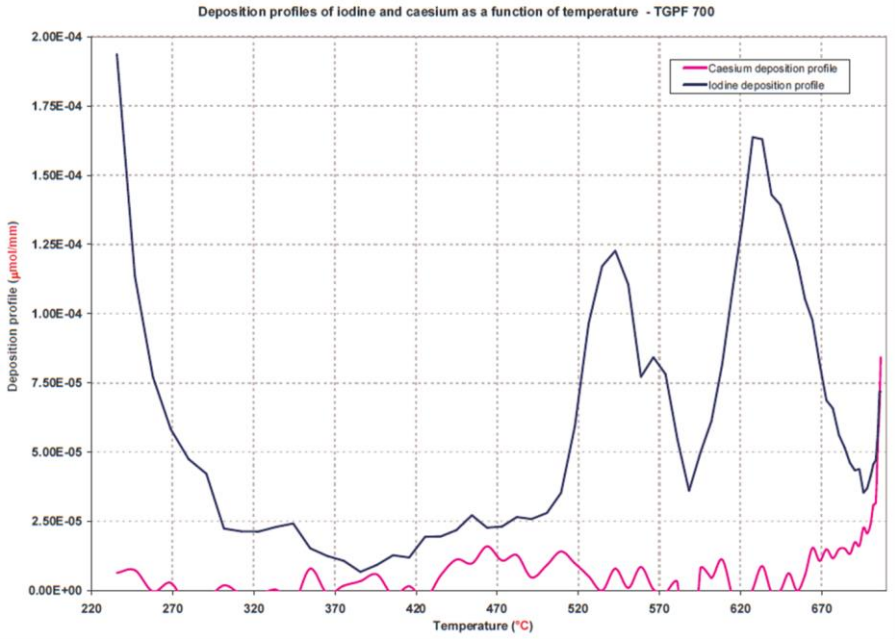

Figure 18. Deposition of iodine and caesium as a function of temperature at the SIC control rod rupture; the two condensation peaks for iodine are very pronounced.

3.6 Behaviour of vapours and gases in the circuit

By definition a gas has one defined state at room temperature whereas vapour is a substance that is in gaseous and liquid equilibrium at room temperature, at a given pressure. A species is volatile if it is gaseous at the highest temperatures in the circuit e.g. in the upper plenum. It is gaseous if it is a gas at the lowest temperatures in the circuit e.g. in the cold leg. It is implicit that volatile species will condense or change chemically into something else somewhere along the circuit.

Some specific zones of FP retention were observed in the circuit. As in previous Phebus tests, two major zones of retention were measured that correspond to sections where the temperatures sharply dropped: the upper plenum, in which the maximum temperature drop was ~1400°C, and the steam generator inlet, in which temperatures cooled from 700°C to 150°C.

In addition, a significant deposition was also measured for some elements in the horizontal line (Ba, Mo, and Te) and in the cold leg of the circuit (Ag, Ba, and Cs). This deposition in the horizontal line and the cold part of the circuit suggests that gravitational settling could be a significant deposition mechanism for some elements. This phenomenon, which was not observed in FPT-1, could be explained by the lower steam flow rate injected in the circuit throughout the FPT-2 test. The deposition pattern of FPs was less dependent on their volatility as compared to previous tests (FPT-0/FPT-1). For example, in the upper plenum, the vertical line, and the steam generator riser, no significant differences were found for the retention of some elements such as Cs, I, Mo despite their marked difference in volatility. This can be partly explained by their unexpected partial retention in zones upstream of the upper plenum (namely, in the upper part of the fuel rods) and upstream of the steam generator riser where a cold temperature spot was identified (***"cold traps"***). Tellurium, as already observed in the previous Phebus FP tests, behaves in a specific manner, characterized by a higher deposited fraction than caesium and iodine (§ 3.6.1).

Particular attention is given to the iodine radiochemistry because of several stable very volatile gaseous and vaporous species present in the circuit and in the containment vessel and of their radiological impact. With regard to the iodine source term issue, measurements performed on-line and off-line on the sequential samplings located both in the circuit hot leg and in the circuit cold leg provide data for the description of the iodine behaviour released, transported and deposited in the various zones of the experimental circuit.

Results of the four sampling channels located in the hot leg of the circuit (Table 2) reveal that iodine was essentially transported in a vapour form, fraction ranged between 56% and 89% of the total iodine sampled in each channel, the remainder being aerosols (Table 2). The gaseous iodine fraction was measured to be lower than 0.3% of total measured iodine whatever the sampling. ^{131}I-emitter deposition profiles were measured in the transition lines (Figure 17A). It's considered that in these lines only ^{131}I-emitter vapour species condensed during the sampling. All iodine deposition profiles indicate that there is one or several iodide vapour species transiting through the circuit hot leg. Figure 19 displays the profile of iodine deposits together with caesium deposits (these two nuclides were the only isotopes measured on this line) for the Point C transition lines sampled between the two oxidation phases (Gregoire, 2009). Results show one caesium condensation peak overlapping one of two iodine peaks. This may be explained by the presence of CsI or Cs_2I_2. The caesium iodide species seem to be only one of the three main metallic iodide vapours observed at sampling time i.e. in oxidizing conditions. During this period, it seems that at least two other iodine species can be found in a metallic vapour not linked to caesium. The three other transition lines only gave one iodine condensation peak without any other nuclide being detected. From the condensation peaks that were measured (line sampled during the first oxidation phase is displayed in Figure 19) one can conclude that CsI appears in some conditions, but cannot be the only species present. Finally, iodine deposits in the circuit hot leg were

relatively low (evaluated at ~0.44% from on-line γ-measurements of Point C (station 2/3) located along the hot leg) at the end of the test. In general the deposits in the hot leg were low as previously discussed in chapter 0.

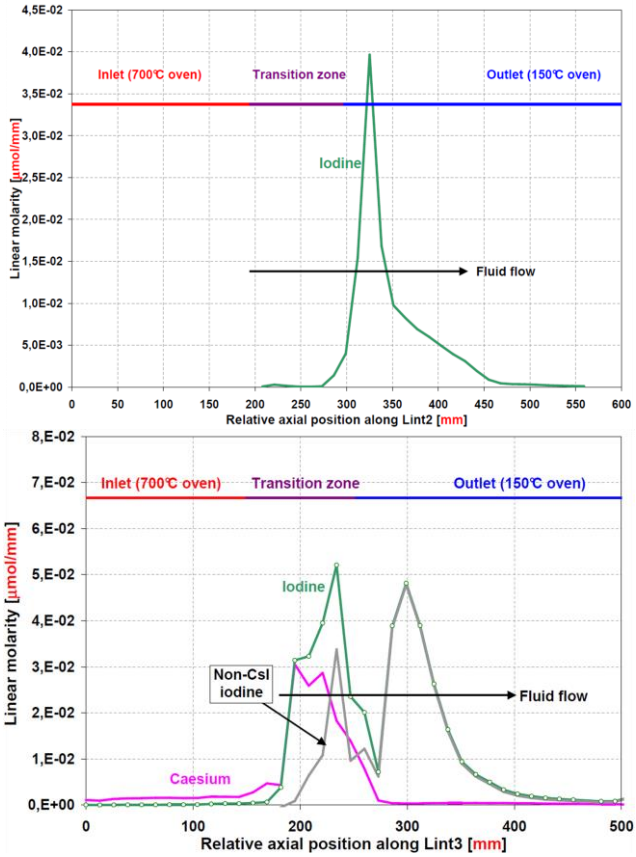

Figure 19. Deposition profile of iodine and caesium along the Point C transition lines of the hot leg (time lapse between first oxidation phase and second oxidation phase, at ca. 10000 s).

Table 2. Iodine repartition [wt%] measured at Point C. Relative uncertainty is estimated to be about 16%.

Time Phase	9126-9311 s oxidation runaway	9955-10144 s first oxidation	13180-13309 s P4 plateau	18676-18806 s late heat-up
Aerosol Vapour Gas	30.2 69.7 0.1	21.0 78.7 0.3	11.0 88.9 0.1	44.2 55.7 0.0
Total	100	100	100	100

The ASTEC/SOPHAEROS code predicted well the iodine deposition along the transition line wall and the Thermal Gradient Tubes (TGT) provided that the iodine species reacted with Cs species. The measured iodine peak at the outlet of the transition line can be identified as CdI_2. If iodine species reacted with other species and not predominantly

with Cs, the predicted behaviour would have been different from the measured one (Gregoire, 2009).

3.6.1 Caesium and Tellurium behaviour

After the core shutdown, about 45% of the deposited Cs in the hot part of the circuit (upper plenum and vertical line) was re-volatilized and then deposited mainly in the steam generator tube. Moreover, Te hot leg deposits (^{131}Te, and ^{132}Te, half-lives 25 minutes and 76.3 hours) decayed into volatile forms of iodine (^{131}I and ^{132}I) that were also conveyed to the steam generator tube. The post-transient revaporisation of Cs is concentration-controlled as in FPT-1. It obviously took place not only after the transient but during the course of the transient, "smoothing" the supply of Cs to downstream parts of the circuit.

Concerning retention of Te, (Girault et al., 2010) find a uniform retention throughout the circuit (ranging from 10 to 20% of the released fraction). This is explained by the significant calculated chemisorption of Te mainly as SnTe in the high-temperature regions of the circuit. A potential explanation for the difference in Te behavior could be that because of incomplete thermodynamic data and/or uncertainties concerning Sn release kinetics, which are strongly linked to the cladding oxidation state, the dominant species for Te is not SnTe. Based on the literature, it is thought that a wide range of Cs_x-Te_y species could be formed that are not yet taken into account in the calculations. These species were however indirectly observed in some of the analytical Vercors HT test loops when the gas-phase composition was reducing. It is interesting to note that if these species were dominant, the chemisorption would be a minor phenomenon and the retention profile of Te more similar to that of caesium.

3.6.2 Iodine deposited in the steam generator

Iodine was found to exist in a vapour form at 700 °C, representing about 85% of the iodine conveyed through the circuit hot leg (with less than 0.1 % of gaseous iodine). The existence of a significant vapour fraction was emphasized for both Cs and I. Materials that were transported in vapour form in the circuit hot leg condensed even before the steam generator inlet.

Iodine deposits measured in the steam generator sections were evaluated at ca. 4.3%. The post-test γ-scanning of first six steam generator sections showed that the iodine deposition profile is similar to that of caesium suggesting that, like caesium, iodine is deposited by aerosol thermophoresis process in this zone. Unfortunately, iodine deposits in the upstream part of the steam generator (between the beginning of cooling at 150°C and the first measured section i.e. 130 mm) were not available, but thanks to the aerosol deposition profile obtained on the six measured sections, the iodine aerosol deposits in the upstream part were evaluated at 1.5%. Nevertheless, when one compares the iodine fraction released from the fuel bundle (~72%) with the fraction conveyed through the circuit cold leg (~56%), it can be assumed that some iodine vapour fraction was deposited in the upstream part of the steam generator.

About 10% of the depositions are expected at the SG inlet bend which was not monitored.

3.6.3 Iodine behaviour in the cold leg of the circuit

In the cold leg of the circuit, most of the iodine was transported in an aerosol form towards the containment vessel (~56.7%). Each sampling only indicated a negligible fraction of gaseous iodine throughout the transient phase, which does not exclude the possibility that gaseous iodine fractions may have been temporarily much higher. The

mass flow rate curve of iodine obtained from on-line γ-measurements is presented in green in Figure 20 which is consistent with the performed samplings (pink points). Additionally, these results prove that most of the iodine species that are not condensed in the hot leg had time to condense on the aerosols before reaching the containment and (or) also to deposit on the steam-generator inner surface. Besides, as reported in Figure 20 the three TGT devices triggered in the hot leg and the on-line γ-measurements viewing the circuit hot leg (point C; which characterize both iodine transport and deposits) are higher than data obtained in the cold leg in agreement with deposits between both locations. It is interesting to observe a peak of γ-signal at point C during the second part of the first oxidation phase. This peak could be attributed either to iodine deposited in the hot leg surface which then re-volatilized or to some more important iodine amount transiting over this period.

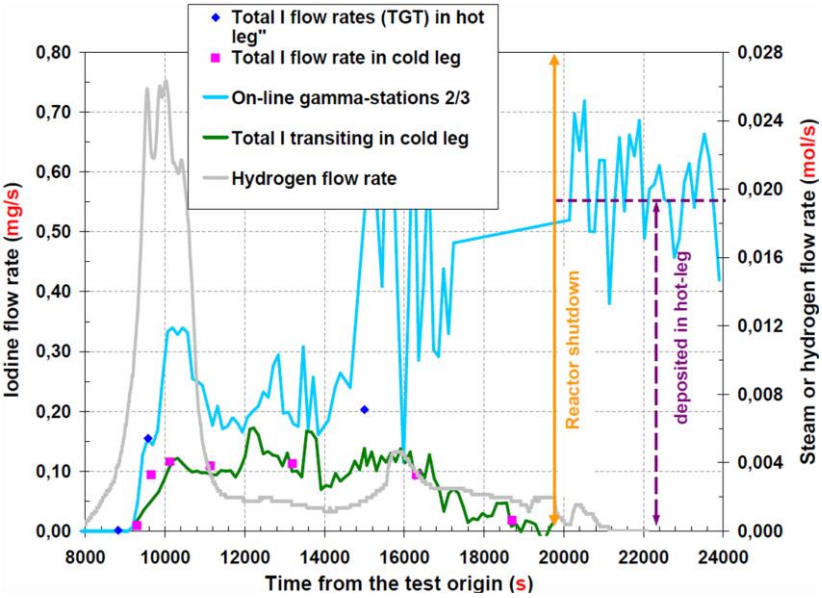

Figure 20. Iodine and on-line γ-spectrometry measurements in the hot leg and the cold leg (stations 2/3 ←→ Point C). see § 0 for details.

All the above is a presentation of experimental findings. Please refer forward to § 0 to read about the calculation results.

3.7 Aerosol characterization

Condensed material was transported in the cold leg as mixed amorphous aerosols (Figure 21): the structure of the aerosol particles was predominantly spherical, with an AMMD (average mass median diameter) of about 2 μm (Gregoire et al., 2009). These very fine particles may have been agglomerated to form larger particles. Larger particles reaching 2 μm are constituted either of Cs/Re, Cs/Ag, Ag-rich, Re, Ag. The aerosol mass composition was dependent on the bundle degradation events. The composition of the aerosols transiting through the cold leg was dominated by fission products (Cs, Mo), control rod materials (Ag, Cd, In) and cladding material (Sn) compared to FPT-1 where structure materials were dominant. The total material mass transiting through the circuit, determined from elements measured in the circuit either by γ-spectrometry or by chemical analyses, amounted to about 60 g in the circuit hot leg (vapour and condensed material) and about 42 g in the circuit cold leg. Based on speciation data gained from the previous FPT-0 and FPT-1 tests, oxidation of material could have increased the total

aerosol masses to about 50 g in the circuit cold leg. The aerosol mass composition was dependent on three bundle degradation events:

1. Large control rod material (almost exclusively Cd) contributions during the first main oxidation phase;
2. Large volatile FP (Cs, Mo) and significant control rod (Ag) and structure material (Sn) contributions during the phase leading to the melt initiation and propagation;
3. Dominant Ag and significant volatile FPs (Cs, Mo), control rod (Cd) and structure material (Sn) contributions during the late oxidation and the final heat-up. There is an interesting dominance of the last phase as regards aerosol mass. And in contrast to the previous Phebus experiments Mo and Cs play major roles.

The aerosol mass concentration was at its highest level during the late oxidation phase: about 12% of the aerosol mass transited through the circuit during the main oxidation phase, 17% during the phase leading to the melt initiation and progression in the fuel bundle and 71% during the second oxidation phase.

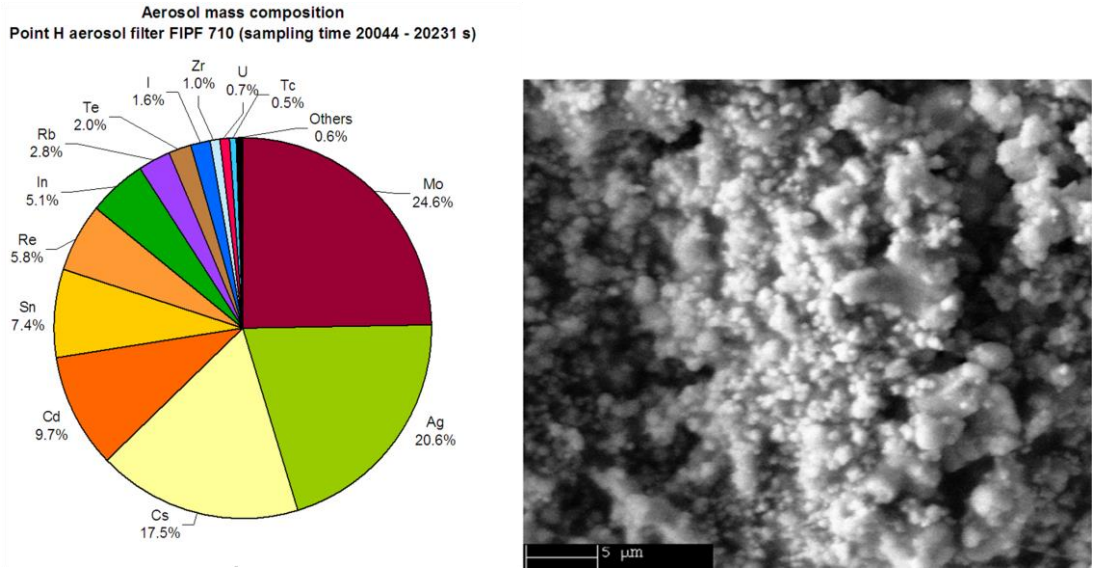

Figure 21. Aerosol morphology and mass composition after core shut-down.

3.8 Aerosol deposition and resuspension

In the inlet section of the steam generator (SG), all detected elements showed a simple exponential decay deposition profile. Deposits in the raising part of the steam generator represented about 84% and 94% of the total mass deposited in the steam generator respectively for low volatile and volatile elements. The deposition before the steam generator and in the cold leg is of minor importance as shown in § 0. In comparison to test results the retention of species in the circuit is generally overestimated by calculations. Considering the large measurement uncertainty the source term into the containment is predicted fairly well (Trambauer et al., 2008).

Deposits e.g. within the reactor vessel head (vessel head ???) and in the hot piping immediately adjacent to the reactor vessel can act as heat sources through self-heating and may subsequently evaporate or be resuspended, thus providing a late source term. Some of this work is documented in CACIC presentations and in publications derived from them (see Appendix 3).

3.9 Insights on calculations

The analysis of the three FPT-2 Thermal Gradient Tubes (TGTs), dedicated to provide information on the chemical speciation and volatility of fission products in the hot leg, was performed with the ASTEC/SOPHAEROS code version 2.1 integrated into ASTEC V1 using a whole-circuit calculations with 42 volumes (20 volumes for the circuit, with a more refined nodalization above the bundle and in the raising part of the steam generator, and 22 volumes for the 1 meter long TGT tube, Dienstbier 2006). These ASTEC/SOPHAEROS analyses were performed with a chemical database including more than 800 species. The input source term for the calculations included 21 elements which are the main released elements during the test and/or elements that have a high affinity for I and Cs. These are respectively H, O, B, for the carrier fluid elements and Ag, In, Cd, Re, Zr, Sn, W, U for control rod, structural and fuel elements and I, Cs, Te, Ba, La, Rb, Ru, Mo, Sb, Sr for the fission products.

Calculated species depositions were broadly similar: HIOSr, CsI (Cs_2I_2) and CdI_2 in decreasing volatility order are the dominant iodine species whereas Cs was mainly transported under Cs_2MoO_4 and $CsReO_4$ species. Further progress in the fission product speciation firstly requires a more accurate determination of mass flow rates of FPs such as Mo, Cd that greatly impact the iodine and caesium chemistry and a general check and improvement of the thermochemical database (as for the Cs-Te systems) used in the calculations.

(Dienstbier, 2006) invoked speciation to explain the differences between the experimental data and the calculated results concerning the retention of the different species and the aerosol and vapour source term to the containment. Much improvement in the simulation of Te was reached by depressing SnTe sorbtion on Inconel while some improvement was found in iodine species deposition by suppressing the H_2MoO_4 vapour - modification of the saturation pressure in material database (MDB) - without changing the Cd source. As a consequence the volatile iodine ”HI” decreased in the hot leg due to the I reaction with Cs and Rb. Accordingly a significant surplus of Cs (Rb) source is calculated over the Mo source. ASTEC/SOPHAEROS is mainly based on equilibrium thermodynamics except for iodine reactions. According to this ASTEC/SOPHAEROS equilibrium chemistry model, the predicted dominant species molar ratio Mo/Cs(Rb) has the largest influence on the fraction of Iodine that can reach the containment in the gaseous or highly volatile form (Girault at al., 2009) when iodine species to the containment are CsI and its dimer. When this surplus is partly reduced due to an increase in the Mo source, some fraction of iodine is available to react also with other FPs/SMs (like Ba, Ag, Cd). Comparing to FPT-1 results the main retention phenomena remains thermophoresis but gravitational settling is responsible for more than 10% of the retention; gravitational settling was small in the case of the FPT-1 experiment. The best estimate calculation slightly improved the prediction for the iodine species, but the Te species retention was significantly under predicted. The test results and thermal gradient tube experiments strongly suggested that caesium was vaporized from the core as the mixed oxide species caesium molybdate, Cs_2MoO_4 (gas). This suggestion has been adopted into the MELCOR computer code with generally good results and greatly increased the predicted releases of radioactive molybdenum so that these predicted releases are in good accord with both the extent and timing of molybdenum release observed in the tests. Because caesium molybdate is less volatile than caesium hydroxide, more caesium deposition is predicted to occur in the reactor coolant system (Powers et al., 2013). ASTEC has not yet been implemented to take into account of depositions along the bundle. The complex chemical interaction throughout the bundle and circuit of molybdenum, caesium and iodine is thus found to influence the nature of the iodine source to the containment to a considerable degree, a fact which may be considered a “discovery” of the Phebus experiments. Modelling of the chemistry can be achieved using kinetics or using static chemistry with a judicious choice of typical species, based on findings from Phebus and other experiments.

The combined ATHLET-CD and ASTEC/SOPHAEROS calculations (K. Trambauer et al., 2002, 2005, 2006, 2008) for the analysis of the thermal behaviour and the deposition in the circuit during the FPT-2 experiment showed a good agreement with the thermal hydraulic part of the experiment, but still have unexplained differences after the steam starvation period. The temperature profile and timing of hydrogen release were well reproduced. The total hydrogen generation was underestimated by 10 % compared to the corrected experimental data. The fission product and aerosol release from the bundle predicted reasonably close to the experimental data. The deposition was overestimated (Cs and I as well as of the absorber materials) and there is no reasonable simulation for the significant aerosol deposition after the steam starvation period. ATHLET found that most of the aerosol deposition was in the steam generator due to the bend impaction. Nevertheless the calculation reproduces fairly well the aerosol deposition in the cold line. The flow conditions in FPT-2 (laminar flow) and FPT-1 (turbulent flow) are different and therefore the temperature differences between the bulk and the wall in case of FPT-1 was smaller helping to interpret the differences between the measured data in the FPT-1 and FPT-2 experiments. The thermal behaviour in the steam generator after the steam-starved period (Figure 22) could not be sufficiently explained. It was assumed at that time that the observation was a result of changed surface properties of the thermocouples and of the steam generator which in consequence changed the heat transfer by radiation (K. Trambauer et al., 2008).

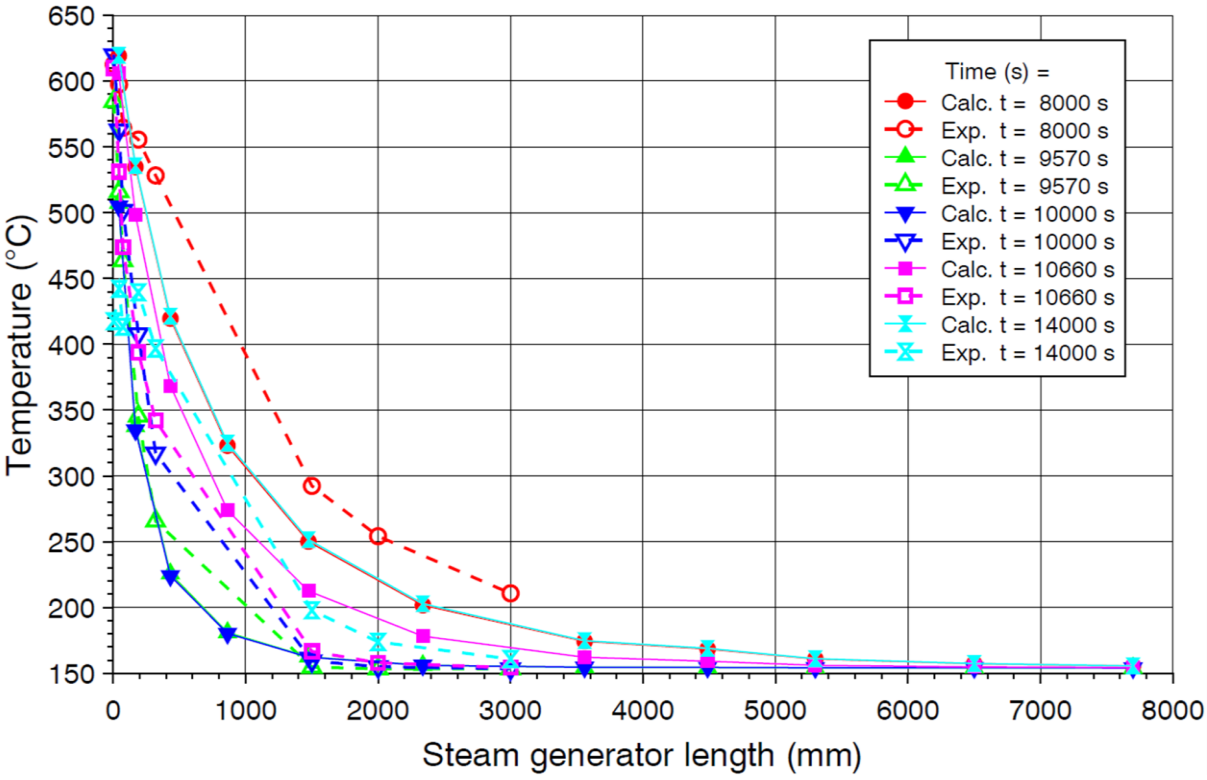

Figure 22. Fluid temperature profile in the steam generator. The values calculated from gamma spectrometric recordings after and before the oxidation phase (between 8000 seconds and 14000 seconds calculation time) are identical as expected; the experimental observed temperature profile after the oxidation phase (Exp. t = 14000) obviously remain on a different level than before (Exp. t = 8000 s).

A MAAP 4.04 (de Pascale, 2004) version that includes models developed by EDF taking into account that it is a fast running code with highly empirical models based on the conservative calculation approach shows a good behaviour overall. For most models

default values of MAAP were used in this simulation. A shortcoming comes from the built-in nodalization of the MAAP code version that affects, for instance, the large deposition in the steam generator (SG) because of the single node nodalization model in the SG. Through models developed by EDF the MAAP 4.04 calculation simulated the entire FPT-2 test reasonably well.

Fission product behaviour during transport in the circuit was analysed with the SOPHAEROS module of the integral code ASTEC, version 1.3, coupling vapour and aerosol phenomena (Girault et al., 2010). The trends in the volatile retention profile show two major zones of retention, namely, the high-temperature zone (the upper plenum at the fuel bundle outlet) and the steam generator riser. The third major zone of retention (the cold leg) was not so strongly evidenced in the calculations (Figure 23).

Very high temperature gradient, increased mass transfer in the upper plenum inlet, and geometric irregularities (bundle outflow and conical flow contraction) are possible causes of an enhancement of the heat and mass transfer in the upper plenum region and thus of FP deposition. In this region, vapour condensation on the wall is the major retention phenomenon for the most volatile elements (such as I and Cs) due to the high thermal gradients between gas and wall. Aerosol deposition that can also, to a lesser extent, occur in this region may be enhanced both by impaction due to the irregular above-bundle geometry and because the laminar flow entering this region probably does not have a thermally and hydraulically parabolic profile. This implies that the mass transfer at the wall can be considerably higher than in a developed flow.

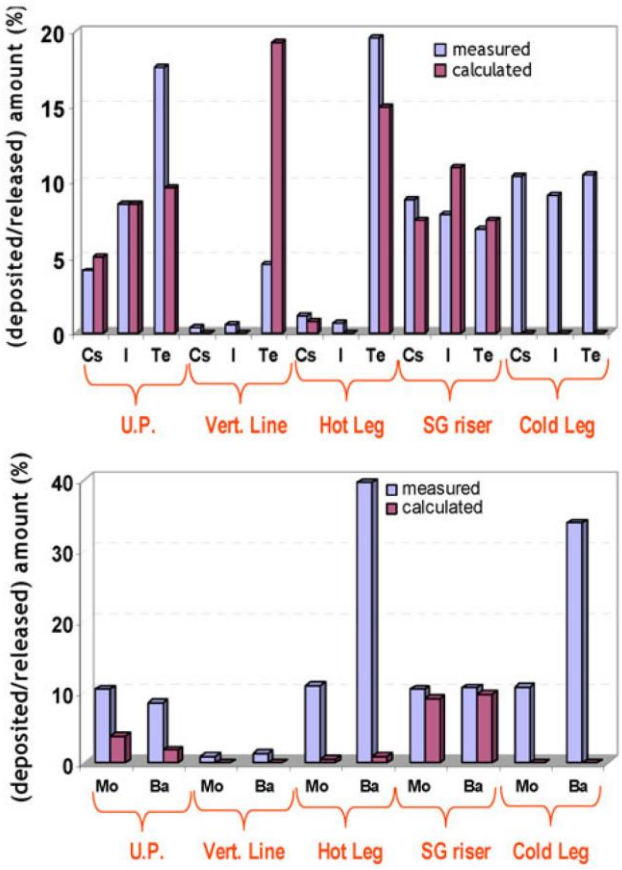

Figure 23: Retention profile of some FPs along the FPT-2 circuit—comparison between total values calculated from gamma spectrometric recordings (light colour) and measured (dark colour) fractions relative to release: cold-leg deposit measurements include descending part of steam generator. (a) Volatiles: I, Cs, and Te and (b) semi volatiles and low volatiles: Mo and Ba. (Girault et al., 2010).

The underestimated retention of Ba and Mo could be explained by an enhanced deposition due to the counter-current that is calculated to form in a very limited part of the upper plenum region during the steam-rich periods of the test (Figure 24a). But further calculations taking into account this counter-current are necessary to check if this effect is sufficient to explain the underestimation of some of the less volatile elements (such as Ba) in this region. The finding that Ba is only weakly released from fuel (less than 1.2% of its initial bundle inventory) is consistent with the previous Phebus FP tests (FPT-0 and FPT-1), but contrasts with observations made in the separate-effects experiments HI/VI and HEVA/VERCORS (Ducros et al., 2001) and the Phebus FPT-4 test. Tc is a low volatile element with less than 2% of its initial inventory released from the fuel over the entire transient.

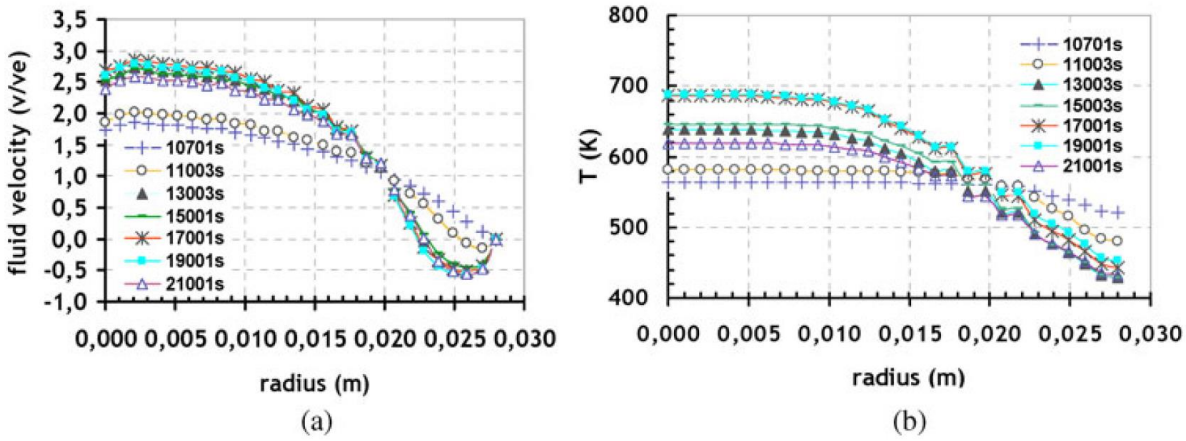

Figure 24: Changes in total values calculated from gamma spectrometric recordings in the radial profiles of (a) fluid velocity and (b) temperature in the Phebus upper plenum (v/ve: non-dimensional value, relative to mean fluid velocity at upper plenum inlet). (Girault et al., 2010).

The calculated behaviour of Mo and Ba both conflict with the behaviour observed during the test (Figure 23). Indeed, the molybdenum was found to be equally deposited in high-temperature gradient zones (i.e., in the upper plenum and rising part of the steam generator), in the horizontal part (in the hot leg), and in the cold part of the circuit. This deposition in the horizontal line and the cold part of the circuit (though not restricted to the horizontal cold leg) suggests that gravitational settling could be a significant deposition mechanism for some species in aerosol form. In the case of barium, this mechanism even becomes predominant. This phenomenon, which was not observed in FPT-1, could be explained by the lower steam flow rate injected in the circuit throughout the FPT-2 test. In turn, this suggests that different types of aerosol population could be formed in the circuit, which is not consistent with the ASTEC/SOPHAEROS models. The only direct evidence from circuit aerosol samples suggests that the aerosol particles are multicomponent and not segregated.

As shown below by the red curve Figure 25 from sampling on the hot leg, silver is mainly released during the heat up oxidising phase of the test at a time where probably the main part of the control rod is relocated in a lower zone. Only a very small part is released during the starvation phase, which corresponds to the degradation-relocation phase of the control rod. Indium (Figure 26) is rather released during the starvation phase whereas, during the heat up phase, some part could be deposited as shown by the increase in gamma spectrometry compared to the rather stable signal from sampling.

The global fractions of both silver and indium are low compared to the FPT-0 and FPT-1 tests; about two per cent for silver and seven per cent for indium. Among the possible effects which could be responsible for the specific behaviour of the control rod there is

the earlier degradation associated to very quick relocation in the cold zone. Also due to strong interactions, a significant amount of zirconium or perhaps also iron, nickel or chromium might have decreased the vapour pressure (of indium notably). Then, very probably, the degradation of the rod and candling of molten alloy occurred during the steam starvation phase, which again might have decreased the indium vapour pressure.

The gas phase composition has a strong effect, notably on Indium vapour pressure. Indeed oxidising composition enhances indium vaporization due to oxide and hydroxide productions. Nevertheless, this effect stops in the oxidising case for which the low volatile oxide In_2O_3 is created. For silver, the effect of the gas phase is probably less important because simple monatomic silver is the main contributor of total vapour pressure of silver in all conditions. In addition, it must be pointed out that silver and indium have a non-ideal behaviour, notably indium. In addition the effect of Zr (probably also iron and chromium) is important for additional decrease of the vapour pressures.

This qualitative explanation for the observed release signatures of Ag and In is plausible but there is not a corresponding quantitative model. This problem could be referred to the Bundle Interpretation Circle.

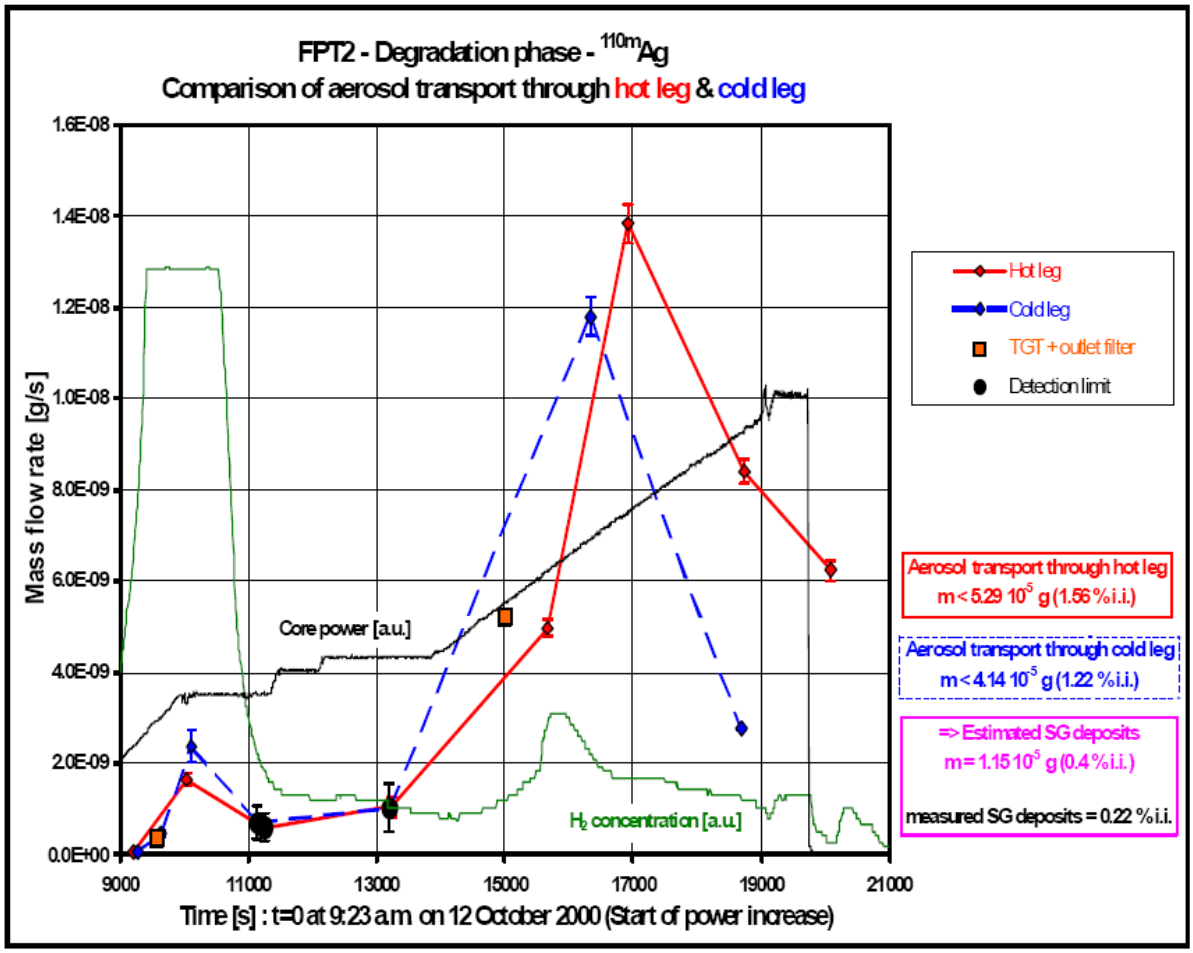

Figure 25. Silver transported at point C during FPT-2.

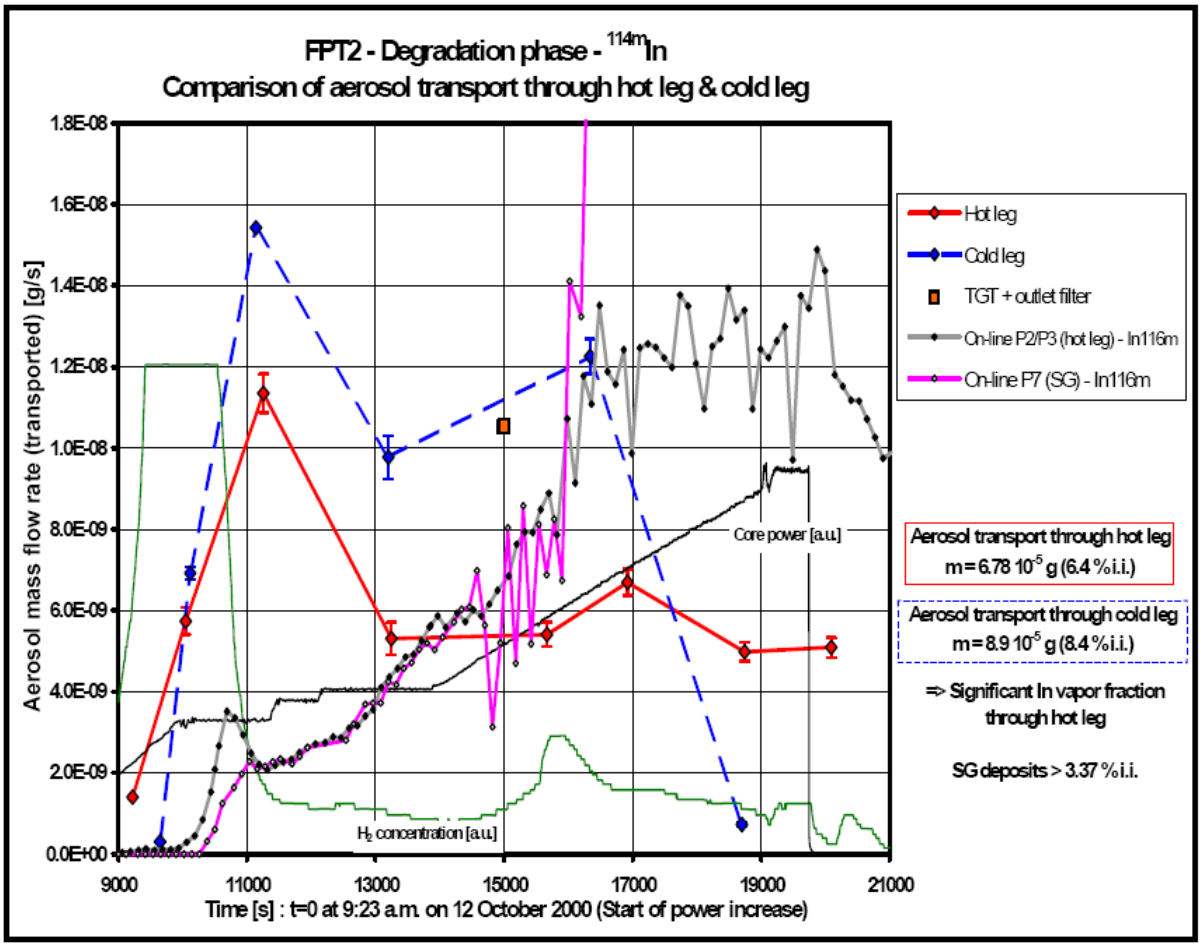

Figure 26. Indium transported at point C during FPT-2.

Most of the codes have no or very simple models to evaluate the release of control and structural material from the core. Releases of tin (from cladding), silver, indium and cadmium were observed. These materials may affect the chemical forms of the radioactive fission product and the extent of their retention in the circuit and containment although they do not directly contribute to the potential radiological source. Silver has an impact on iodine chemistry in the containment, while tin and cadmium also affect the fission product chemistry, most notably that of tellurium. In particular the release of silver was much lower (though probably still significant) in FPT-2 than FPT-0/FPT-1. It is possible that the silver drained to cooler parts of the bundle more readily in FPT-2, but this is not confirmed and the controlling mechanism has not been identified.

Due to its volatile character, iodine was strongly released from the fuel bundle. As shown in Figure 27, about 28% of initial bundle inventory remained in the fuel bundle at the end of the test (Gregoire 2009). This figure displays the post-test γ-scanning of ^{131}I together with this one of ^{58}Co. The first one gives the final iodine distribution profile and the second one is representative of the short lived FP distribution before the transient. Indeed, the ^{58}Co is an activation product of the test device pressure tube and, as such, it characterizes the irradiation profile of the Phebus driver core. From γ-measurements, it is interesting to note very little iodine located along the molten pool and the cavity, in agreement with the volatile character of iodine and the temperature reached in this area during the degradation phase. On the other hand, the post-test iodine distribution profile is higher than that of ^{58}Co in the lower rods (1) and in the upper rods (2):

1. The relocation of fuel and structural material towards the lower part of the test device during the degradation phase is responsible of the iodine accumulation in this zone;
2. Iodine deposits occurred during its transit on the various surfaces in the upper part as observed also beyond the top of the fissile column.

Thermal hydraulic conditions encountered in fuel bundle outlet led to iodine deposits in the upper plenum and vertical line zones (i.e. respectively 4.1% and 0.4% of the initial bundle inventory).

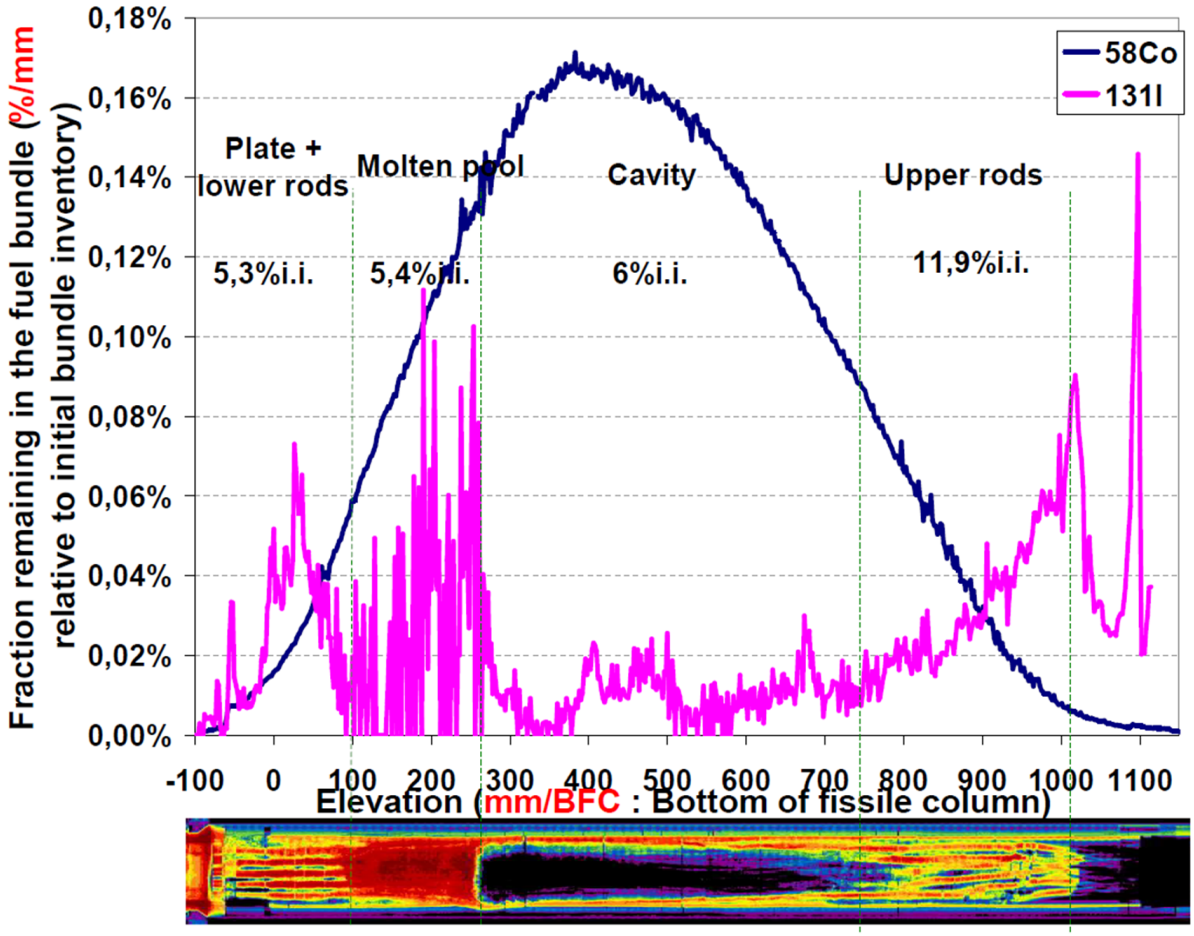

Figure 27. Test bundle activity profiles of ^{131}I and ^{58}Co.

The transport models that are used in the codes and that are based on the deposition of volatile species are generally confirmed by the results coming from the Phebus experiment (Birchley et al., 2005). Some discrepancies observed in the deposition profile for the volatile species could also be ascribed by uncertainties in the boundary conditions rather than the models for the processes. Some studies suggest that the application of models which are based on fully developed flow in a uniform channel to conditions like the upper plenum with an irregularly shaped geometry can be at the origin of the underestimation of deposition in that region.

Some discrepancies in the deposition profile (e.g. for caesium) seem to be linked to differences between available data for chemical species and calculations. Treatment of chemistry is not considered in all system-type codes. But its implementation, like in VICTORIA or ASTEC/SOPHAEROS, would likely improve estimates of the speciation, provided bundle release histories are correct. The information coming from separate

effect experiments within the SARNET project can provide additional data for model improvements.

However, the speciation computed by such codes is based on equilibrium conditions, which represent a great deal when considering species formed due to non-equilibrium effects. Gaseous iodine has been identified among these species that current equilibrium models are not able to calculate. New non-equilibrium models are only in fair agreement with the results of Phebus tests (Cantrel and Krausmann, 2004).

4. CONTAINMENT VESSEL

Steam, hydrogen and all released materials including fission products are collected in a safe way into the vessel; moreover the vessel has facilities for condensing the steam and thus keeping the system pressure under control, and for examining the physics and chemistry of the released aerosols and vapours.

4.1 Design, objectives and scenario

The containment vessel is a 10 m^3 electro-polished stainless steel cylinder with elliptical end caps, mounted vertically and equipped with features to induce typical containment phenomena for study with the representative source from the Phebus circuit. Recessed into the bottom of the vessel is a water-filled cavity called «the sump». Above the sump is a vertically oriented injection nozzle connected to the circuit, and suspended above the nozzle are three condensers. The condensers are cylinders with temperature-controlled surfaces: wet and dry. Their wet surfaces are cooled during the early injection phase of the experiment so that steam condenses upon them. The down flowing condensate is collected and periodically discharged to the sump. The dry surfaces are heated so that no condensation occurs and they are included for comparison with the wet surfaces.

The aerosol phase was devoted to studying fission product, bundle, structural and control rod material removal in the containment. The aerosol phase lasted approximately 37 hours. This phase was conducted with containment thermal hydraulic conditions identical to those of the degradation phase such that no condensation could occur on the condensers after 25960 seconds. During the aerosol phase, the containment humidity steadily decreased from 60% to 50%.

The 23-minute washing phase aimed at washing aerosols from the containment bottom, where they had settled, towards the sump, in order to take full benefit of their radiolytic contribution during the subsequent chemistry phase. This phase was preceded by about 5-hour preparatory phase to establish appropriate boundary conditions and limit vaporisation of the water from the sump and the containment bottom. The spray didn't work properly (the mass flow was too weak) and, thus, the FP wash down of the elliptic bottom into the sump was incomplete, but this problem affects only the sump composition and hence containment chemistry. The thermal hydraulic conditions were changed by decreasing the temperature of the sump water and the condensers wet part to about 40 °C , the containment bottom to about 100 °C and by increasing the temperature of the condensers' dry part and the vessel walls to about 120 °C in order to minimise condensation on the associated surfaces.

The aerosol calculation objectives included:

- Determine the thermal-hydraulics within the containment vessel, such as temperature, pressure, relative humidity and condensation rates on the condensers and in the sump, well enough to drive the aerosol physics.
- Determine the evolution of the airborne mass of aerosol in several specific containment portions, including aerosol removal to condensers, heated surfaces, and sump
- Determine the aerosol size distribution as a function of time

4.2 Source term into the containment

The composition of the aerosols injected into the containment vessel was dominated by fission products (Cs - 19%, Mo - 20%), control rod materials (Ag - 16%, Cd - 15%, In - 11%) and cladding material (Sn - 7%). The total mass is estimated to be 55 grams

taking into account the oxidation of the aerosol material. This value is very low compared to the FPT-1 value of 160 grams:

- The fission product Tc, Ru and Te had a containment inventory lower by a factor of 23, 6 and 2.5 respectively compared to the previous FPT-1 test;
- The control rod materials Ag and Cd had a containment inventory lower by a factor of 4.5 and 2 respectively compared to the previous FPT-1 test;
- The fuel material had a containment inventory lower by a factor of 43 for U compared to the previous FPT-1 test. Pu was not detected;
- Structural elements (Sn) and thermocouple material (Re) had a containment inventory lower by a factor of 5 and 20 respectively compared to the previous FPT-1 test.

This remarkable difference between FPT-2 and FPT-1 is partly explained by the lower injection steam flow rate in the FPT-2 experimental circuit (lower by a factor of about 4) that led to higher transit times in the experimental test device and the circuit and resulted in higher aerosol deposits in the upper plenum and the circuit hot leg for some elements. The lower steam injection flow rate also induced some differences in the fuel bundle degradation processes and led to release kinetics and release amounts from the test device notably different from those obtained in FPT-1, which in return directly impacted both the aerosol mass injected into the containment and the aerosol elemental composition.

The elements may be classified according to their release fractions in the containment:

- noble gases such as Xe and Kr elements have containment inventories which can reach 80% of the bundle initial inventory since these elements are not retained on the circuit surfaces. Release fractions of noble gases are quite similar for all the Phebus experiments;
- highly volatile fission products have containment inventories higher than 40% of the initial bundle inventory. They only include I (57% i.i.) and Cs (41% i.i.) whose behaviours are rather similar to FPT-1;
- some elements have intermediate release fractions in the containment ranging from 10% to 40% of the initial inventory, such as Rb (32% i.i.), Mo (31% i.i.) Te (28% i.i.) and Cd (23% i.i.). Rb, Te and Cd appear to be significantly less released than in FPT-1 where they belonged to highly volatile fission products with containment inventories respectively of 49% i.i, 53% i.i., and 51% i.i.;
- other elements have low release fractions in the containment such as Sn (6.8% i.i.), In (5.7% i.i.), W (3.7% i.i.), Ag (1.5% i.i.), and Tc (0.92% i.i.). Among these elements, Sn, Ag and Tc are significantly less released than in FPT-1 where they had containment inventories respectively of 33% i.i., 6.7% i.i., and 21% i.i.;
- some elements have negligible release fractions in the containment (lower than 0.5% i.i.) such as low-volatile fission products Sr (0.43% i.i.), Ba (0.37% i.i.), Re (0.33% i.i.), Ru (0.083% i.i.), La (0.056% i.i.), fuel material U (0.0028% i.i.), and Zr (0.0076% i.i.) coming from the structures. Among these elements, fuel elements and Re are remarkably less released than in FPT-1 and Pu is not even detected in FPT-2. Ba, Ru and Zr are also less released than in FPT-1 where they had containment inventories respectively of 0.7% i.i., 0.5% i.i., and 0.015% i.i.. In terms of mass released to the containment Re, Cs and Mo rank highest, in contrast to FPT-0 and FPT-1.

Figure 28 indicates that iodine discharged into the containment in relation to the H_2 flow rate is completely different depending on the test. In contrast with the FPT-1 test, which gave rise to three distinct iodine release phases concomitant with the first three hydrogen production phases detailed above (the molten pool formation and the fuel relocation were events which occurred in the secondary oxidation phase), the curve of

iodine injected in the containment for the FPT-2 test shows that there was no variation related to the bundle events. In particular, the peak absence during the first oxidation phase, which produces the strongest iodine release amplitude in FPT-1, may be due to the considerable deposits in FPT2 in the upper bundle and upper plenum which provided a reservoir of fission products which were released when their concentrations in the carrier gas stream from the degrading bundle fell, so smoothing out the release to the containment.

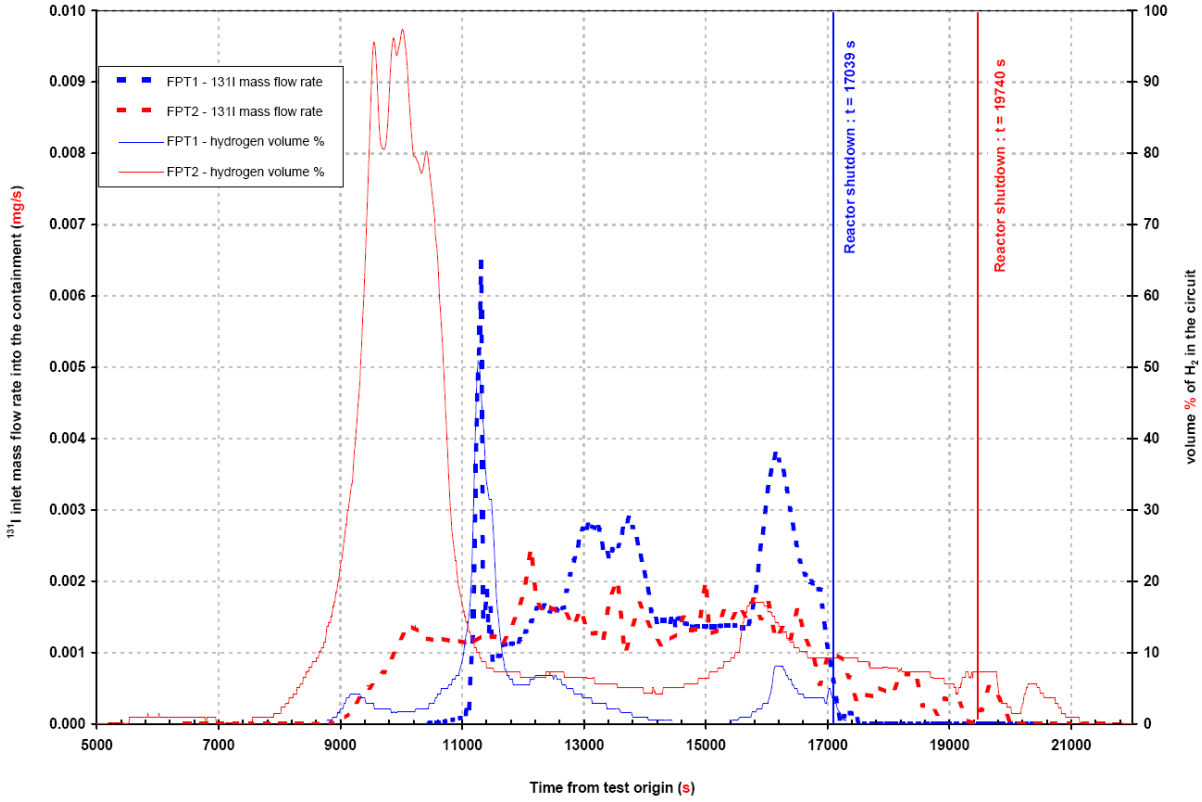

Figure 28. I^{131} mass flow rate in the cold leg (point G, 150°C) of the circuit during the test transient. FPT-1 and FPT-2 comparison.

4.3 Thermal-hydraulic conditions

Although the thermal hydraulics within the Phebus containment vessel was not a major concern in the test, there were certain objectives in calculating the vessel conditions. These included checking that the experimental measurements were self-consistent and that certain code parameters had been correctly assigned, providing evidence for the degree of spatial homogenisation (mixing) achieved in the test and generating information upon which to base the aerosol and iodine chemistry calculations. In general, FP will be well mixed in the containment atmosphere except during the injection phase.

Special features of the Phebus vessel, such as fixed wall temperatures and multiple thermal hydraulic phases were very useful to analysts, as was spatial temperature information from a grid of suspended thermocouples. Single-volume and multivolume calculations were made with standard containment codes such as ASTEC/CPA, CONTAIN, COCOSYS, and MELCOR.

Numerous two-and three-dimensional analyses of the containment thermalhydraulics were performed with general purpose CFD codes such as CFX (Gyenes and Ammirabile,

2010). A variety of turbulence models have been deployed and various assumptions implemented. By using a certain number of fictitious internal "volumes" and ad-hoc junctions among them, lumped parameters codes could predict flows similar to those determined with CFD tools. However, no increased accuracy was observed with the prediction of bulk parameters which are important for the aerosol physics such as temperature, pressure and relative humidity. Discrepancies with the measured values were in the range of a few degrees or tenth of bars.

The test was simulated (Kljenak, 2003) with the lumped-parameter CONTAIN code in order to verify the consistency of the data. The steam injection rate in the containment vessel was calculated from time-dependent atmosphere humidity, steam condensation rate and gas sampling rate. No inconsistency of the data was detected when comparing experimental and calculated results. The calculated steam injection rate in the containment was found adequate and suitable to be used for further simulations and analyses.

MELCOR calculations for FPT-1 (Birchley, 2003) have shown quite good, though not outstanding agreement with data for the thermal-hydraulic and aerosol response. It was important to confirm (or otherwise) whether similar good agreement could be obtained for the different conditions in FPT-2, using the same physical model, and whether the experimentally observed difference in aerosol depletion rate would be reflected in the calculations. Concerning the pressure history, a similar level of agreement is obtained, although the much smaller range in pressures meant that small discrepancies are more noticeable, including the effect of sampling.

Calculations were performed with CONTAIN 2.0 code (Herranz and del Pra, 2004) using a single cell model, the same as used for the analysis of the FPT-1 experiment; also the aerosol parameters were set to the same values as in FPT-1. It was found that the single-cell approach is detailed enough to simulate the thermal behaviour of the Phebus containment during the FPT-2 test. However, the instantaneous thermal response of CONTAIN 2.0 to fluctuations in steam injection rates could have an influence on aerosol behaviour. The relative humidity is a more adequate thermal-hydraulic parameter of the behaviour of the Phebus vessel than the condensation rate, since the relative humidity can be measured while the condensations are just estimated.

Similar calculations were performed with the ASTEC/CPA code (Fontanet et al., 2005) in the Phebus containment, modelling it with three zones: the dry and wet condensers and the whole volume below the condensers. It was found that the thermo-hydraulic and aerosol deposition results for the FPT-2 experiment are quite similar to CONTAIN results, with ASTEC/CPA consistently predicting the settling as the main aerosol depletion mechanism. The author concludes that a three-cell approach in ASTEC/CPA is good enough.

4.4 Calculated Aerosol Behaviour

In the containment vessel, aerosols experienced three main deposition processes:

- diffusiophoresis, which corresponded to the driving of aerosols by condensing steam towards the cooled wet painted condensers;
- gravitational settling on the containment floor;
- deposition on the vertical walls and the elliptic top lid of the containment vessel.

It was shown that most of detected isotopes had a similar global deposition behaviour:

- deposition by gravitational settling was the major aerosol deposition mechanism with an average value of 74 %c.i. [1] and τ_{grav} [2] = 5320 s on the containment

[1] containment inventory
[2] aerosol concentration follows the decay law $c(t) = c_0 * exp(-t/\tau_{grav})$

bottom. This fraction is higher than in FPT-1 (65-70% of the containment inventory), probably because the steam flow rate was higher in FPT-1 (2 g/s instead of 0.5 g/s) and led to a higher contribution of thermophoresis. The slower gravitational settling kinetics in FPT-2 may partly be explained by the smaller size of the aerosols in FPT-2 than in FPT-1.

- diffusiophoresis resulted in deposition of 12 % c.i. on the painted condensers surfaces. Deposition by diffusiophoresis may also be satisfactorily described as a first order process (with respect to the aerosol mass in suspension in the containment atmosphere) with a time constant of 8.5 h instead of 2.2 h in FPT-1. The ratio of these two time constants (equal to 3.8) is quite comparable with the ratio of the different condensation mass flow rates of 0.5 g/s in FPT-2 and 2 g/s FPT-1 (equal to 4), indicating that the diffusiophoresis kinetics is rather proportional to the steam flow rate.
- deposition on the containment vertical walls was shown to be about 11% c.i. with an average τ_{wall} = 38750 s at the end of the aerosol settling phase. This value was much higher than that observed for the FPT-1 test (maximum of about 2%c.i.). Assuming that wall deposition can be described as a first order process (with respect to the aerosol mass in suspension in the containment atmosphere), the time constant is about 11 h instead of 37 h in FPT-1. The different deposits on the wall versus settling may be partly explained by the smaller aerosol size in FPT-2 than in FPT-1, since smaller particles have a slower settling velocity.

The faster aerosol depletion kinetics in FPT-1 (t_{susp} = 0.65 h) is mainly due to the faster gravitational settling and to the higher condensation rate.

Impactor data suggest that the aerosol mass distribution in the containment may be characterized by an AMMD of 2.5 to 3.5 µm and a standard deviation of 2, which is smaller than the AMMD of 3.5 to 4 µm measured in FPT-1. The impactor data also reveal that the aerosol size is increasing as a function of time in the containment because of agglomeration processes. Unlike FPT-1, the agreement between experimental data and the log-normal distribution is not fully satisfactory, indicating that the assumption of an uni-modal log-normal distribution of the aerosol population is probably not fully justified and that the aerosol population in the containment vessel is probably more complex than the expected description (possibly multi-modal aerosol population).

At the end of the aerosol phase, containment inventory fractions deposited on the containment walls (11 %c.i.) and on the containment floor (67 %c.i.) were almost the same for all elements whereas the repartition between the sump and the condensers' wet part of elements depended on their solubility. Soluble elements (especially caesium and rubidium) were almost totally recovered into the sump whereas non soluble elements remained on both the sump and the condensers' wet part since they were not fully washed away.

During the transient and the early aerosol phase, water solubility of the aerosols can be classified as follows:

- elements that were mostly found in the water solution (Cs, Rb, and I, Figure 29);
- elements that lay in between, e.g. partly water soluble elements (Ba, Mo, Cd, Re, and Tc, Figure 30);
- elements that remained almost completely water non soluble (Ce, Te, Zr, Ru, Sn, In, Ag, W, and U, Figure 31).

This behaviour was the same as that observed for the FPT-1 test except for iodine that behaved as a water soluble element during the entire transient and underwent a very low deposition during the aerosol phase in the FPT-2 conditions. In the atmosphere of the containment the aerosol particles tended to agglomerate and grow as a function of time with an Aerodynamic Mass Median Diameter increasing from 1.4 µm during the first oxidation phase to 3.68 µm at the beginning of the aerosol phase.

Both reactor containment codes and CFD codes were applied and benchmarked. Again the CACIC served to coordinate and integrate analysis efforts. Single-volume codes did as well as multivolume codes and CFD codes in predicting the macroscopic thermal hydraulics. The CFD codes predict rather complex flow patterns during the injection phase with some inhomogeneity.

The experimental results confirm the applicability for the simple geometry of lumped-parameter, coarse-node models for calculating the global response of the Phebus containment. Some discrepancies in the aerosol deposition rate and split between gravitational settling and diffusiophoretic deposition reflect a difficulty to calculate the particle sizes (Herranz et al., 16th and 17th CACIC meetings). It is necessary to use a sufficient number of size classes (at least 10 and possibly 20) to resolve the distribution. The internal circulation is not represented in the coarse node models and may have influenced the particle sizes but did not otherwise appear to strongly affect the aerosol behaviour.

There is no indication that detailed models or CFD methods are needed to calculate the global behaviour, although they would be necessary to calculate the transient hydrogen distribution.

It was observed that the containment thermalhydraulics and aerosol behaviour are not tightly coupled, meaning that the presence of aerosols had no significant effect on the thermalhydraulics, while the containment thermalhydraulic processes affected the aerosol deposition but without playing a dominant role. The aerosol behaviour depends on the source from the circuit and a high aerosol concentration leads to faster agglomeration and hence more settling.

It can be said that, due to the simple Phebus configuration, care should be taken when extrapolating these conclusions to much more complex situations that can be found in a real plant. Also, the remarks concerning coupling between phenomena might not apply in a real plant where the fission products deliver energy through their decay heat and disruptive events such as hydrogen burning may occur.

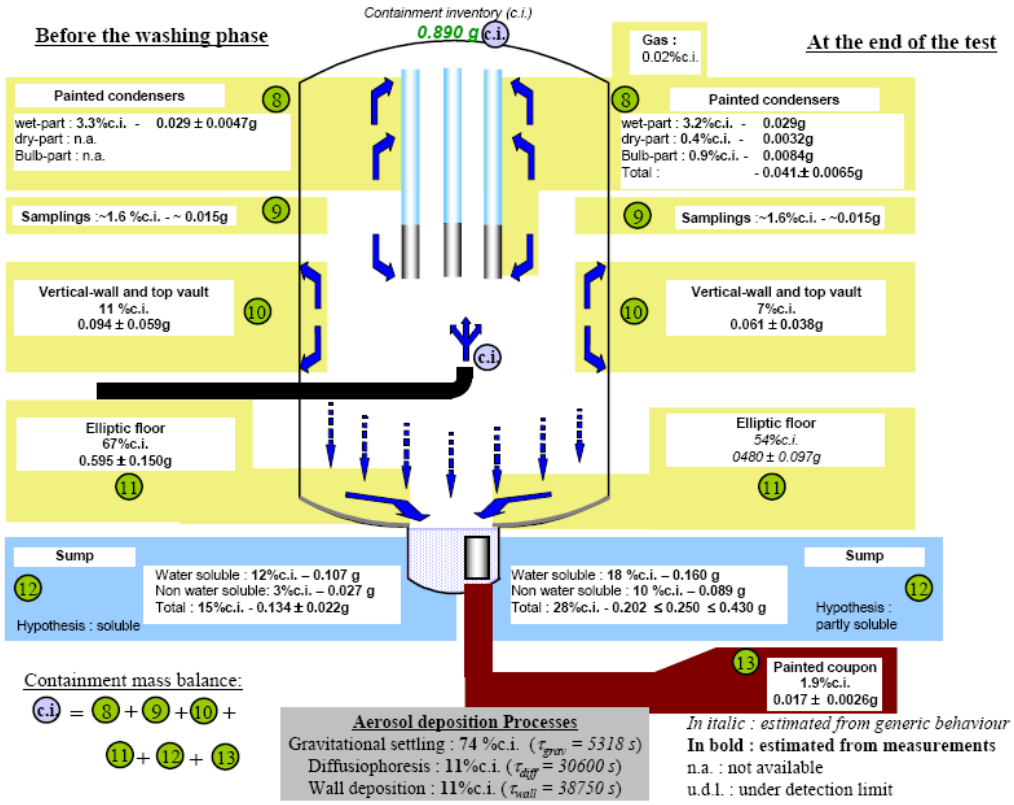

Figure 29. FPT-2 containment vessel: material distribution of soluble element I^{131}.

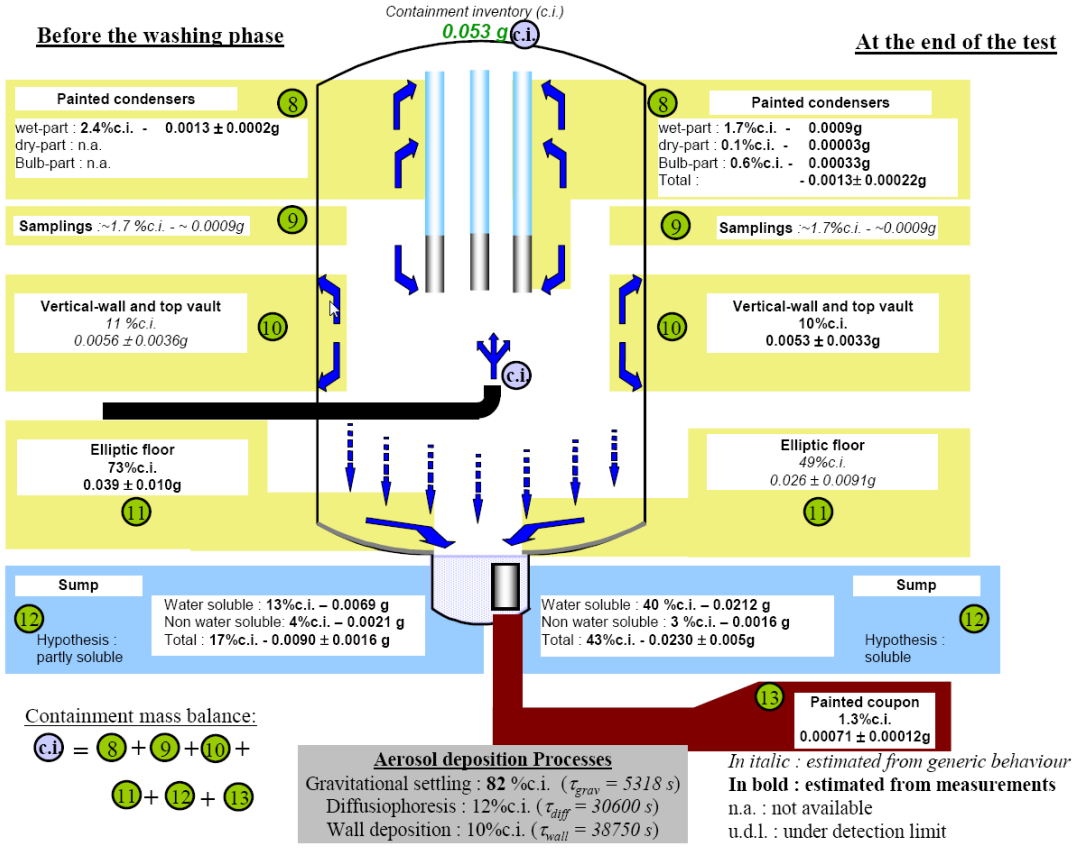

Figure 30. FPT-2 containment vessel: material distribution of partly soluble element Ba ($^{140}Ba/^{140}La$).

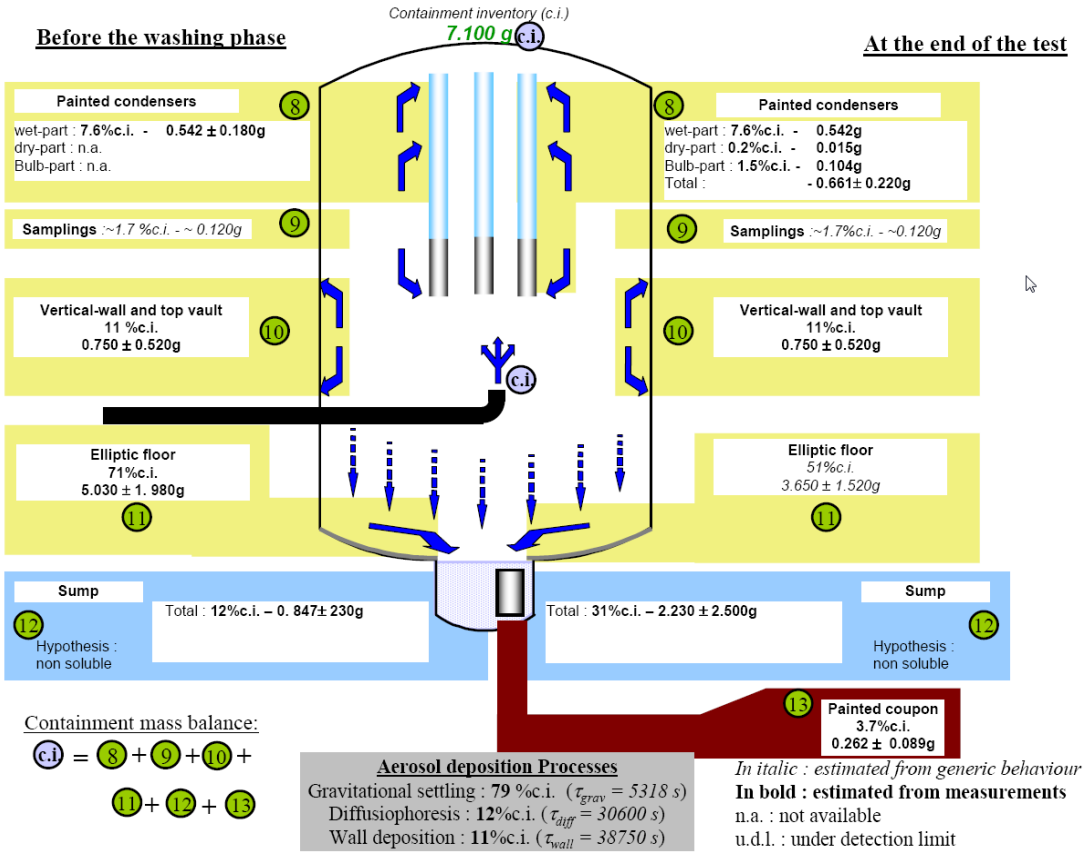

Figure 31. FPT-2 containment vessel: material distribution of non-soluble element Ag^{110m}.

This behaviour was the same as that observed for the FPT-1 test except for iodine which behaved as a water soluble element during the entire transient and hence left no deposits on the wet surfaces of the condensers in the FPT-2 conditions. This difference in iodine behaviour is currently unexplained. In the atmosphere of the containment, size and variance of the aerosol particles tended to grow as a function of time with an Aerodynamic Mass Median Diameter increasing from 1.4 μm during the first oxidation phase to 3.68 μm at the beginning of the aerosol phase.

4.4.1 The Injection phase

According to (Kljenak, 2005) the overall aerosol deposition was slower than in the FPT-1 experiment and the total deposition on the condensers was also lower. The differences in the aerosol settling might be explained by the differences in particles size or by the different circulation of steam into the Phebus vessel during the two experiments. The CFD calculations done by NRG (Gyenes, 2005) showed that the circulation patterns are complex: in case of higher steam injection rates two vortices were formed along the length of the vessel and when the steam injection is lower only single vortices were formed. Possibly there is a different interaction between downward flow near condensers and upward flow in FPT-1 and FPT-2. These differences should also be considered in discussion of aerosol deposition on condenser wet parts.

4.4.2 The settling phase

MELCOR calculations for FPT-1 (Birchley, 2003) had shown quite good, though not absolute agreement with data for the thermal-hydraulic and aerosol response, Figure 32. Contrary to experiment, the calculated aerosol depletion rate for FPT-2 is similar to the case of FPT-1, having been underestimated in FPT-1 but showing better agreement in FPT-2, Figure 33. The calculated depletion rates decrease over time as the dominant process of gravitational settling removes the larger particles preferentially. However, the experiment shows a more constant depletion rate. These differing trends suggest that physical processes in addition to settling may have played a role.

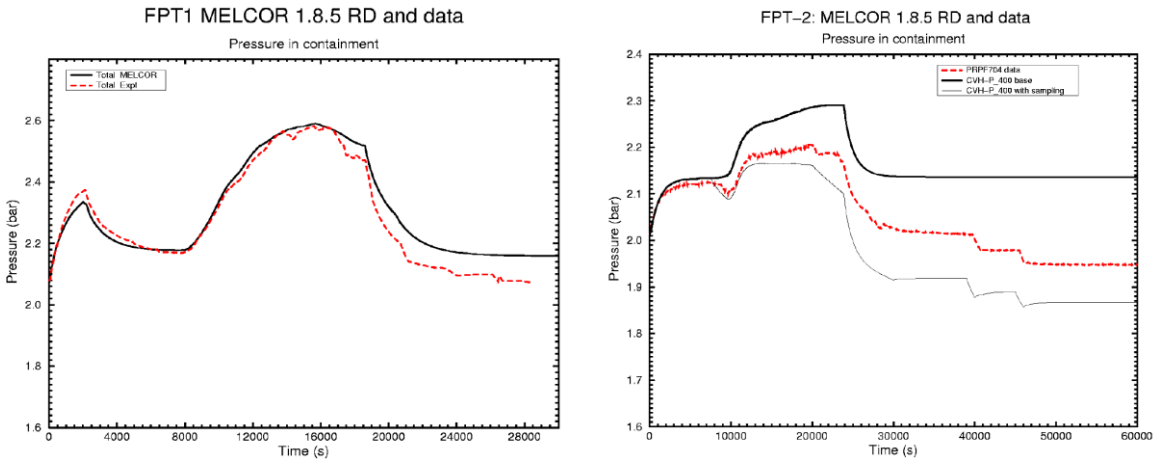

Figure 32. MELCOR calculation of pressure in the containment for FPT-1 and FPT-2.

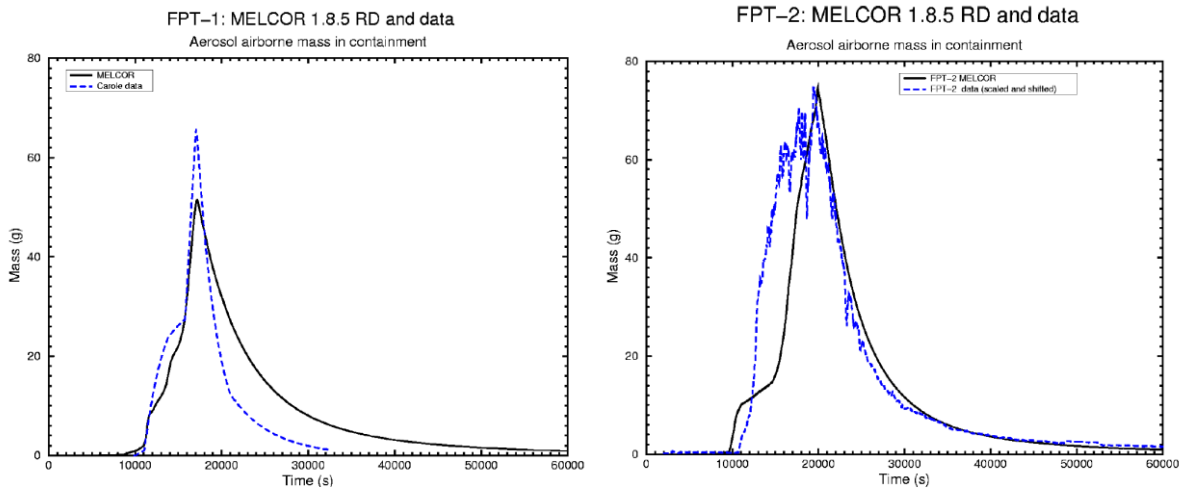

Figure 33. MELCOR calculation of aerosol airborne mass in the containment for FPT-1 and FPT-2.

The calculations performed with CONTAIN 2.0 code (Herranz and del Pra, 2004) using a single cell model and the same aerosol parameters as used for the analysis of the FPT-1 experiment, consistently predicted that settling was the main deposition mechanism in FPT-2 and the characteristic removal time was predicted satisfactorily, but the settling was somewhat over-predicted, Figure 34 and Figure 35. However the wall deposition and the effect of the sampling were under-predicted.

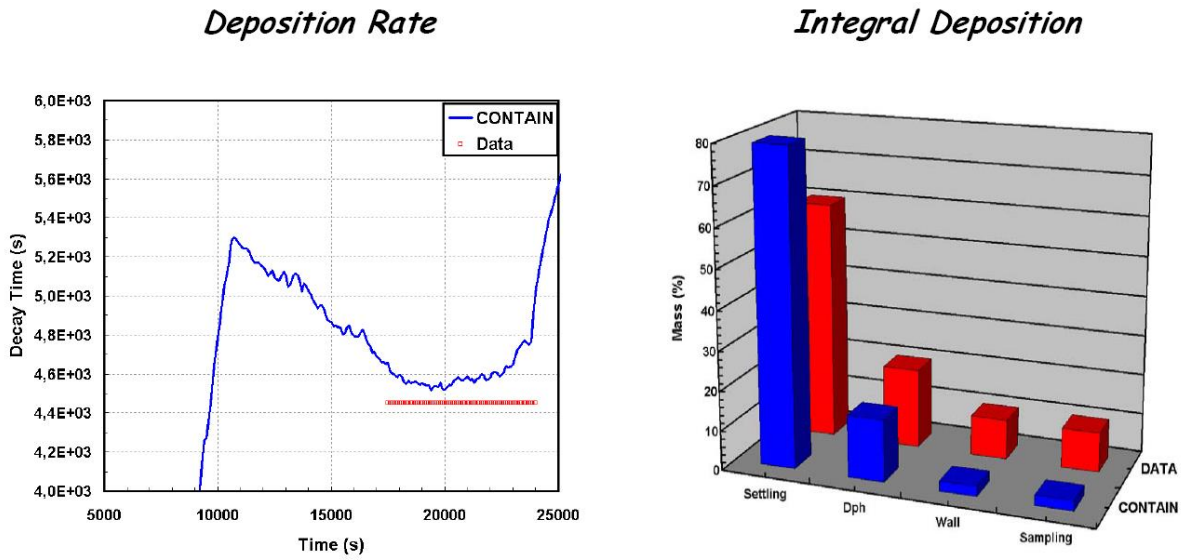

Figure 34. CONTAIN calculation of deposition in the containment for FPT-2[3].

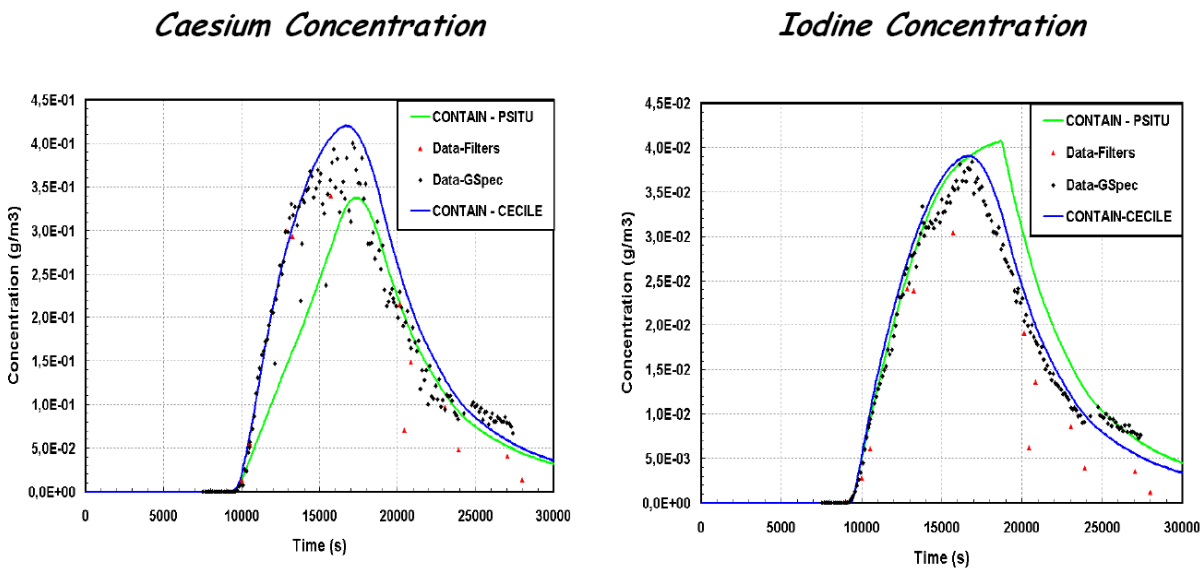

Figure 35. CONTAIN calculation of Cs and I concentration in the containment for FPT-2.

Similar calculations were performed with the ASTEC/CPA code (Fontanet et al., 2005) in the Phebus containment, modelling it with three zones: the dry and wet condensers and the whole volume below the condensers. It was found that the thermo-hydraulic and aerosol deposition results for the FPT-2 experiment are quite similar to CONTAIN results (Figure 36), with ASTEC/CPA consistently predicting sedimentation as the main aerosol depletion mechanism. However, ASTEC/CPA over predicted the settling rate and underestimated deposition by diffusiophoresis like other codes. Practically no deposition on the containment wall was predicted. The comparison of ASTEC/CPA and CONTAIN results shows that according to ASTEC/CPA particle growth is faster than was predicted by the CONTAIN code.

[3] Dph stands for diffusiophoresis

A code-to-code calculation benchmark was performed using CONTAIN, ASTEC/CPA and MELCOR (Herranz, 2005), with almost identical input parameters and finding that all codes predicted similar scenarios and no major differences could be attributed to the nodalization of the containment vessel. All codes were found to overestimate the steam condensation during the first 2000 seconds. The comparisons with the experimental data showed that the gravitational settling calculated by the codes was overestimated and consequently the diffusiophoresis on the wet condensers was underestimated. Sensitivity calculations showed that the overestimation of the gravitational settling cannot be explained by the reasonable changes in the input parameters of the gravitational settling models like aerosol density, aerosol shape factor or particle diameter.

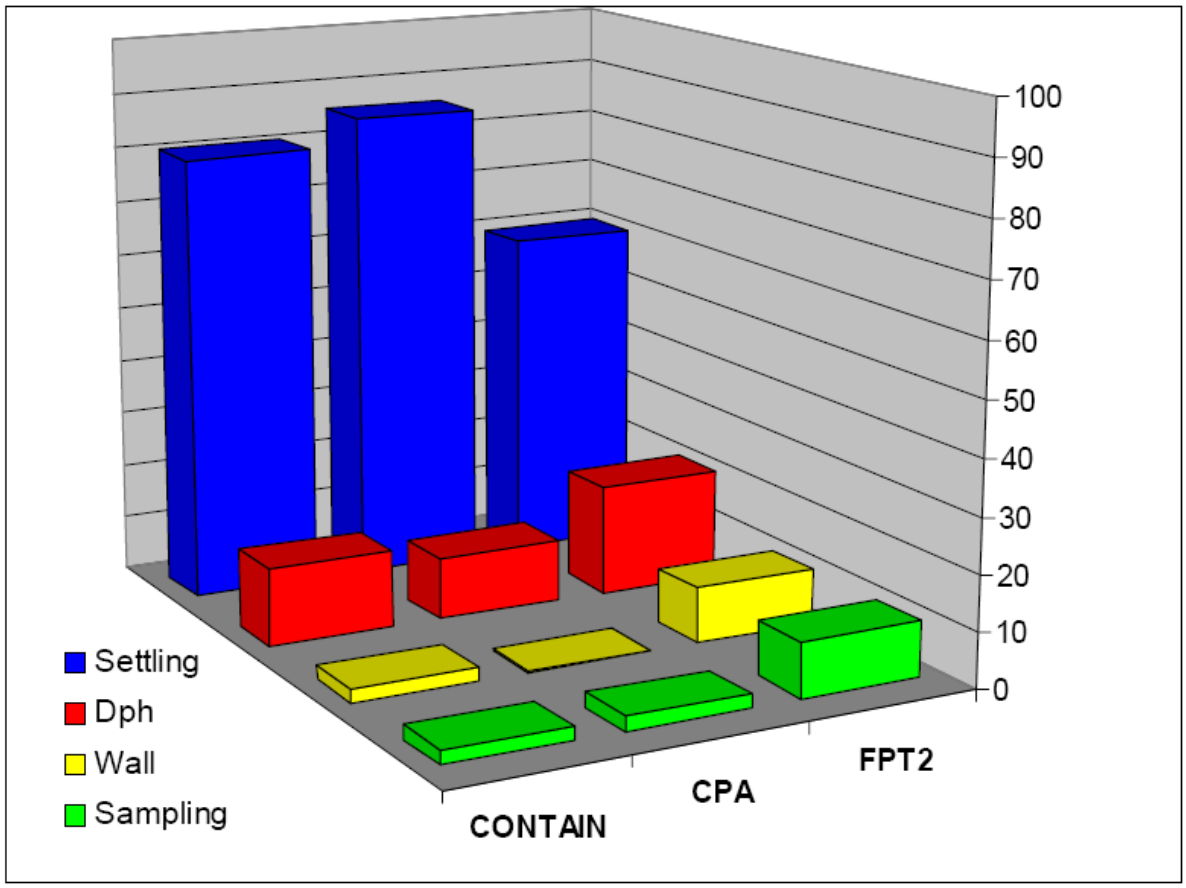

Figure 36. CONTAIN and ASTEC/CPA calculation of deposition (as a percentage of airborne mass) in the containment for FPT-2[4].

4.4.3 Aerosol deposition on the walls

In the former Phebus FPT-0 and FPT-1 tests, significant (a few percent of the mass released in the containment) and unexpected deposition on the containment vessel wall had been observed (Layly and Plumecocq, 2004). This unexpected behaviour (according to the current modelling) was also observed in the Phebus FPT-2 test. As most of the fission products and structural materials were released in aerosol form into the containment, such a deposition must be linked only to the mechanics of aerosols.

[4] Dph stands for diffusiophoresis

In a first step, 3D computations of the flow pattern (Layly et al., 1996) showed that the velocity field near the walls could not produce significant inertial deposition. On the other hand, because the vessel was slightly warmer than the atmosphere and humidity remained in the range 60%-70% during the aerosol depletion phase, no phoretic or hygroscopic mechanism could happen to be efficient.

In a second step, the possible electrophoretic deposition had been explored (Layly 1998). Because of the space charge electric field oriented toward the steel wall, positively charged particles could have been captured. The conclusion of this study was that small particles were negatively charged, their charge becoming positive for a size much higher than the one encountered in the Phebus containment. This result was linked to the weakness of the specific activity. Measurements of the charging effect on aerosols had been considered after FPT1 but never realised in the Phebus containment. (We could not only mention Layly but Gendarmes thesis and C. Clement references)

No other mechanism than diffusive deposition could explain the experimental results. This mechanism, often referred in the literature as "Brownian diffusion deposition", is mainly a hydrodynamic process: particles are brought by turbulent flow up to a region close to the wall where their deposition can occur by Brownian diffusion. The deposition velocity is written as the diffusion coefficient divided by a width, the numerical value of the latter being a user input of the codes, and depends more often on the user's personal judgement. In the current understanding of this mechanism, it is equal to the viscous sub layer thickness, the value of which may be deduced from numerical simulations of the flow. In the Phebus case, a reasonable value is roughly one millimetre. For a one-micron diameter particle, one then gets a deposition velocity, which is four orders of magnitude lower than the settling velocity. A model was developed based on the viscous sub layer width. As a result, the deposition velocity versus the particle size follows an $r^{-2/3}$ or $r^{-3/4}$ law, to be compared to the previous r^{-1} law. This allows larger particles, which actually carry most of the suspended mass, to be captured.

The thermal-hydraulic conditions were very similar in FPT-0, FPT-1 and FPT-2. With respect to FPT-0, more mass was released in FPT-1, and thus one can expect a lower fraction deposited on the vessel wall, because of the increasing settling. With respect to FPT-1, less mass was released in FPT-2, and also the temperature of the condenser was slightly higher in comparison to the wall, so one could predict a larger fraction deposited on the wall.

4.5 Calculated gas behaviour

The only significant non-noble gas entering the containment apart from hydrogen was gaseous iodine, Figure 37. This form of iodine is depleted by a variety of processes including absorption on aerosol particles and the vessel wall, capture by the wet and dry painted surfaces of the condensers and transfer to the sump, and also replenished by radiochemical reactions in the sump and possibly elsewhere. The subject is a complex and specialised one of considerable safety importance, is a central concern of the Containment Chemistry Interpretation Circle (Bosland et al. 2010), and is outside the scope of this report.

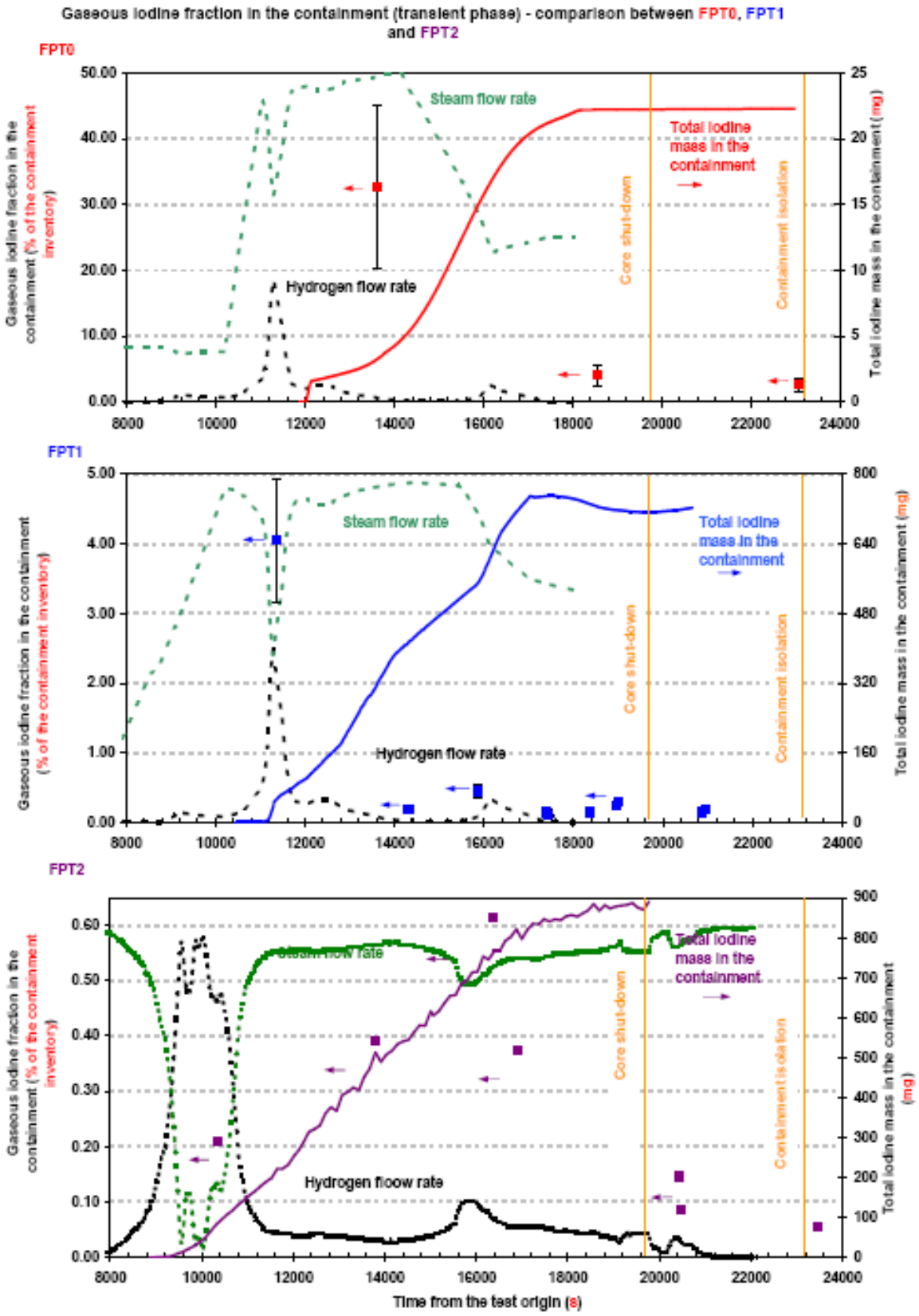

Figure 37. Gaseous iodine fraction in the containment for FPT-0, FPT-1 and FPT-2.

5. CONCLUSIONS AND OPEN ISSUES

The experimental results and modelling of the Phebus FPT-2 test have significantly improved our understanding of the fission products source term. However the number of calculations for FPT-2 is limited and not all aspects are fully covered as no benchmark or ISP was organized as it was done for FPT-1 and FPT-3 experiments.

- *Higher retention in upper plenum → different source term*

The Phebus experiment FPT-2 provides several results contrasting with those obtained in previous FPT-0 and FPT-1 tests. The FP release from the bundle is greater in FPT-2 than in FPT-1 due to higher bundle temperature and the FP deposition is greater in FPT-2 than in FPT-1 due to lower carrier velocity. The lower injection steam flow rate in the FPT-2 experimental circuit (lower by a factor of about 4) led to higher transit times in the experimental test device and the circuit, and that resulted in higher aerosol deposits in the upper plenum and the circuit hot leg for some elements. The lower steam injection flow rate also induced some differences in the fuel bundle degradation processes and led to release kinetics and release amounts from the test device notably different from those obtained in FPT-1.

- *Different degradation + different flow → different speciation to the circuit*

Compared to the mass injected into the containment, a generic behaviour could be identified for volatile (Cs) and low volatile material deposit (Ag, Ba) allowing estimating the cold leg deposits for the unmeasured elements. In the hot leg, material deposition could be determined experimentally for a larger set of elements (Cs, I, Te, Ba, Ag); for the unmeasured elements, the deposits in the hot leg were estimated using generic behaviour for volatile and low volatile material as in the cold leg.

Calculated species depositions were broadly similar: HIOSr, CsI (Cs_2I_2) and CdI_2 in decreasing volatility order are the dominant iodine species whereas Cs was mainly transported under Cs_2MoO_4 and $CsReO_4$ species. It's worth noting that $CsReO_4$ is non-prototypic or not reactor-typical and can only be the result of rhenium aerosols from thermocouples Further progress in the fission product speciation firstly requires a more accurate determination of mass flow rates of FP such as Mo, Cd that greatly impact the iodine and caesium chemistry and secondly a general check and improvement of the thermochemical database (as for the Cs-Te systems) used in the calculations.

The deposition pattern of FPs was less dependent on their volatility as compared to previous tests (FPT-0/FPT-1). For example, in the upper plenum, the vertical line, and the raising part of the steam generator, no significant differences were found for the retention of volatiles (Cs, I, Mo) despite their marked difference in volatility. This can be partly explained by their unexpected partial retention in zones upstream of the upper plenum (namely, in the upper part of the fuel rods) and upstream of the raising part of the steam generator where a cold temperature spot was measured. Tellurium, as already observed in the previous Phebus FP tests, behaves in a specific manner, characterized by a higher deposited fraction than caesium and iodine. This can be explained by the specific properties of some of its species that readily chemisorb on surfaces at high temperatures.

- *Circuit deposition, re-vaporization*

Both resuspension and revaporisation phenomena were observed in the test. Even if resuspension may be characteristic of the procedures in the facility we cannot exclude the possibility that it might occur in a plant accident for reasons we are not aware of, or we are unable to predict. The possibility that airborne fission product mass may increase

later during an accident can have a negative potential impact on source term evaluation following later containment failure or venting.

After reactor shutdown, about 45% of the caesium deposited in the hot part of the circuit (upper plenum and vertical line) was re-volatilized and then deposited mainly in the steam generator tube. Moreover, tellurium hot leg deposits decayed to volatile forms of iodine that were also conveyed to the steam generator tube.

Comparing to FPT-1 results, the main retention phenomena remains thermophoresis but gravitational settling accounts for more than 10% of the retention; gravitational settling was small in FPT-1. The best estimate calculation slightly improved the prediction for the iodine species, but the Te species retention was significantly under predicted.

According to (Birchley, 2005) and based on studies which showed a sensitivity to noding, a more detailed representation of the Phebus facility with a better choice of input related to the geometry could improve the results of the analyses rather than new aerosol physics models. What is not clear is whether the noding sensitivity is specific to the Phebus set-up. Further studies should also be pursued to evaluate if a plant calculation would be similarly affected by details in the geometry.

- *U-tube temp. drop (cold trap)*

The important deposits measured both in the cold leg of the circuit differs with those obtained for both previous tests. On the contrary, measured steam-generator deposits are significantly lower in FPT-2 than in FPT-0 and FPT-1 (less than 5% versus ~10-20% for volatile FPs). It was nevertheless observed that the fluid temperature at the steam generator inlet dropped down to 400-450°C through most of the release phase of the FPT-2 test, instead of the expected 700°C. Although this behaviour remains unexplained, it could account for some additional inventory being deposited upstream the steam generator inlet where the temperature gradient was located (Haste et al., 2013).

- *Interaction with materials especially Te*

Tellurium, as already observed in the previous Phebus FP tests, behaves in a specific manner, characterized by a higher deposited fraction than caesium and iodine. A potential explanation for the difference in Te behaviour could be that because of incomplete thermodynamic data and/or uncertainties concerning Sn release kinetics, which are strongly linked to the cladding oxidation state, the dominant species for Te is not SnTe. Literature suggests that a wide range of Cs_x-Te_y species could be formed that are not yet taken into account in the calculations. If these species were dominant, the chemisorption would be a minor phenomenon and the retention profile of Te more similar to that of caesium.

- *Bend effect not observed*

Experimentally no particular deposition in the circuit bends was found in FPT-2 test. With reasonable approximations to the observed aerosol size distribution most of the codes applied predicted deposition in the steam generator bend whereas no significant bend deposition was observed. However, several calculations predict bend deposition, using models based on experimental data from other sources. This point is also relevant to the calculation of deposition in the hot and cold leg and may merit further investigation. Bend deposition correlations have considerable experimental underpinning and are considered well validated for particles in the Phebus size range, and some bend deposition would be expected in the SG bend under Phebus conditions. The same problem was also seen with bend deposition in the hot section of the circuit. Possibly the dry fluffy nature of the Phebus deposits favoured resuspension, so that although particles deposited in the SG bend they were immediately resuspended.

- *Inconel effect*

The re-vaporisation testing on the vertical line samples (stainless steel and inconel sections) initially planned as a part of the PTA plan were cancelled, since deposits on those samples were not significant. We have thus no data concerning the layered composition of the aerosols or of the deposits in the circuit line (vertical line, steam generator tube).

- *Boric acid expected to change Cs and I chemistry*

Investigation on how diluted boric acid in the injected steam had influenced FP speciation showed that besides Mo, other important "consumers" of Cs were found, namely, Re (from thermocouples and not reactor-typical material) and B (indeed from boric acid), forming $CsReO_4$ and $CsBO_2$, respectively. Nevertheless, part of Cs is also calculated to leave the bundle as CsOH. On the other hand, during the hydrogen/steam-poor phases, when Mo and Re release is largely prevented, caesium borates and molybdates should be predominantly formed at high temperatures, while only a minor part ~1% of the released Cs is converted into CsI. There was probably a B-rich blockage in the circuit occasioned by the boric acid injection (Haste et al., 2012). A pressure difference was measured between the hot leg and the cold leg of about a third of that seen in FPT-3, which is approximately proportional to the mass of boron injected, and with similar time dependence. Anyway, this effect has never been studied in detail in FPT-2.

- *Gaseous iodine non equilibrium chemistry*

Although CsI is the main volatile iodine species predicted to be formed at high temperatures, a small amount of CdI_2 and volatile HI that persists in a gaseous form at low temperatures is also predicted. The transport of some of the iodine as gaseous species is not understood and cannot be explained on the basis of equilibrium chemistry.

Though limited cadmium release could explain the fraction of gaseous iodine persisting at low temperature under HI in the Phebus tests, non-equilibrium chemistry is currently under investigation through performance of small-scale analytical tests in the CHIP facility (part of the ISTP program) and development of chemical kinetics models. The presence of a gaseous iodine source may have a strong impact on the atmospheric iodine concentration in the long term and hence the potential for significant iodine release.

- *Containment*

It was shown that most isotopes detected had similar global deposition behaviour as in FPT-1. Deposition by settling was the major aerosol deposition mechanism in the containment and diffusiophoresis resulted to be the cause for deposition on the painted condenser surfaces. Deposition by diffusiophoresis was shown to be slower compared to FPT-1 by a factor of about 4, corresponding to the steam condensation mass flow rate ratio between the two tests. Deposition on the containment wall was shown to be of the same order of magnitude of the condenser, but much higher than that observed for the FPT-1 test. The different deposits on the wall versus settling can be partly explained by the smaller aerosol size in FPT-2 than in FPT-1; mainly FP and control rod materials in FPT-2, structural materials (Sn, Re) largely exceeded the FP and the fuel content was quite significant in FPT-1. This deposition issue rather speculative, it is still an open issue and some further "brainstorming" of the mechanism is required.

At the end of the aerosol phase, containment inventory fractions deposited on the containment walls (11 % c.i.) and on the containment floor (67 % c.i.) were almost the same for all the elements, while the repartition between the sump and the condensers' wet part of elements depended on their solubility.

Iodine behaved as a water-soluble element during the entire transient and underwent a very low deposition during the aerosol phase in the FPT-2 conditions in comparisons to other experiments.

Internal circulation in the containment vessel is not represented in the coarse node models and may have influenced the particle sizes but did not otherwise appear to affect the aerosol behaviour; however, this is not confirmed. Anyway, it is not expected to have a dominant effect on the aerosol deposition rate.

Both reactor containment codes and CFD codes were applied and benchmarked. Single-volume codes did as well as multivolume codes and CFD codes in predicting the macroscopic thermal hydraulics. The CFD codes predict rather complex flow patterns during the injection phase with some inhomogeneity. The experimental results confirm the applicability of lumped-parameter, coarse-node models for calculating the global response of the containment.

The calculations performed on the containment consistently predicted that settling was the main deposition mechanisms in FPT-2 and the characteristic removal time was predicted satisfactorily, but the settling was somewhat over predicted. The wall deposition and the effect of the sampling were under-predicted. In general the codes produced better results for the containment than for the circuit. Anyway, caution should be taken in generalising to the reactor containment, since the Phebus vessel was deliberately kept simple and the thermal-hydraulic conditions dry to facilitate calculation.

The new developed model implemented in ASTEC/CPA based on bench-scale experimental results and integrating turbulence damping in the viscous boundary layer was found to reproduce the deposition on the containment side walls satisfactorily, allowing larger particles to be captured. This deposition is largely underestimated based on the current Brownian diffusion modelling.

ANNEX 1: Phebus FP Test Matrix

Test n°	Type of fuel	Fuel Degradation	Primary Circuit	Containment	Date
FPT-0	Fresh Fuel 1 Ag-In-Cd rod 9 days pre-irradiation	Melt Progression & FP release in steam-rich environment	FP chemistry and deposits in non condensing steam generator	Aerosol deposition Iodine radiochemistry at pH5	Dec. 2 1993
FPT-1	BR3 fuel ≈ 23 GWd/tU 1 Ag-In-Cd rod Re irradiation	As FPT-0 with irradiated fuel	As FPT-0	As FPT-0	July 26 1996
FPT-2	As FPT-1 BR3 fuel ≈ 32 GWd/tU	As FPT-1 under steam poor conditions	As FPT-1 with effect of boric acid	pH9 evaporating sump	Oct. 12 2000
FPT-3	As FPT-1 with B_4C instead of Ag-In-Cd BR3 fuel ≈ 24 GWd/tU	As FPT-2	As FPT-0	pH5 evaporating sump, recombiner coupons	Nov. 18 2004
FPT-4	EDF fuel 38 GWd/tU no pre-irradiation	Low volatile FP& actinide release from UO2-ZrO2 debris bed	Integral filters in test device Post-test analyses on samples		July 22 1999

ANNEX 2: Summary of Phebus phenomenology

(Birchley et al., 2005)

Parameter / process	Value / characteristics	Remarks	Significance for reactor plant
		Significance for code models and their application to plant	
Zircaloy oxidation	Oxidation fraction: ca. 70%	Occurred on intact cladding and also during debris formation and movement	Rapid generation and large total fraction (equivalent to 500-600 kg, max 1 kg/s) points to appraisal of hydrogen mitigation measures
	Rapid peak oxidation rate (up to 0.2 g/s); significant or total consumption of steam at typical steam flow rates	Potential for further oxidation following water injection (not included in experiments)	Spatial variations in plant reactor core may reduce oxidation
		Oxidation simulated well by Urbanic-Heidrick model, despite known limitations	
Interaction of molten metallic with fuel and oxidised cladding	Failure of oxide shell at ca. 2400 K led to moderate relocated mass (up to 10%)	Indirectly lead to debris formation and major fuel movement	Resolidified (U, Zr)O can act as in-core crucible for heating of fuel debris (as in TMI-2)
	Predominantly (U, Zr)O mixture	Interaction with both cladding (Zr) and other metallic (steel, etc.)	
		Onset of relocation within normal parametric band (2300-2500 K)	
Bulk fuel movement/melt pool formation	Indicated to start at 2500-2650 K	Occurrence not expected by experimental team at start of programme;	Possibility of early formation of melt pool and transition to late phase; possible reduced time window for re-establishing core cooling
	Up to 25% of fuel melted, 50% displaced	Driving mechanism connected with interaction with metallic but not yet understood	
	Mostly ceramic molten pool near bottom of the bundle (debris bed in FPT-4) maximum temperature 2800-2900 K	Occurred well below theoretical ceramic melting temperature (>2800 K)	
		Sensitivity studies are needed to cover uncertain behaviour	

Release of materials from fuel bundle	Large (>80%) release of gases and highly volatile species	Volatiles: total as expected but kinetics slower (by a factor of about 4); modest effect of fuel burnup (c/f FPT-0, FPT-1)	On balance, releases are smaller/slower than typically calculated by system level codes
	Wide range (1-50%) release of semi-volatile species	Semi-volatile: comparison with models and other sources of data indicate strong effect of chemistry	Plant sequence likely to include reflooding, which could lead to additional release in short and long term
	Low release (ca. 0.1% or less) of refractory species including actinides	Refractory/fuel: no significant fuel release resulting from UO2 oxidation	Release of structural and control material has strong influence on FP chemistry in containment
	Other: significant release, up to 70% of Cd, Sn, up to 15% of Ag; made up bulk of aerosol mass	Other: sensitivity to transient conditions; mechanism partly understood but not adequately modelled; In and Sn release associated with cladding oxidation; Ag release associate with fuel movement; large early release of Cd when control rod failed	
		Certain parameters in empirical models being reviewed; sensitivity studies needed	
		Need for credible model for control/structural material release	
Transport of material in circuit	Transported fraction in range 30-70%, depending on volatility	Enhanced retention in regions of changing geometry	Plant geometry more complex than Phebus; more retention possible
	Almost all aerosols deposited in regions of large thermal gradient (upper plenum and SG up-side)	Revaporisation of Cs in circuit not adequately explained	Aerosol scrubbing in liquid regions in path to break (loop seal, etc.) could lead to very high retention
	Revapourisation of Cs in circuit	No liquid regions in Phebus circuit	
	Multi-component aerosol particles made up of most of the released materials	Aerosol models adequate, but deposition affected by complex geometry	
		Models mostly adequate for plant safety studies	

Chemistry in circuit	Little direct data available	Mechanism for production of vapour phase iodine and species not identified; may be due to finite rate chemical kinetics	Vapour phase iodine transport to containment has strong impact on potential source to environment
	Some iodine transported as vapour	Common assumption that all Cs, I are CsI, CsOH is refuted by Phebus results	
	Indication of Cs2MoO4 as dominant Cs species	Transport of gaseous iodine should be modelled (or accommodated) in codes	
		Importance of other aspects of circuit chemistry not yet clear	
Thermal-hydraulics in containment	Modest pressure increase (<1 bar)	Global response determined by balance of steam inflow and condensation; small contribution from hydrogen	Phebus behaviour is benign; plant containment has more complex geometry; other processes occur (H_2 burning, gases from core-concrete interaction, spray operation)
	Significant internal convective flows (deduced from temperature differences between surfaces)	CFD methods needed to calculate detailed internal flow and hydrogen distribution, but no data to test models	
		Simple models are entirely sufficient to calculate global behaviour	
		Simple geometry and boundary conditions in Phebus, and absence of disruptive events means models are not strongly tested	
Aerosol behaviour in containment	Smooth and monotonic decrease in airborne concentration; depletion rates ca. 40 min (FPT-0, FPT-1), 75 m (FPT-2)	Circulation velocity much larger than settling velocity, but role of circulation flow is not clear	Aerosol-borne FP release to environment would be negligibly small following uncontrolled discharge if it occurred several hours after release to containment
	Deposition: floor, ca. 70%; condensing surface, ca. 25%; smaller fraction on walls		Additional aerosols produced by core-concrete interaction; effect on FP concentration can be positive or negative
		Overall behaviour adequately simulated by classical models (gravity settling, diffusiophoresis)	

		Simple geometry and boundary conditions in Phebus, and absence of disruptive events means models are not strongly tested	
Iodine chemistry in sump	Almost all iodine retained in the sump	Different conditions in FPT-1/-2 make interpretation complicated	Release of Ag and/or maintaining basic sump conditions are important agents for limiting iodine volatility
	AgI (insoluble) was predominant in FPT-1; a significant fraction was soluble but non-volatile in FPT-2, possibly iodate.	FPT-1 (acidic sump): Ag was effective sink; radiolytic decomposition of AgI did not have significant effect	Additional species in reactor sump could modify iodine behaviour;
		FPT-2: basic sump conditions limited iodine volatility in FPT-2	
		Both semi-empirical and detailed models can reproduce observed behaviour, given suitable input, but unclear how well they extrapolate to wider range of conditions	
Iodine in containment atmosphere	Small but non-negligible concentration of volatile iodine, ca. 0.05 increasing to 0.1% in FPT-1, ca. 0.1 decreasing to 0.01% in FPT-2	Initial source of gaseous iodine is important	Gaseous iodine in containment is largest biological hazard following a severe accident
	Trend for organic iodide to dominate in long term	Formation of organic iodine believed to be from interaction with painted surfaces	Scaling to plant is uncertain due to limited knowledge of formation and destruction processes, and might affect gaseous iodine concentration
	Presence of gaseous iodine is very persistent	Concentrations and of inorganic/organic due mainly to balance of chemical formation and radiolytic destruction	
		Evaporating sump led to lower long term concentration in FPT-2	
		Possible to obtain fair agreement with known data but only by careful choice of model parameters; little confidence in blind prediction	
		Effort still in progress to gather and interpret data; credible models still lacking	
		The most difficult quantity to reproduce; current target is within a factor of 10.	

Integral effects	Degradation and fission product release are controlled by coupled processes (fluid and heat transport, oxidation, material interaction and chemistry)	Behaviour is very complex, challenging to interpret and calculate, and not fully understood sufficiently for reliable modelling purposed	Degradation behaviour is still subject to basic uncertainty; must be addressed by sensitivity studies
	Iodine chemistry in containment is controlled by coupled processes (chemistry in liquid pool, gas space, walls, radiation, mass transfer pool/gas space interface)	Phenomena can differ from those observed in separate effects experiments	Plant geometry and boundary conditions are more complex, and several additional processes occur in plant sequence
	Phenomena in one region or time period influence those in others; they may have impacts away from their origin	Propagation of physical quantities, means uncertainties are propagated and may be amplified	
		Direct quantitative Phebus-plant translation is not possible; it must be achieved via code calculations for both Phebus and plant, using similar modelling strategies	

References

Bottomley, P.D.W. Clément, B. Haste, T. Jacquemain, D. Powers, D. A. Schwarz, M. Teisseire, B. Zeyen, R.	2013	Special Issue : Phebus FP Final Seminar	Annals of Nuclear Energy Volume 61, Pages 230 (November 2013)
Clément, B. Zeyen, R.	2013	The objectives of the Phébus FP experimental programme and main findings	Annals of Nuclear Energy, Volume 61, November 2013, p. 4-10
Grégoire, A.-C. Haste, T.	2013	Material release from the bundle in Phébus FP	Annals of Nuclear Energy, Volume 61, November 2013, p. 102-121
Haste, T. Payot, F. Bottomley, P.D.W.	2013	Transport and deposition in the Phébus FP circuit	Annals of Nuclear Energy, Volume 61, November 2013, p. 102-121
Cousin, F. Kissane, M.P. Girault, N.	2013	Modelling of fission-product transport in the reactor coolant system	Annals of Nuclear Energy, Volume 61, November 2013, p. 135-142
Cantrel, L. Louis, F. Cousin, F.	2013	Advances in mechanistic understanding of iodine behaviour in PHEBUS-FP tests with the help of ab initio calculations	Annals of Nuclear Energy, Volume 61, November 2013, p. 170-178
Laurie, M. March, P. Simondi-Teisseire, B. Payot, F.	2013	Containment behaviour in Phébus FP, Annals of Nuclear Energy	Volume 61, November 2013, p. 122-134
Girault, N. Payot, F.	2013	Insights into iodine behaviour and speciation in the Phébus primary circuit	Annals of Nuclear Energy, Volume 61, November 2013, p. 88-95
Powers, D.A. Lee, R.Y. Salay, M.A.	2013	Applications of results from the Phébus-FP programme in the US regulatory process	Annals of Nuclear Energy, Volume 61, November 2013, p. 225-229
Brillant, G. Marchetto, C., Plumecocq, W.	2013	Fission product release from nuclear fuel I. Physical modelling in the ASTEC code	Annals of Nuclear Energy, Volume 61, November 2013, p. 88-95
Brillant, G. Marchetto, C., Plumecocq, W.	2013	Fission product release from nuclear fuel II. Validation of ASTEC/ELSA on analytical and large scale experiments	Annals of Nuclear Energy, Available online 12 April 2013

Birchley, J.	2003	Comparison calculations for FPT-1 and FPT-2 using MELCOR	Proceedings of the 14th Meeting of the Phébus Circuit and Containment Aerosol Interpretation Circle, 2003, Aix-en-Provence.
Birchley, J. Haste, T. Bruchertseifer, H. Cripps, R. Guntay, S., Jackel, B.	2005	Phebus-FP: Results and significance for plant safety in Switzerland	Nuclear Engineering and Design Volume 235, Issue 15, Pages 1557-1674 (July 2005)
Bosland, L. Cantrel, L. Girauld, N. Clement, B.	2010	Modelling of iodine radiochemistry in the ASTEC severe accident code: description and application to FPT-2 Phebus test	Nuclear Technology, Volume 171, Number 1, 2010, Pages 88-107
Bujan, A. Tóth, B. Bieliauskas, A. Zeyen, R. Housiadas, C.	2010	Interpretation of the Phebus FPT-0 and FPT-1 circuit results using the SOPHAEROS/ASTEC V1 module	Nuclear Technology Volume 169, Number 1, January 2010, Pages 1-17
Cantrel, L. Krausmann, E.	2004	Reaction Kinetics of a Fission-Product Mixture in a Steam-Hydrogen Carrier Gas in the Phebus Primary Circuit	Nuclear Technology, Volume 144, Number 1, 2003, Pages 1-15
Clement, B. Girault, N., Repetto, J. Jacquemain, D. Jones, A.V. Kissane M.P. von der Hardt, P.	2003	LWR severe accident simulation: synthesis of the results and interpretation of the first Phebus FP experiment FPT-0	Nuclear Engineering and Design, Volume 226, Issue 1, Pages 1-82 (November 2003)
Clement, B. Zeyen, R.	2013	The objectives of the Phebus FP experimental programme and main findings	Annals of Nuclear Energy, Special Issue on Phébus FP Final Seminar, Volume 61 (2013) 4-10
de Pascale, C.	2004	MAAP4 re-calculation of FPT-2 test, from bundle degradation to FP behaviour in circuit and containment and iodine chemistry during the aerosol phase	Proceedings of the 15th Meeting of the Phébus Circuit and Containment Aerosol Interpretation Circle, 2004, Bergen, The Netherlands.

Dienstbier, J.	2006	Findings from fission product transport analyses in Phebus FPT-1, FPT-2 circuits using the SOPHAEROS code	Proceedings of the 19th Meeting of the Phébus Circuit and Containment Aerosol Interpretation Circle, 2006, Alkmaar, The Netherlands.
Drosik, I.	2005	FPT-2 interpretation: Preliminary analysis of Caesium and Iodine species transported through hot leg during the FPT-2 fuel degradation process	Phebus Progress Report April-Sept 2005
Drosik, I.	2006	Preliminary analysis of the profiles of caesium and iodine in FPT-2 transition lines using the SOPHAEROS code	Proceedings of the 19th Meeting of the Phébus Circuit and Containment Aerosol Interpretation Circle, 2006, Alkmaar, The Netherlands.
Dubourg, R. Plumecoq, W.	2005	FPT-2 interpretation: Silver-Indium-Cadmium behaviour in the FPT-2 test	Phebus PROGRESS REPORT April-September 2005
Ducros, G. Malgouyres, P.P. Kissane, M. Boulaud, D. Durin, M.	2001	Fission product release under severe accidental conditions: general presentation of the program and synthesis of VERCORS 1–6 results	Nuclear Engineering and Design, 208, September 2001, Pages 191-203
EC CEA/IPSN	1988	Convention concernant le programme Phebus FP entre la communauté européenne de l'énergie atomique et le commissariat à l'énergie atomique	EC/CEA convention: 3428-88-07 TP ISP F of 12/07/1988
Fontanet, J. Vela-Garcia, M. Herranz, L.E.	2005	Preliminary results of Phebus FPT-2 simulation with CPA code	Minutes of the 17th meeting of the Circuit and Containment Interpretation Circle, 2005, Bergen (NH), The Netherlands.
Garnier, E.	2009	FPT-2 interpretation: CFD simulations of flow in the Phebus vertical line for tests FPT-1 and FPT-2	Phebus Progress Report October 2004- March 2005
Girault, N. Bosland, L. Dienstbier, J. Dubourg, R. Fiche, C.	2010	LWR severe accident simulation fission product behaviour in FPT-2 experiment	Nuclear Technology, Volume 169, Number 3, 2010, Pages 218-238

Girault, N. Bosland, L. Dickinson, S. Funke, F. Güntay, S. Herranz, L.E. Power, D.	2012	LWR severe accident simulation: iodine behaviour in FPT-2 experiment and advances on containment iodine chemistry	Nuclear Engineering and Design Volume 243, Pages 371-392
Girault, N. Fiche, C. Bujan, A. Dienstbier, J.	2009	Towards a better understanding of iodine chemistry in RCS of nuclear reactors	Nuclear Engineering and Design Volume 239, Issue 6, Pages 1162-1170 (June 2009).
Gregoire, A.C. Payot, F.	2009	PHEBUS FPT-1 TEST: Overview of fission product and material release and transport in the experimental circuit	ICAPP Tokyo, May 10-14, 2009.
Gregoire, A.C. March, P.	2005	FPT-2 data evaluation: TGT	Phebus Progress Report October 2004- March 2005
Gregoire, A.C. March, P. Payot, F. Ritter, G. Zabiego, M. de Bremaecker, A. Biard, B. Gregoire, G. Schlutig, S.	2008	FPT-2 Final Report	IP/08/579, 2008, IRSN.
Gyenes, G. Ammirabile, L.	2011	Containment analysis on the Phebus FPT-0, FPT-1 and FPT-2 experiments	Nuclear Engineering and Design, Volume 241, Issue 3, Pages 854-864 (March 2011)
Haste, T. Payot F. Dominguez C. March Ph. Simondi-Teisseire B. Steinbrück M.	2012	Study of boron behaviour in the primary circuit of water reactors under severe accident conditions: A comparison of Phébus FPT3 results with other recent integral and separate-effects data	Nuclear Engineering and Design, 246 (2012), p.147-156
Herranz, L.E.	2005	Analysis of In-Containment Aerosol Behaviour during the Phebus-FPT-2 Test	Proceedings of the 18th Meeting of the Phébus Circuit and Containment Aerosol Interpretation Circle, 2005, Aix-en-Provence.
Herranz, L.E. del Prá, C.L.	2004	CONTAIN 2.0 Simulation of Phebus-FPT-2: Preliminary Results	Proceedings of the 16th Meeting of the Phébus Circuit and Containment Aerosol Interpretation Circle, 2004, Aix-en-Provence.

Herranz, L.E. Vela-Garcia, M. Fontanet, J. del Pra, C. L.	2007	Experimental interpretation and code validation based on the Phebus-FP programme: Lessons learnt from the analysis of the containment scenario of FPT-1 and FPT-2 tests	Nuclear Engineering and Design, Volume 237, Issue 23, Pages 2210-2218 (December 2007)
Jones, A. Zeyen, R. Sangiorgi M.	2015	Circuit and Containment Aspects of PHÉBUS Experiments FPT0 and FPT1	EUR 27218. Luxembourg (Luxembourg): Publications Office of the European Union; 2015. JRC95357
Kljenak, I.	2005	Discussion on steam injection in Phebus containment vessel during FPT-1 and FPT-2 tests based on TOSQAN experimental results	Proceedings of the 18th Meeting of the Phébus Circuit and Containment Aerosol Interpretation Circle, 2005, Aix-en-Provence.
Kljenak, I.	2003	Inspection of containment thermal-hydraulic experimental data during the Phebus FPT-2 degradation phase using the CONTAIN code	Proceedings of the 14th Meeting of the Phébus Circuit and Containment Aerosol Interpretation Circle, 2003, Aix-en-Provence.
Langhans, J.	2004	Thermo-hydraulic and aerosol behaviour in the Phebus-FPT-2 containment vessel calculated with the GRS-code COCOSYS	Proceedings of the 15th Meeting of the Phébus Circuit and Containment Aerosol Interpretation Circle, 2004, Bergen, Netherlands.
Layly, V.D. Plumecocq, W.	2004	Aerosol deposition on the vertical walls of the Phebus containment vessel	Phebus Progress report April-September 2004
Payot, F. Haste, T. Biard, B. Bot-Robin, F. Devoy, J. Garnier, Y. Guillot, J. Manenc, C. March, P.	2011	FPT-3 Final Report	IP/11/589, 2011, IRSN.

Tirini, S.	2004	ASTEC CPA and FPT-2 Experimental Data	Minutes of the 15th meeting of the Circuit and Containment Interpretation Circle, 2004, Bergen (NH), The Netherlands.
Trambauer, K.	2008	Phebus FPT-2 post-test calculation with ATHLET-CD/SOPHAEROS: Deposition profile in steam generator	Minutes of the 23rd meeting of the Circuit and Containment Interpretation Circle, 2008, Bergen (NH), The Netherlands.
Trambauer, K.	2002	Athlet-CD Analysis of Phebus Tests: Comparison of Fission-Product Release and Transport in FPT-1, FPT-2 and FPT-3	Minutes of the 12th meeting of the Circuit and Containment Interpretation Circle, 2002, Aix-en-Provence.
Trambauer, K.	2006	Phebus-FPT-2 ATHLET-CD post-test calculation FP and aerosol transport	Minutes of the 20th meeting of the Circuit and Containment Interpretation Circle, 2006, Aix-en-Provence.
Trambauer, K. Erdmann, W.	2005	ATHLET-CD/SOPHAEROS analysis of Phebus FPT-2: Thermal behaviour and deposition in the circuit	Minutes of the 18th meeting of the Circuit and Containment Interpretation Circle, 2005, Aix-en-Provence.
Trambauer, K.	2008	Nachrechnung des Versuchs PHEBUS FPT-2 mit dem Rechenprogramm ATHLET-CD	GRS Report TN-TRB-08-01, 2008.
Layly, V.D. Spitz, P. Tirini, S. Mailliat, A.	1996	Analysis of the Phebus FPT-0 containment thermal hydraulics with the Jericho and Trio-VF codes	Nuclear Engineering and Design, Volume 166, Issue 3, 1 November 1996, Pages 413-426
Gouello, M. Mutelle, H. Cousin, F. Sobanska, S. Blanquet, E.	2013	Analysis of the iodine gas phase produced by interaction of CsI and MoO3 vapours in flowing steam	Nuclear Engineering and Design, Volume 263, October 2013, Pages 462-472

List of abbreviations and definitions

AMMD	average mass median diameter
BIC	Bundle Interpretation Circle
CACIC	Circuit and Containment Interpretation Circle
CCIC	Containment Chemistry Interpretation Circle
CFD	Computational Fluid Dynamics
EC	European Commission
EU	European Union
FP	Fission product
HL	Horizontal line
IC	Interpretation Circle
i.i.	Initial inventory
ISP	International Standard Problem
JRC	Joint Research Centre
MDB	material database
PSI	Paul Scherrer Institute
PTA	Post Test Analysis
PWR	Pressurized Water Reactor
SIC	Silver Indium Cadmium
SG	Steam Generator
SM	Structural materials
TGT	Thermal gradient tubes
TL	Transition lines
UP	Upper plenum
VL	Vertical line

List of figures

List of tables

LD-NA-27631-EN-N

JRC Mission

As the Commission's in-house science service, the Joint Research Centre's mission is to provide EU policies with independent, evidence-based scientific and technical support throughout the whole policy cycle.

Working in close cooperation with policy Directorates-General, the JRC addresses key societal challenges while stimulating innovation through developing new methods, tools and standards, and sharing its know-how with the Member States, the scientific community and international partners.

Serving society
Stimulating innovation
Supporting legislation

doi: 10.2790/94418

ISBN 978-92-79-54085-1